STRUCTURAL CHARACTERIZATIONS OF THE DIMERIC ANTI-HIV ANTIBODY 2G12 AND THE HIV-2 ENVELOPE GLYCOPROTEIN

Thesis by

Yunji Wu

In Partial Fulfillment of the Requirements for the

degree of

Doctor of Philosophy

CALIFORNIA INSTITUTE OF TECHNOLOGY

Pasadena, California

2015

(Defended April 29, 2015)

© 2015
Yunji Wu
All Rights Reserved

This work is dedicated to the memory of my grandmother

LU FENGYING

who showed me what it is to be a good human being

no matter where you come from or how little you have.

ACKNOWLEDGEMENTS

I'd like to express my unending gratitude to the people whose support was invaluable in the completion of my thesis. As someone who is stubbornly independent to a fault, I can say without a doubt that none of this could ever have been accomplished without my academic family.

To my advisor, Pamela Bjorkman, thank you for the last six years of training me in your lab and for always holding me to the highest standards. Especially when everyone else told me to give up on very low-resolution crystallography (Chapter 2), you were the only person that kept encouraging me to push harder and persevere – and we got it done! Thank you for being an example of a tireless, thoughtful scientist who does her work with integrity and pride. I know that I will carry what I learned from you for the rest of my career. (Pamela, I'm sorry that there are lots of sentence fragments on this page – it's hard to write in this format!) To my thesis committee – David Chan, Doug Rees, and David Baltimore – thank you for your perpetual support and constructive discussions. I've enjoyed some of my most fruitful conversations at Caltech with you. Thanks for always keeping an open door for me to talk about science, career, or life, even though I know you're all so busy. To Dianne Newman, thank you for awakening the love of microbes in me and for trusting me to help teach your class for so many years. Your generosity in both mentorship and friendship has truly been one of the highlights of my time at Caltech.

I want to thank so many people in the Bjorkman lab for making it a wonderful place to "grow up", but I only have space to mention a few here. To Anthony, you have been my scientific rock during grad school. I really don't know what I would have done

without you. Thank you for always listening to my conflicted and confused ramblings, and in spite of them, never failing to set me back on the exact right course. To Beth S., you were the best back-to-back baymate/mentor/friend I could have asked for. Thank you for always giving me your time and insights on crystallography and life. You have never once told me you were too busy to help me, and I don't take that for granted. To Rachel, Jennifer, and Marta, I want to thank you for a lot of other things, but mostly for your warmth, kindness, and humanness. Grad school can be a tough environment, and knowing that I could always rely on you to be there for me in a "real people" way was truly comforting and profoundly important. To my undergrads who gave your own time to help me – Salam, Dan, Gloria, and Sumana – I hope you got something out of it! Thanks for keeping the lab fun and young.

For those people in other labs who had absolutely no reason to help me except for the goodness of your hearts, especially Jost Vielmetter, Jens Kaiser, Justin Chartron, Matt Swulius, and Alasdair McDowell – my biggest breakthroughs would not have been possible without your altruism. All I can say is that because of you, I will pass it on to others. The same goes for the developers of the CCP4 suite and Phenix software, especially Nat Echols, Pavel Afonine, and Tom Terwilliger.

I could not have done any of this without the love and support of my family. To my hardworking, loving parents – thank you for always believing in me and teaching me to value and respect myself. To my brother, thank you for brightening up a huge part of my life by just being you. Finally, to my very soon-to-be husband, Andy, thank you for your steady love, devotion, and support, and for always giving me a safe place to be myself.

ABSTRACT

More than thirty years after the discovery that Human Immunodeficiency Virus (HIV) was the causative agent of Acquired Immunodeficiency Syndrome (AIDS), the disease remains pandemic as long as no effective universal vaccine is found. Over 34 million individuals in the world are infected with the virus, and the vast majority of them have no access to the antiretroviral therapies that have largely reduced HIV to a chronic disease in the developed world. The first chapter of this thesis introduces the history of the virus. The key to the infectious mechanism of the virus lies in its envelope glycoprotein (Env), a trimeric spike on the viral surface that utilizes host T cell receptors for entry. Though HIV-1 Env is immunogenic, most infected patients do not mount an effective neutralizing antibody response against it. Broadly-neutralizing anti-Env antibodies (bNAbs) present in the serum of a minority of infected individuals are usually sufficient to prevent the progression to full blown AIDS. Thus, the molecular details of these bNAbs as well as the antibody-antigen interface are of prime interest for structural studies, as insight gained would contribute to the design of a more effective immunogen and potential vaccine candidate. The second chapter of this thesis describes the low-resolution crystal structure of one such antibody, 2G12 dimer, which targets a high mannose epitope on the surface of Env. Patients infected with HIV-2, a related virus with ~35% sequence identity in the Env region, can generally mount a robust antibody response sufficient for viral control for reasons still unknown. The final two chapters of this thesis focus on the first reported structural studies of HIV-2 Env, the molecular details of which may inform HIV-1 therapy and immunogen design.

TABLE OF CONTENTS

Chapter 1: Introduction

Discovery of HIV/AIDS

The first official record of the AIDS epidemic was published in a Morbidity and Mortality Weekly Report (MMWR) by the Centers of Disease Control and Prevention (CDC) on June 5, 1981(Centers for Disease, 1981). The report described the unusual incidence of *Pneumocystis carinii pneumonia* (PCP) and other secondary infections in five previously healthy, young, gay men, two of whom had already died. In the months that followed, numerous national newspapers converged on this story. Reports of similar opportunistic infections in patients with similar profiles began emerging from hospitals across the United States, including many cases of Kaposi's Sarcoma, a rare but aggressive cancer (Altman 1981)(Hymes et al., 1981). By the end of the following year, immunodeficiency was determined to be the direct cause of these mysterious infections, and the term acquired immunodeficiency syndrome (AIDS) was used for the first time to describe the litany of illnesses that plagued a growing population of patients (AIDS.gov).

In 1983, through the efforts of Drs. Luc Montagnier, Francoise Barre-Sinoussi, and Robert Gallo, analysis of viral DNA within human T cells of infected patients revealed that AIDS was caused by a retrovirus – namely, a virus that uses reverse transcriptase to transcribe viral RNA into DNA before integrating into the host genome (Barre-Sinoussi et al., 1983). Human immunodeficiency virus (HIV) was subsequently isolated in the lab and characterized as a member of the genus *lentivirus*, in the family *retroviridae*, meaning that it uses positive sense single-stranded RNA as its genetic material and employs a long latency period as a part of its lifecycle. Over the next ten

years, the first clinical trials of ziduvidine (AZT) and other antiretroviral therapies (ART) targeting reverse transcriptase were conducted in the U.S. with significant but fairly unsatisfying results (Fischl et al., 1987). At the 11th International Conference on AIDS in 1996, a series of new studies presented promising trends from trials of triple-drug cocktails, including potent HIV protease inhibitors (Gulick et al., 1997; Hammer et al., 1997). From that point on, multi-drug therapy using a combination of reverse transcriptase and/or protease inhibitors has been the standard of treatment, resulting in a 60-80% decline in AIDS incidence and death just over the first decade in patients treated with highly-active antiretroviral therapy (HAART) (Michaels et al., 1998).

AIDS has afflicted nearly 75 million people thus far (UNAIDS 2013). As of 2012, around 34 million living people were infected with HIV worldwide, up from about 8 million in 1990 (World Health Organization). Around 70% of this global epidemic is made up of patients in sub-Saharan Africa, whose underdeveloped infrastructure and low income preclude the use of the most effective ART therapies. For the minority of patients who live in in developed countries with access to HAART, HIV infection is now a manageable, chronic infection (Palella et al., 1998). A total of 1.7 million AIDS-related deaths still occur each year, with 1.2 million in sub-Saharan Africa (World Health Organization). There are initiatives underway to improve the sexual education and healthcare infrastructures in those countries, but an inexpensive HIV vaccine would be the true solution for reducing HIV incidence and AIDS deaths.

In 1984, after the isolation of HTLV-III (later known as HIV), the CDC triumphantly predicted that they hoped "to have a vaccine ready for testing in about two years." (Watkins, 2008). Over 30 years later, the goal of an effective HIV vaccine has

still not been realized. In pursuit of this, however, the scientific community has contributed to an enormous body of knowledge surrounding HIV biology, pathogenesis, mode of infection, potential therapies, and patient outcomes. To date, many different types of HIV vaccines have been tested in volunteers. Trials of live attenuated or inactivated HIV vaccines like those used for influenza or poliovirus have been done in non-human primates (Daniel et al., 1992). These have been found to be either unsafe or risky, as many test subjects still progressed to AIDS (Baba et al., 1995).

Much work has been done to develop a vaccine based on the individual protein components of HIV. Especially extensive strides have been made in the study of the HIV envelope spike glycoprotein gp160 (composed of gp120 and gp41), which the virus requires to infect human host cells. Efforts to study the details of these protein subunits and their interactions with components of the human immune system have been greatly aided by the tools of structural biology, including X-ray crystallography and electron microscopy. The first co-crystal structure of HxBc2 gp120 in complex with the CD4 human host receptor and a fragment of 17b, an anti-HIV antibody, was solved in 1998 (Kwong et al., 1998). This set off the determination of a series of crystal structures of various gp120 proteins from different strains of HIV type 1 in the presence of neutralizing antibodies. The collective knowledge amassed from those studies has been contributing toward a more comprehensive and accurate view of the interface at which HIV engages the immune system. The ultimate goal is to rationally design a vaccine, scaffold, or therapeutic using detailed molecular insight into what HIV looks like during an infection. The studies described in this work were conducted with that goal in mind. Presented here are the low-resolution crystal structure of a potent, dimeric form of 2G12,

an antibody against HIV-1 (Chapter 2), as well as the first crystal structure of the envelope glycoprotein from HIV-2 in complex with the CD4 host receptor (Chapter 3). Additionally, I describe preliminary results from efforts to create a soluble, cleaved, native-like HIV-2 envelope glycoprotein trimer (Chapter 4).

Evolutionary history of HIV

HIV exists in two types, 1 and 2, each of which can be classified into many different groups, subtypes, and strains. Both types are thought to have resulted from zoonotic transmission events from Simian Immunodeficiency Virus (SIV), which infects non-human primates. After the first formal documented incidence of HIV-1, the origins were traced back to SIV via a case of HIV-2 infection in 1986 (Clavel et al., 1986a). HIV-2, unknown at the time, was found to be closely related to a simian lentivirus that infected macaques and caused a mild AIDS-like illness, later termed SIV (Chakrabarti et al., 1987; Clavel et al., 1986b). Most SIVs are nonpathogenic, and chronic infection with an SIV is not uncommon in primates, sometimes affecting 50% of an entire species (Sharp and Hahn, 2011). It eventually became clear that HIV-1 and HIV-2 emerged from simian viruses infecting non-human primates in Africa – chimpanzees (cpz) and sooty mangabey monkeys (smm), respectively (Hirsch et al., 1989; Huet et al., 1990). SIV infections have only been found in African primates, so it is thought that primate lentiviruses emerged after the split of Old World Monkeys into Asia and Africa. Non-human primate cross-species transfers of SIV have been known to occur, but it is uncertain what role this may have played in the emergence of HIV (Hahn et al., 2000; Sharp et al., 2000).

A study conducted between 2000-2009 in Gombe National Park, Tanzania revealed that SIV_{cpz} spreads sexually and leads to a 10- to 16- fold increased risk of death in infected chimpanzees (*Pan troglodytes troglodytes*) after an AIDS-like illness featuring progressive CD4+ T cell depletion (Santiago et al., 2002). HIV-1 Group M, the type responsible for the global AIDS epidemic, is most closely related to SIV_{cpz} found in these animals (Lemey et al., 2004). It has been hypothesized that human encounters with apes in the early 1900s via injuries incurred during bush meat hunting were the cause of zoonotic transfers of SIV (Korber et al., 2000; Lemey et al., 2004). HIV-2 was proposed to have descended from SIV_{smm} in sooty mangabeys, which is nonpathogenic but widespread in its natural host organism (Gao et al., 1992). HIV-2 Groups A and B are most commonly found in humans, and generally cause a much milder illness than HIV-1 Group M does (Popper et al., 2000). For unknown reasons, patients infected with HIV-2 often sustain appreciable CD4+ T cell counts and mount a robust immune response with broadly neutralizing antibodies (Berry et al., 2002). The last two chapters of this work represent the first structural studies of the HIV-2 envelope glycoprotein in an effort to investigate the reasons for the differences in pathogenicity between the two types of HIV.

From recent viral archaeology studies, the AIDS pandemic is thought to have originated from HIV-1 group M infections in Kinshasa (formerly Leopoldville), Republic of Congo around the early 1920s (Faria et al., 2014; Sharp and Hahn, 2011). An increasingly trafficked railway network in Kinshasa combined with a robust sex trade facilitated the rapid explosion of HIV to surrounding urban centers in the 1960s. The virus then mutated rapidly via its error-prone reverse transcriptase and short generation times as it spread farther, leading to diversification into geographically distinct subtypes

over a short period of time. Through various genetic bottlenecks, epidemics broke out in different regions of the world: notably subtype C in Africa and subtypes A and B in Europe and the Americas (Faria et al., 2014). Subtype B is thought to have spread to Haiti from Africa in the 1960s, then spread to the United States via a single migration event at the end of the decade (Worobey et al., 2008). These results suggest that HIV was circulating in the United States well before the first officially documented cases. The traits of the virus that enabled its rapid spread throughout the globe are the very ones that help it to successfully evade the human immune system.

The role of *Env* in HIV infection

HIV is an enveloped virus, which means that it utilizes a mainly host-derived membrane enclosing a protein capsid containing genetic material, all of which it synthesizes and assembles using host machinery. The key to infecting host cells lies in the envelope glycoprotein (Env), which is a trimer of heterodimeric proteins embedded in the envelope. The virus uses this protein to recognize and bind to a host cell via host receptors, and it subsequently fuses to the host cell via choreographed steps (Marsh and Helenius, 2006). Enveloped viruses generally enter host cells by directly fusing to the plasma membrane, or via pH dependent endocytosis, leading to fusion within an endosome (Blumenthal et al., 2012). HIV is able to infect cells at neutral pH by directly fusing to the plasma membrane, but there has been some evidence that it can fuse via endosomes as well (Wilen et al., 2012).

The envelope glycoprotein gp160 is expressed in the endoplasmic reticulum and trafficked to the Golgi, where it undergoes post-translational cleavage into the

noncovalently associated gp120 and gp41 subunits by the protease furin (Checkley et al., 2011). These subunits are then incorporated into the plasma membrane as a trimer of heterodimers (gp120-gp41). Gp120 contains five constant domains (C1-C5), which are highly conserved and concealed in a core structure, and five variable loops (V1-V5), which are well exposed on the surface of gp120 and undergo rapid mutation to evade the immune system. Further, gp120 can be roughly divided into inner and outer (with respect to the N- and C-termini) domains, and a set of four β-strands bridging the gap between the two, dubbed the "bridging sheet".

HIV initially approaches the host membrane via electrostatic forces or nonspecific attachment to host membrane elements, allowing the envelope spike to access and bind to the CD4 host receptor on the surface of T cells (Pantophlet and Burton, 2006) using a conserved CD4 binding site (CD4bs, (Kwong et al., 1998)). CD4 is normally responsible for mediating T cell receptor signaling, a critical component of host physiology that the virus exploits for its own infection mechanism. CD4 binding results in a conformational change in gp120, inducing shifts in the variable loops V1/V2 and V3 as well as the bridging sheet and inner domain elements to expose key elements for subsequent coreceptor binding. Binding also induces a hinging of the CD4 domains, which may bring the virus closer to the membrane as well as structural rearrangements in regions of gp41, which prepare the envelope spike for fusion (Blumenthal et al., 2012). HIV strains can be distinguished by their chemokine receptor usage, with the majority binding to the G-protein coupled receptors CCR5 (termed R5 viruses) or CXCR4 (termed X4 viruses) to trigger subsequent fusion. Some laboratory adapted strains of HIV-1 can trigger cell entry with only coreceptor binding in the absence of CD4, suggesting that singular coreceptor

usage may have been an archaic fusion mechanism for HIV (Borsetti et al., 2000). After coreceptor binding, the virus positions itself for viral fusion along the plasma membrane (Marsh and Helenius, 2006). There is also some evidence that HIV gets endocytosed at the plasma membrane and fuses with endosomes in a dynamin-dependent fashion (Miyauchi et al., 2009).

The gp41 fusion peptide is exposed by conformational changes during coreceptor binding, and inserts into the host cell membrane. The gp41 trimer then forms a six-helix bundle (Chan et al., 1997) and brings the viral and host membranes into close proximity to form a stabilized fusion pore (Melikyan, 2008). Gp120 is then likely disengaged from the gp41 stalk to allow for refolding of the fusogenic coiled coil. To complete pore formation, the trimeric gp41 six-helix bundle forms upon refolding and brings its two membrane-anchored regions into range in a hairpin-like fashion (Melikyan, 2008).

Broadly neutralizing antibodies against HIV

Env is the sole known antigenic target of neutralizing antibodies against HIV (Pantophlet and Burton, 2006). Patients infected with HIV-1 produce many antibodies against Env, but few of them are effective enough to neutralize across several strains. As a result, most patients progress to full blown AIDS. In contrast, HIV-2 Env is highly immunogenic and elicits much more effective and broad antibodies in patients (Kong et al., 2012a; Kong et al., 2012b). HIV-2 patients retain high CD4+ T cell counts and exhibit low transmissibility of the virus (see Chapter 3) (Kong et al., 2012a; Kong et al., 2012b).

The causes of an ineffective neutralizing antibody response against HIV-1 are several fold: conformational masking (Kwong et al., 2002) and steric occlusion of

conserved epitopes (Labrijn et al., 2003), glycan shielding and rapid mutation of variable regions to produce variants resistant to therapy (Wei et al., 2003), and sparse distribution of envelope spikes (Klein and Bjorkman, 2010). Vaccines that have been developed against other enveloped viruses such as influenza and poliovirus are sufficient to elicit neutralizing antibodies to control infection (Kwong and Wilson, 2009). While the envelope spike protein of many of these viruses also exhibit traits that make it difficult to make antibodies against HIV, a key difference lies in the sparse distribution of spikes on HIV compared to relatively abundant spikes on the other viruses (Klein and Bjorkman, 2010). Therefore, antibodies against other viruses can exploit avidity effects via inter-spike crosslinking, i.e., bivalent binding to adjacent spikes using both antibody arms. Antibodies against HIV are unable to accomplish this without intervention (Galimidi et al., 2015) due to there being only ~14 spikes on the surface of the virus (Klein and Bjorkman, 2010; Zhu et al., 2003). Despite this, up to 25% of infected individuals, called long-term nonprogressors, are able to make neutralizing antibodies against HIV-1 Env (Doria-Rose et al., 2009; Montefiori et al., 1996) and do not progress to full blown AIDS (Migueles et al., 2000).

The first structure of HIV-1 gp120, from the strain HxBc2, was in complex with an antigen binding fragment (Fab) of the CD4-induced antibody 17b as well as two domains of the CD4 receptor (Kwong et al., 1998). Since then, especially after the development of single-cell antibody cloning (Scheid et al., 2009), more than dozens of antibody Fab structures have been solved in complex with gp120. The molecular details of their epitopes have been systematically elucidated, and these include the CD4-binding site, nonspecific high mannose glycans, the Asn332 N-linked glycosylation site and

associated V3 loop, the Asn160 N-linked glycosylation site and associated V1/V2 loops, and the membrane proximal region (MPER) (West et al., 2014).

In 2013, X-ray crystallographic and cryo-electron microscopy structures of a soluble, cleaved form of the Env trimer were solved at 4.7 Å and 5.8 Å, respectively (Julien et al., 2013; Lyumkis et al., 2013). Key to this remarkable advance was a recombinant gp140 protein from the BG505 strain, dubbed "SOSIP", featuring a trimer-stabilizing mutation within gp41 and covalent linkage of the gp120 and gp41 subunits via a disulfide bond (Sanders et al., 2013). This long-pursued target revealed important quaternary interfaces of the HIV-1 trimer that could not be appreciated via crystal structures of monomeric gp120. Epitope mapping using EM reconstructions of antibody Fabs bound to the trimer have revealed several epitopes that were previously incompletely defined in the context of gp120 monomers (Derking et al., 2015). Chapter 4 of this work describes preliminary data resulting from initial attempts to create a HIV-2 version of the SOSIP trimer.

References

Baba, T.W., Jeong, Y.S., Pennick, D., Bronson, R., Greene, M.F., and Ruprecht, R.M. (1995). Pathogenicity of live, attenuated SIV after mucosal infection of neonatal macaques. Science *267*, 1820-1825.

Barre-Sinoussi, F., Chermann, J.C., Rey, F., Nugeyre, M.T., Chamaret, S., Gruest, J., Dauguet, C., Axler-Blin, C., Vezinet-Brun, F., Rouzioux, C.*, et al.* (1983). Isolation of a T-lymphotropic retrovirus from a patient at risk for acquired immune deficiency syndrome (AIDS). Science *220*, 868-871.

Berry, N., Jaffar, S., Schim van der Loeff, M., Ariyoshi, K., Harding, E., N'Gom, P.T., Dias, F., Wilkins, A., Ricard, D., Aaby, P.*, et al.* (2002). Low level viremia and high CD4% predict normal survival in a cohort of HIV type-2-infected villagers. AIDS research and human retroviruses *18*, 1167-1173.

Blumenthal, R., Durell, S., and Viard, M. (2012). HIV entry and envelope glycoprotein-mediated fusion. The Journal of biological chemistry *287*, 40841-40849.

Borsetti, A., Parolin, C., Ridolfi, B., Sernicola, L., Geraci, A., Ensoli, B., and Titti, F. (2000). CD4-independent infection of two CD4(-)/CCR5(-)/CXCR4(+) pre-T-cell lines by human and simian immunodeficiency viruses. Journal of virology *74*, 6689-6694.

Centers for Disease, C. (1981). Kaposi's sarcoma and Pneumocystis pneumonia among homosexual men--New York City and California. MMWR Morbidity and mortality weekly report *30*, 305-308.

Chakrabarti, L., Guyader, M., Alizon, M., Daniel, M.D., Desrosiers, R.C., Tiollais, P., and Sonigo, P. (1987). Sequence of simian immunodeficiency virus from macaque and its relationship to other human and simian retroviruses. Nature *328*, 543-547.

Chan, D.C., Fass, D., Berger, J.M., and Kim, P.S. (1997). Core structure of gp41 from the HIV envelope glycoprotein. Cell *89*, 263-273.

Checkley, M.A., Luttge, B.G., and Freed, E.O. (2011). HIV-1 envelope glycoprotein biosynthesis, trafficking, and incorporation. Journal of molecular biology *410*, 582-608.

Clavel, F., Brun-Vezinet, F., Guetard, D., Chamaret, S., Laurent, A., Rouzioux, C., Rey, M., Katlama, C., Rey, F., Champelinaud, J.L.*, et al.* (1986a). [LAV type II: a second retrovirus associated with AIDS in West Africa]. Comptes rendus de l'Academie des sciences Serie III, Sciences de la vie *302*, 485-488.

Clavel, F., Guyader, M., Guetard, D., Salle, M., Montagnier, L., and Alizon, M. (1986b). Molecular cloning and polymorphism of the human immune deficiency virus type 2. Nature *324*, 691-695.

Daniel, M.D., Kirchhoff, F., Czajak, S.C., Sehgal, P.K., and Desrosiers, R.C. (1992). Protective effects of a live attenuated SIV vaccine with a deletion in the nef gene. Science *258*, 1938-1941.

Derking, R., Ozorowski, G., Sliepen, K., Yasmeen, A., Cupo, A., Torres, J.L., Julien, J.P., Lee, J.H., van Montfort, T., de Taeye, S.W.*, et al.* (2015). Comprehensive Antigenic Map of a Cleaved Soluble HIV-1 Envelope Trimer. PLoS pathogens *11*, e1004767.

Doria-Rose, N.A., Klein, R.M., Manion, M.M., O'Dell, S., Phogat, A., Chakrabarti, B., Hallahan, C.W., Migueles, S.A., Wrammert, J., Ahmed, R.*, et al.* (2009). Frequency and phenotype of human immunodeficiency virus envelope-specific B cells from patients with broadly cross-neutralizing antibodies. Journal of virology *83*, 188-199.

Faria, N.R., Rambaut, A., Suchard, M.A., Baele, G., Bedford, T., Ward, M.J., Tatem, A.J., Sousa, J.D., Arinaminpathy, N., Pepin, J.*, et al.* (2014). HIV epidemiology. The early spread and epidemic ignition of HIV-1 in human populations. Science *346*, 56-61.

Fischl, M.A., Richman, D.D., Grieco, M.H., Gottlieb, M.S., Volberding, P.A., Laskin, O.L., Leedom, J.M., Groopman, J.E., Mildvan, D., Schooley, R.T.*, et al.* (1987). The efficacy of azidothymidine (AZT) in the treatment of patients with AIDS and AIDS-related complex. A double-blind, placebo-controlled trial. The New England journal of medicine *317*, 185-191.

Galimidi, R.P., Klein, J.S., Politzer, M.S., Bai, S., Seaman, M.S., Nussenzweig, M.C., West, A.P., Jr., and Bjorkman, P.J. (2015). Intra-spike crosslinking overcomes antibody evasion by HIV-1. Cell *160*, 433-446.

Gao, F., Yue, L., White, A.T., Pappas, P.G., Barchue, J., Hanson, A.P., Greene, B.M., Sharp, P.M., Shaw, G.M., and Hahn, B.H. (1992). Human infection by genetically diverse SIVSM-related HIV-2 in west Africa. Nature *358*, 495-499.

Gulick, R.M., Mellors, J.W., Havlir, D., Eron, J.J., Gonzalez, C., McMahon, D., Richman, D.D., Valentine, F.T., Jonas, L., Meibohm, A.*, et al.* (1997). Treatment with indinavir, zidovudine, and lamivudine in adults with human immunodeficiency virus infection and prior antiretroviral therapy. The New England journal of medicine *337*, 734-739.

Hahn, B.H., Shaw, G.M., De Cock, K.M., and Sharp, P.M. (2000). AIDS as a zoonosis: scientific and public health implications. Science *287*, 607-614.

Hammer, S.M., Squires, K.E., Hughes, M.D., Grimes, J.M., Demeter, L.M., Currier, J.S., Eron, J.J., Jr., Feinberg, J.E., Balfour, H.H., Jr., Deyton, L.R.*, et al.* (1997). A controlled trial of two nucleoside analogues plus indinavir in persons with human

immunodeficiency virus infection and CD4 cell counts of 200 per cubic millimeter or less. AIDS Clinical Trials Group 320 Study Team. The New England journal of medicine *337*, 725-733.

Hirsch, V.M., Olmsted, R.A., Murphey-Corb, M., Purcell, R.H., and Johnson, P.R. (1989). An African primate lentivirus (SIVsm) closely related to HIV-2. Nature *339*, 389-392.

Huet, T., Cheynier, R., Meyerhans, A., Roelants, G., and Wain-Hobson, S. (1990). Genetic organization of a chimpanzee lentivirus related to HIV-1. Nature *345*, 356-359.

Hymes, K.B., Cheung, T., Greene, J.B., Prose, N.S., Marcus, A., Ballard, H., William, D.C., and Laubenstein, L.J. (1981). Kaposi's sarcoma in homosexual men-a report of eight cases. Lancet *2*, 598-600.

Julien, J.P., Cupo, A., Sok, D., Stanfield, R.L., Lyumkis, D., Deller, M.C., Klasse, P.J., Burton, D.R., Sanders, R.W., Moore, J.P.*, et al.* (2013). Crystal structure of a soluble cleaved HIV-1 envelope trimer. Science *342*, 1477-1483.

Klein, J.S., and Bjorkman, P.J. (2010). Few and far between: how HIV may be evading antibody avidity. PLoS pathogens *6*, e1000908.

Kong, R., Li, H., Bibollet-Ruche, F., Decker, J.M., Zheng, N.N., Gottlieb, G.S., Kiviat, N.B., Sow, P.S., Georgiev, I., Hahn, B.H.*, et al.* (2012a). Broad and potent neutralizing antibody responses elicited in natural HIV-2 infection. Journal of virology *86*, 947-960.

Kong, R., Li, H., Georgiev, I., Changela, A., Bibollet-Ruche, F., Decker, J.M., Rowland-Jones, S.L., Jaye, A., Guan, Y., Lewis, G.K.*, et al.* (2012b). Epitope mapping of broadly neutralizing HIV-2 human monoclonal antibodies. Journal of virology *86*, 12115-12128.

Korber, B., Muldoon, M., Theiler, J., Gao, F., Gupta, R., Lapedes, A., Hahn, B.H., Wolinsky, S., and Bhattacharya, T. (2000). Timing the ancestor of the HIV-1 pandemic strains. Science *288*, 1789-1796.

Kwong, P.D., Doyle, M.L., Casper, D.J., Cicala, C., Leavitt, S.A., Majeed, S., Steenbeke, T.D., Venturi, M., Chaiken, I., Fung, M.*, et al.* (2002). HIV-1 evades antibody-mediated neutralization through conformational masking of receptor-binding sites. Nature *420*, 678-682.

Kwong, P.D., and Wilson, I.A. (2009). HIV-1 and influenza antibodies: seeing antigens in new ways. Nature immunology *10*, 573-578.

Kwong, P.D., Wyatt, R., Robinson, J., Sweet, R.W., Sodroski, J., and Hendrickson, W.A. (1998). Structure of an HIV gp120 envelope glycoprotein in complex with the CD4 receptor and a neutralizing human antibody. Nature *393*, 648-659.

Labrijn, A.F., Poignard, P., Raja, A., Zwick, M.B., Delgado, K., Franti, M., Binley, J., Vivona, V., Grundner, C., Huang, C.C.*, et al.* (2003). Access of antibody molecules to the conserved coreceptor binding site on glycoprotein gp120 is sterically restricted on primary human immunodeficiency virus type 1. Journal of virology *77*, 10557-10565.

Lemey, P., Pybus, O.G., Rambaut, A., Drummond, A.J., Robertson, D.L., Roques, P., Worobey, M., and Vandamme, A.M. (2004). The molecular population genetics of HIV-1 group O. Genetics *167*, 1059-1068.

Lyumkis, D., Julien, J.P., de Val, N., Cupo, A., Potter, C.S., Klasse, P.J., Burton, D.R., Sanders, R.W., Moore, J.P., Carragher, B.*, et al.* (2013). Cryo-EM structure of a fully glycosylated soluble cleaved HIV-1 envelope trimer. Science *342*, 1484-1490.

Marsh, M., and Helenius, A. (2006). Virus entry: open sesame. Cell *124*, 729-740.

Melikyan, G.B. (2008). Common principles and intermediates of viral protein-mediated fusion: the HIV-1 paradigm. Retrovirology *5*, 111.

Michaels, S.H., Clark, R., and Kissinger, P. (1998). Declining morbidity and mortality among patients with advanced human immunodeficiency virus infection. The New England journal of medicine *339*, 405-406.

Migueles, S.A., Sabbaghian, M.S., Shupert, W.L., Bettinotti, M.P., Marincola, F.M., Martino, L., Hallahan, C.W., Selig, S.M., Schwartz, D., Sullivan, J.*, et al.* (2000). HLA B*5701 is highly associated with restriction of virus replication in a subgroup of HIV-infected long term nonprogressors. Proceedings of the National Academy of Sciences of the United States of America *97*, 2709-2714.

Miyauchi, K., Kim, Y., Latinovic, O., Morozov, V., and Melikyan, G.B. (2009). HIV enters cells via endocytosis and dynamin-dependent fusion with endosomes. Cell *137*, 433-444.

Montefiori, D.C., Pantaleo, G., Fink, L.M., Zhou, J.T., Zhou, J.Y., Bilska, M., Miralles, G.D., and Fauci, A.S. (1996). Neutralizing and infection-enhancing antibody responses to human immunodeficiency virus type 1 in long-term nonprogressors. The Journal of infectious diseases *173*, 60-67.

Palella, F.J., Jr., Delaney, K.M., Moorman, A.C., Loveless, M.O., Fuhrer, J., Satten, G.A., Aschman, D.J., and Holmberg, S.D. (1998). Declining morbidity and mortality among patients with advanced human immunodeficiency virus infection. HIV Outpatient Study Investigators. The New England journal of medicine *338*, 853-860.

Pantophlet, R., and Burton, D.R. (2006). GP120: target for neutralizing HIV-1 antibodies. Annual review of immunology *24*, 739-769.

Popper, S.J., Sarr, A.D., Gueye-Ndiaye, A., Mboup, S., Essex, M.E., and Kanki, P.J. (2000). Low plasma human immunodeficiency virus type 2 viral load is independent of proviral load: low virus production in vivo. Journal of virology *74*, 1554-1557.

Sanders, R.W., Derking, R., Cupo, A., Julien, J.P., Yasmeen, A., de Val, N., Kim, H.J., Blattner, C., de la Pena, A.T., Korzun, J.*, et al.* (2013). A next-generation cleaved, soluble HIV-1 Env Trimer, BG505 SOSIP.664 gp140, expresses multiple epitopes for broadly neutralizing but not non-neutralizing antibodies. PLoS pathogens *9*, e1003618.

Santiago, M.L., Rodenburg, C.M., Kamenya, S., Bibollet-Ruche, F., Gao, F., Bailes, E., Meleth, S., Soong, S.J., Kilby, J.M., Moldoveanu, Z.*, et al.* (2002). SIVcpz in wild chimpanzees. Science *295*, 465.

Scheid, J.F., Mouquet, H., Feldhahn, N., Seaman, M.S., Velinzon, K., Pietzsch, J., Ott, R.G., Anthony, R.M., Zebroski, H., Hurley, A.*, et al.* (2009). Broad diversity of neutralizing antibodies isolated from memory B cells in HIV-infected individuals. Nature *458*, 636-640.

Sharp, P.M., Bailes, E., Gao, F., Beer, B.E., Hirsch, V.M., and Hahn, B.H. (2000). Origins and evolution of AIDS viruses: estimating the time-scale. Biochemical Society transactions *28*, 275-282.

Sharp, P.M., and Hahn, B.H. (2011). Origins of HIV and the AIDS pandemic. Cold Spring Harbor perspectives in medicine *1*, a006841.

Watkins, D.I. (2008). The vaccine search goes on. Scientific American *299*, 69-74, 76.

Wei, X., Decker, J.M., Wang, S., Hui, H., Kappes, J.C., Wu, X., Salazar-Gonzalez, J.F., Salazar, M.G., Kilby, J.M., Saag, M.S.*, et al.* (2003). Antibody neutralization and escape by HIV-1. Nature *422*, 307-312.

West, A.P., Jr., Scharf, L., Scheid, J.F., Klein, F., Bjorkman, P.J., and Nussenzweig, M.C. (2014). Structural insights on the role of antibodies in HIV-1 vaccine and therapy. Cell *156*, 633-648.

Wilen, C.B., Tilton, J.C., and Doms, R.W. (2012). HIV: cell binding and entry. Cold Spring Harbor perspectives in medicine *2*.

Worobey, M., Gemmel, M., Teuwen, D.E., Haselkorn, T., Kunstman, K., Bunce, M., Muyembe, J.J., Kabongo, J.M., Kalengayi, R.M., Van Marck, E.*, et al.* (2008). Direct evidence of extensive diversity of HIV-1 in Kinshasa by 1960. Nature *455*, 661-664.

Zhu, P., Chertova, E., Bess, J., Jr., Lifson, J.D., Arthur, L.O., Liu, J., Taylor, K.A., and Roux, K.H. (2003). Electron tomography analysis of envelope glycoprotein trimers on HIV and simian immunodeficiency virus virions. Proceedings of the National Academy of Sciences of the United States of America *100*, 15812-15817.

Chapter 2*

Structural basis for enhanced neutralization of HIV-1 by a dimeric IgG form of the glycan-recognizing antibody 2G12

*This chapter, first published in *Cell Reports* in 2013, was written by Yunji Wu[1], Anthony P. West, Jr.[1], Helen J. Kim[2], Matthew E. Thornton[1,3], Andrew B. Ward[2], and Pamela J. Bjorkman[1,4]

[1]Division of Biology and Biological Engineering 114-96, California Institute of Technology, 1200 East California Boulevard, Pasadena, CA 91125, USA

[2]Department of Integrative Structural and Computational Biology, The Scripps Research Institute, La Jolla, CA 92037, USA

[3]Present address: University of Southern California Keck School of Medicine, Division of Maternal Fetal Medicine at the Saban Research Institute of Children's Hospital of Los Angeles, Los Angeles, CA 90027, USA

[4]Howard Hughes Medical Institute, California Institute of Technology, 1200 East California Boulevard, Pasadena, CA 91125, USA

ABSTRACT

2G12 is a human IgG that recognizes high-mannose carbohydrates on the HIV-1 envelope protein gp120. Its two antigen-binding fragments (Fabs) are intramolecularly domain exchanged, resulting in a rigid $(Fab)_2$ unit including a third antigen-binding interface not found in antibodies with flexible Fab arms. We determined crystal structures of dimeric 2G12 IgG created by intermolecular domain exchange, which exhibits increased breadth and 50- to 80-fold increased neutralization potency compared with monomeric 2G12. The four Fab and two Fc regions of dimeric 2G12 were localized at low resolution in two independent structures, revealing IgG dimers with two $(Fab)_2$ arms analogous to the Fab arms of conventional monomeric IgGs. Structures revealed three conformationally-distinct 2G12 dimers, demonstrating flexibility of the $(Fab)_2$–Fc connections that was confirmed by single particle electron microscopy, small angle X-ray scattering, and binding studies. We conclude that a combination of intermolecular domain exchange, flexibility, and bivalent binding to allow avidity effects is responsible for the high neutralization potency and increased breadth of dimeric 2G12.

INTRODUCTION

Difficulties in generating broadly neutralizing antibodies against human immunodeficiency virus type 1 (HIV-1) lie in structural features of the gp120-gp41 envelope spike trimer: the spike's variable loops are highly susceptible to rapid mutation (Starcich et al., 1986), its few conserved regions are often sterically occluded via conformational masking (Kwong et al., 2002), and a host-derived glycan shield covers much of the spike surface, making gp120 one of the most heavily glycosylated proteins in nature (Poignard et al., 2001). As such, surface carbohydrates contribute to roughly 50% of gp120's molecular weight (Botos and Wlodawer, 2005). Despite the fact that most antibodies elicited against HIV-1 are strain-specific, there exists a small set of broadly neutralizing antibodies that have demonstrated efficacy across strains (Kwong and Mascola, 2012; Mascola and Haynes, 2013). Isolated from the blood of infected individuals, these antibodies have been found to target conserved epitopes on either the gp120 or gp41 subunits of the envelope spike protein.

Human monoclonal antibody 2G12 recognizes clusters of *N*-linked high-mannose ($Man_{8\text{-}9}GlcNAc_2$) glycans on the surface of gp120 (Calarese et al., 2005; Sanders et al., 2002; Scanlan et al., 2002) and effectively neutralizes many Clade B and some Clade A strains of HIV-1 (Trkola et al., 1996). 2G12's ability to target glycan clusters is facilitated by three-dimensional domain swapping (Liu and Eisenberg, 2002) of its heavy chains to form a rigid $(Fab)_2$ antigen-binding unit (Calarese et al., 2003). By contrast, two independent antigen-binding units are found in conventional IgGs, which contain two heavy chains and two light chains arranged into two fragment antigen-binding (Fab) regions and a single fragment crystalline (Fc) region (Figure 1A). In a typical Fab, the

two domains of the light chain (the variable light (V_L) and constant light (C_L) domains) pair with the variable heavy (V_H) and constant heavy 1 (C_H1) domains, respectively, of a single heavy chain. In the domain-swapped $(Fab)_2$ unit of monomeric 2G12, each light chain is associated with both heavy chains, such that the C_L domain of a light chain contacts C_H1 from one heavy chain, and the V_L domain from that light chain contacts the V_H domain from the second heavy chain (Calarese et al., 2003). The result is a single rigid $(Fab)_2$ unit that contains a third antigen binding site at the V_H/V_H' interface in addition to the two primary antigen binding sites formed by the V_H/V_L interfaces (Figure 1B). The unique V_H/V_H' site allows for increased glycan contacts at the binding surface of 2G12, allowing it to target densely clustered carbohydrates that might be inaccessible to conventional IgG antibodies (Calarese et al., 2003).

During the purification of recombinant 2G12, we previously found that 2G12 formed monomers (two Fabs and one Fc) plus a small fraction of a higher molecular weight species, which was 50- to 80-fold more potent than 2G12 monomer in neutralization of clade A and B HIV-1 (West et al., 2009). This species, identified as 2G12 dimer (four Fabs, two Fcs), was proposed to form through intermolecular domain swapping rather than the intramolecular domain swapping that results in 2G12 monomer (Figure 1C; Figure S1A). Both monomer and dimer were produced during expression in mammalian cells and could be separated by size-exclusion chromatography into purified samples that did not interconvert upon storage or concentration.

Because 2G12 dimer is extremely potent and some 2G12 monomer-resistant HIV strains were neutralized by dimer, increasing the proportion of 2G12 dimer could lead to a more effective reagent for gene therapy or passive immunization. Indeed, introduction

of a higher dimer/monomer ratio 2G12 cell line (West et al., 2009) into HIV-1-infected humanized mice increased protection against infection compared with the wild-type 2G12-expressing cell line, and injection of 2G12 dimer, but not monomer, controlled HIV-1 infection in mouse models (Luo et al., 2010). In addition to its increased capacity for antigen recognition, 2G12 dimer also has the potential for protection via effector functions because it can mediate antibody-dependent cellular cytotoxicity (ADCC) *in vitro* (Klein et al., 2010), indicating that it retains binding to the CD16 Fc receptor on natural killer cells despite its unusual structure.

To investigate the structural and mechanistic basis of the increased potency of 2G12 dimer compared with the monomer, we solved two independent, low-resolution structures of 2G12 dimer by X-ray crystallography. Our efforts were aided by high resolution structures of the 2G12 $(Fab)_2$ (Calarese et al., 2003) and an IgG Fc (Krapp et al., 2003). We performed several structural validations to confirm the 2G12 dimer structures. Collectively the structures revealed three conformationally-distinct forms of the dimer, suggesting that the two $(Fab)_2$ units can adopt different positions relative to the Fcs, analogous to the flexibility of the two Fab arms of a conventional IgG. Consistent with the crystal structures, single particle electron microscopy and small-angle X-ray scattering studies confirmed the flexible nature of 2G12 dimer. Additionally, we showed that 2G12 dimer, but not 2G12 monomer, could bind bivalently to immobilized gp120 in a biosensor assay and confirmed that both Fc regions in the 2G12 dimer were accessible to an Fc receptor using binding and stoichiometry measurements. Our results provide a structural explanation for the superior neutralization potency of 2G12 dimer compared

with monomer (West et al., 2009) and rationalize the dimer's ability to mediate Fc-mediated effector functions (Klein et al., 2010).

RESULTS

Crystallization and structure determination of 2G12 dimer

Structure determinations of intact antibodies are inherently limited by flexibility between domains, and in the case of 2G12, the existence of multiple oligomeric states. Despite these challenges, we were able to readily obtain crystals of intact purified 2G12 dimer. The best crystals (space group $P6_122$) diffracted to only 7.4 Å (Table S1) despite optimizing crystallization conditions and screening >500 crystals. We obtained preliminary phases using molecular replacement with the 2G12 $(Fab)_2$ (pdb entry 1OP3) and IgG Fc (pdb entry 1H3X) structures as search models and verified the solution using heavy atom derivative data (Figure 2; Figure S2, Table S1). Three 2G12 $(Fab)_2$ units were initially located in the crystallographic asymmetric unit (Figure 2A). The Fc regions were found only in molecular replacement searches involving a fixed partial solution including the $(Fab)_2$ units. Crystallographic *R* values after rigid body and B-factor domain refinement decreased from 0.50 to 0.37 after placing the Fc regions. The final model at 8.0 Å resolution (R_{work} = 0.35; R_{free} = 0.37) (Table S1) contained three $(Fab)_2$ units and three Fc regions representing three separate half-dimers (Figure 2A). Applying crystallographic two-fold symmetry operations generated three physiological 2G12 dimers, each with two $(Fab)_2$ units and two Fc regions (Figure 2B). The $(Fab)_2$ units of the 2G12 dimers contacted each other at their antigen binding sites (Figure 2A). They were flanked by pairs of Fc regions that formed a hexamer via a six-fold non-

crystallographic symmetry (NCS) axis coincident with a crystallographic 6_1 screw axis (Figure 2C). The Fc regions forming the hexamers contacted each other at the hinge between the C_H2 and C_H3 domains, the so-called "hot spot" on IgG Fc for interactions with receptors and other proteins (DeLano et al., 2000).

The placement of the $(Fab)_2$ and Fc regions in the $P6_122$ unit cell was dependent upon NCS relating the three half-dimers in the crystallographic asymmetric unit, which we sought to validate to confirm model accuracy. A self-rotation function yielded no peaks for NCS (data not shown). However, NCS axes that are parallel to crystallographic axes of the same or higher symmetry are not detected in self-rotation functions because their peaks coincide with peaks corresponding to crystallographic axes (Rupp, 2010). An NCS axis parallel to a crystallographic can be detected as a peak in a native Patterson map (Rupp, 2010). A native Patterson calculated using the 8 Å $P6_122$ data showed peaks at positions 1/6, 1/3, and 1/2 along the *w* axis (Figure 3A,B). These peaks resulted from the six-fold rotational NCS axis formed by the hexamer of Fc regions along (and parallel to) the crystallographic 6_1 screw axis (Figure 3C). Structure factors calculated from the model of 2G12 half-dimers in the $P6_122$ asymmetric unit reproduced these peaks in a native Patterson calculation (Figure 3A,B), validating the placement of the $(Fab)_2$ and Fc regions in the low-resolution 2G12 dimer structure.

Overall structure of 2G12 dimer

Two of the 2G12 dimers (dimers B and C) in the $P6_122$ crystals were conformationally identical, whereas the third dimer (dimer A) was distinct (Figure 4A,B; Figure S4A,B). The $(Fab)_2$ arms of dimers B and C were related by an angle of ~ 100˚, similar to a typical

angle between a pair of Fab arms in a conventional, non-domain-swapped IgG antibody (Roux, 1999), and the $(Fab)_2$ arms of dimer A were related by ~ 180° (Figure 4A,B). The difference in relative positions of the $(Fab)_2$ arms is consistent with flexibility between the two $(Fab)_2$ portions of the 2G12 dimer structure, in contrast to the inflexibility of the single rigid $(Fab)_2$ of 2G12 monomer. The span between the combining sites of the two $(Fab)_2$ arms of 2G12 dimers, ranging from 105 to 170 Å, was similar to the combining sites of the two Fab arms of a conventional IgG, which are separated by ~ 150 Å (Klein and Bjorkman, 2010). These findings suggest that 2G12 dimer exhibits enhanced neutralization potency due to its ability to bind HIV spikes bivalently with flexible $(Fab)_2$ arms, as compared with 2G12 monomer, which binds monovalently using a single $(Fab)_2$ arm.

Our data also support a novel mechanism for creating IgG dimers via 3-D domain swapping. In this model, each Fc is a hybrid, with each chain derived from a different monomer (Figure S1A). The heavy chain portions of each $(Fab)_2$ unit in the 2G12 dimer each pair with the C_H2-C_H3 region (i.e., the Fc) extending from a neighboring $(Fab)_2$ to form a hybrid Fc. As in other intact IgG structures (Guddat et al., 1993; Harris et al., 1997; Harris et al., 1998; Kratzin et al., 1989; Saphire et al., 2001), the hinge regions of the 2G12 dimers were not resolved in the electron density maps. However, the orientation of the Fc regions in the three 2G12 dimers supported the connectivity model. The model was also consistent with the propensity of 2G12 to form higher order oligomers, including trimers (Figure S1B), which were evident in size-exclusion chromatography profiles of 2G12 (Figure S1C).

Crystallization and structure determination of 2G12 dimer/2G12.1 peptide complex

Packing in the $P6_122$ 2G12 dimer crystals involved contacts between the antigen binding sites of adjacent $(Fab)_2$ units (Figure 2A). We reasoned that disrupting these contacts could allow 2G12 dimer to crystallize in a different packing arrangement that might diffract to higher resolution. To disrupt the contacts, we crystallized 2G12 dimer in the presence of 2G12.1, a 21-residue synthetic inhibitor peptide that binds to the combining site of 2G12 $(Fab)_2$ with an affinity of ~200 μM (Menendez et al., 2008). Clustered hexagonal crystals of 2G12 dimer formed in crystallization trials involving a 19:1 peptide-to-protein molar ratio. By isolating regions of singularity from the clusters, we were able to collect a 6.0 Å data set in space group P6 from a single crystal. We solved the 2G12 dimer/2G12.1 peptide complex structure to 6.5 Å using molecular replacement as described for the 2G12 dimer structure (Table S1). The angle between the $(Fab)_2$ units and Fcs in the 2G12 dimer in this crystal form (Figure 4C) was different from either dimer A or dimer B in the $P6_122$ 2G12 dimer crystals (Figure 4A,B), and thus molecular replacement worked only when we used separate $(Fab)_2$ and Fc search models, resulting in an *R*-value decrease from 0.45 to 0.40 after the Fc region was correctly introduced into the model. Although low resolution precluded visualization of the 2G12.1 peptide in the antigen binding site, introduction of the peptide altered the packing such that there were no crystal contacts involving the $(Fab)_2$ antigen binding site (Figure S3A). However, the Fc regions of 2G12 dimer were arranged as hexamers in the 2G12/2G12.1 crystals (Figure S3B), as also found in the packing of the 2G12 dimer crystals (Figure 2C; Figure 3C).

It was initially difficult to determine the connectivity between the $(Fab)_2$ and Fc regions of the 2G12 dimer in the 2G12/2G12.1 structure because the Fc regions were arranged almost parallel to the $(Fab)_2$ units (Figure 4C). The $(Fab)_2$–Fc connections in the 2G12 dimer/2G12.1 complex structure were interpreted by assigning probable connectivity between the N-termini of the four heavy chains of the two Fc regions and the C-termini of the four heavy chains of the two $(Fab)_2$ units. Taken together, 19 residues within the 2G12 hinge region were missing from the $(Fab)_2$ and Fc structures used as search models for molecular replacement. Distances from the N-termini of the four Fc polypeptide chains to the C-termini of the four $(Fab)_2$ heavy chains were measured using coordinates for high resolution models placed into the 2G12 dimer/2G12.1 structure for residues Pro-238 (N-terminus of Fc) and Lys-228 (C-terminus of the $(Fab)_2$ heavy chain) (residue numbering based on the structures of 2G12 $(Fab)_2$ (pdb ID 1OP3) and Fc (pdb ID 1H3X). Using the shortest combinations of distances as the most plausible choice for connectivity between the chains, we derived the same hybrid Fc model of intermolecular domain exchange as deduced for the formation of the 2G12 IgG dimer (Figure S1A). Assuming this connectivity, the 2G12 dimer in the 2G12/2G12.1 crystal structure adopted a conformation distinct from the two found in the 2G12 dimer alone structure: the Fc regions were oriented at 180° with respect to each other and were essentially parallel to the $(Fab)_2$ units, which were also splayed ~180° apart (Figure 4C), similar to dimer A from the $P6_122$ structure (Figure 4A). Comparison of the three 2G12 dimer conformations obtained from the 2G12 dimer and 2G12 dimer/2G12.1 complex structures demonstrated a large range of conformations accessible to the 2G12 dimer (Figure 4; Figure S4).

Electron microscopy (EM) studies of 2G12 dimer and higher-order oligomers

Negative stain EM and reference-free 2D classification is a powerful method for generating observations of single particles. Here we studied the different fractions eluted from an SEC purification (Figure S1C) that corresponded in apparent molecular weights to 2G12 monomer, dimer, and trimer. Reference-free 2D classes for each of the 2G12 species, including isolated 2G12 $(Fab)_2$, were calculated (Figure 5). In many of the classes for 2G12 dimer and higher-order oligomers, the 2G12 $(Fab)_2$ was discernable and the Fc less clear. The classes corresponding to the dimer and trimer were consistent with an intermolecular domain-swapping model as deduced from the crystal structures. The lack of well-defined class averages for 2G12 IgGs in comparison to a 2G12 $(Fab)_2$ alone (Figure 5A) suggested that 2G12 IgG monomers, dimers, and trimers are flexible structures (Figure 5B-D). In the case of 2G12 monomer, the flexibility presumably resulted solely from the connection between the Fc and the rigid $(Fab)_2$ unit, whereas the 2G12 multimers could adopt different positions of their $(Fab)_2$ units with respect to their Fc regions and each other. Attempts to generate 3-D reconstructions of these particles produced maps that were difficult to interpret, also indicative of conformational heterogeneity. To assess the similarity of the 2G12 IgG dimer models analyzed via crystallography and negative stain EM, the crystal structure of dimer A (Figure 2B; Figure 3A) was filtered to 25 Å and back projected at a 20° Euler angle sampling (Figure 5E). The back projections of 2G12 dimer A showing different orientations of the two $(Fab)_2$ pairs with respect to the Fcs consistently matched the independently generated EM class averages of the 2G12 dimer. Small-angle X-ray scattering (SAXS) data collected

on the 2G12 IgG dimer were also consistent with the dimensions and flexibility observed by EM (Figure 5; Figure S5).

Biosensor assays demonstrate bivalent binding by 2G12 dimer

The crystal structures, single particle EM images, and SAXS analyses of 2G12 dimer suggested that the $(Fab)_2$ units of the IgG dimer are flexible with respect to the Fc region, analogous to the two Fab arms of a conventional IgG antibody. If so, then like a conventional IgG, 2G12 dimer should be capable of bivalent binding to a tethered antigen. By contrast, the intramolecular domain exchange in 2G12 monomer results in a rigid structure that does not have two independently movable Fab arms for bivalent binding (Figure 1B). Rather, the $(Fab)_2$ unit behaves as a single unit using its conventional combining sites at the V_H/V_L interfaces plus the site created by the domain-swapped V_H/V_H' region to bind to clusters of glycans (Calarese et al., 2003) and should therefore exhibit apparently monovalent binding.

To verify these predictions, we compared the binding of 2G12 dimer, 2G12 monomer, and conventional anti-gp120 IgGs to a clade B gp120 using a surface plasmon resonance (SPR) binding assay. 2G12 monomer, 2G12 dimer, or monomeric anti-gp120 IgGs (NIH45-46^{G54W} and 2909) (Diskin et al., 2011; Gorny et al., 2005) were injected over a gp120 protein from the clade B SF162 strain that was immobilized on the surface of a biosensor chip. The gp120 protein was coupled at high and medium coupling densities to permit bivalent binding and at a low density to reveal the potential loss of bivalent binding when the $(Fab)_2$ arms of 2G12 dimer or the Fab arms of the conventional anti-HIV-1 IgGs could not cross-link between two gp120 molecules. To distinguish

between monovalent and bivalent binding, we fit the sensorgram data to a 1:1 binding model and assessed the residuals for the goodness of fit (Figure 6; Figure S6). We found that 2G12 monomer exhibited apparently monovalent binding to gp120 at all coupling densities (Figure 6A-C). As predicted, 2G12 dimer exhibited apparently bivalent binding to gp120 at high and medium coupling densities (Figure 6A,B), but monovalent binding at low coupling density (Figure 6C). Conventional anti-gp120 IgGs bound with apparent bivalency at high coupling density but monovalently at medium and low densities, suggesting a smaller reach between combining sites than 2G12 dimer (Figure 6A-C).

The Fc regions of 2G12 dimer are accessible to Fc receptor binding

The 2G12 dimer structures suggested that the dimer's Fc regions would be accessible to Fc receptor binding, consistent with a study demonstrating that 2G12 dimer triggered ADCC (Klein et al., 2010). This effector function is mediated by CD16, an Fc receptor that interacts with the hinge-proximal region of the Fc C_H2 domain (Sondermann et al., 2000). The C_H2-C_H3 domain interface, the binding site for the neonatal Fc receptor (FcRn) (Burmeister et al., 1994) and the site of contacts that form the NCS 6-fold axis (Figure 2C; Figure 3C; Figure S3B), was also predicted to be accessible for binding. Two FcRn proteins bind to the Fc region of a conventional IgG monomer, one per polypeptide chain in the Fc (Huber et al., 1993; Sanchez et al., 1999). Since 2G12 dimer contains two Fc regions with four potential FcRn binding sites, up to four FcRn proteins could bind per 2G12 dimer.

To characterize the binding interaction between FcRn and 2G12 dimer, we used equilibrium gel filtration, a technique that can be used to determine the stoichiometry of a

complex that might dissociate during conventional gel filtration chromatography (Hummel and Dreyer, 1962). This method was previously used to demonstrate that two FcRn molecules bind per IgG monomer (Sanchez et al., 1999; West and Bjorkman, 2000). For the 2G12 experiments, a gel filtration column was equilibrated with a buffer containing 5 μM FcRn, a concentration ~10-fold higher than the K_D of the interaction between FcRn and IgG in solution (Huber et al., 1993). We then injected various ratios of FcRn to 2G12 monomer or dimer.

Figure 7 shows gel filtration profiles for 2G12 monomer and 2G12 dimer interacting with FcRn. In both chromatograms, the first peak corresponded to the 2G12 complex with FcRn, which migrated at an apparently higher molecular mass for the dimer complex than for the monomer complex. Both chromatograms also showed a peak or a trough at the position where unbound FcRn migrated: a peak in the case of the 3:1 ratio of FcRn per Fc region in 2G12 monomer and the 6:2 ratio of FcRn per Fc region in 2G12 dimer (indicating excess FcRn) and troughs in the cases of lower ratios of FcRn per Fc. Since excess FcRn was present when a 3:1 (or 6:2) ratio of FcRn per Fc was injected, the stoichiometry for both complexes is two FcRn proteins bound per Fc region. Thus two FcRn molecules were bound per 2G12 monomer, which contains one Fc region, and four FcRn molecules were bound per 2G12 dimer, which contains two Fc regions.

DISCUSSION

Among known broadly neutralizing anti-HIV-1 antibodies, 2G12 is unusual in two respects: first, it recognizes a carbohydrate epitope on gp120 (Botos and Wlodawer, 2005), and second, its Fab arms are domain swapped to form a rigid single $(Fab)_2$ unit (Calarese et al., 2003). The $(Fab)_2$ unit in monomeric 2G12 is formed by intramolecular domain swapping involving the two IgG heavy chains. We hypothesized that intermolecular domain swapping could create a dimeric species of 2G12 IgG that was observed by size-exclusion chromatography (West et al., 2009). 2G12 dimers can be isolated as a stable species that contains two Fc regions and four Fabs arranged into two $(Fab)_2$ units. Compared with 2G12 monomer, purified 2G12 dimer is 50- to 80-fold more potent in *in vitro* neutralization assays (West et al., 2009), more effective in protection from HIV infection in *in vivo* experiments (Luo et al., 2010), and mediates ADCC at lower concentrations (Klein et al., 2010). The present structural studies were initiated to investigate the structural mechanism for the increased activity of 2G12 dimer versus monomer.

Although crystal structures of intact IgGs are rare, with few examples in the literature (Guddat et al., 1993; Harris et al., 1997; Harris et al., 1998; Kratzin et al., 1989; Saphire et al., 2001), intact 2G12 IgG dimer formed crystals, both alone and complexed with the 2G12.1 inhibitor peptide. Both crystal forms diffracted weakly to low resolution, but we were able to solve crystal structures by molecular replacement for 2G12 dimer and the 2G12 dimer/2G12.1 complex at resolutions between 6.5 and 8 Å. The molecular replacement solutions were verified by heavy atom methods and native Patterson calculations. The model for connectivity to produce an intermolecular domain-swapped

IgG dimer was consistent with the orientation of the Fc domains in both the 2G12 and 2G12/2G12.1 structures.

The low resolution structures revealed three distinct conformations of 2G12 dimer. In each conformation, the two $(Fab)_2$ units in the dimer were arranged as arms at an obtuse angle, analogous to the Fab arms of a conventional IgG monomer that can bind bivalently to tethered antigens. The two Fc regions were separated from each other, suggesting they would not block each other's interactions with Fc receptors. Indeed, 2G12 dimer interacted with FcRn with proportional stoichiometry as 2G12 monomer in equilibrium gel filtration studies, corroborating the idea that Fc regions in 2G12 dimer are as accessible for effector functions as the Fc regions in conventional IgGs. 2D class averages from negative stain electron microscopy provided unbiased, reference-free profiles that visually confirmed the flexibility and orientations of the 2G12 dimers observed in crystal structures. The presence of three distinct conformations of 2G12 dimer indicated that different conformational intermediates were trapped in the two crystal forms. Consistent with this suggestion, 2G12 dimer could bind bivalently to immobilized gp120, allowing avidity effects to increase the apparent affinity of 2G12 dimer for its carbohydrate epitope. By contrast, the single rigid $(Fab)_2$ unit of monomeric 2G12 bound monovalently to immobilized gp120, regardless of the density of the gp120 on the surface.

These results are relevant to a hypothesis that a general inability of many anti-HIV-1 antibodies to bind with avidity is one reason that the antibody response against HIV is generally ineffective (Klein and Bjorkman, 2010). Briefly, we proposed that most anti-Env antibodies do not bind bivalently to HIV spike trimers because (*i*) the small

number and low density of HIV spike trimers does not normally permit inter-spike crosslinking, and (*ii*) the distance between the same epitope on individual monomers within a spike trimer usually exceeds the armspan of a conventional IgG, thereby preventing most instances of intra-spike crosslinking. To assess potential bivalent binding by anti-viral IgGs, we defined the molar neutralization ratio (MNR) as the concentration at which an Fab achieves 50% inhibition of viral infectivity (IC_{50}) divided by the IC_{50} for the parental IgG in an in vitro neutralization assay (Klein and Bjorkman, 2010). An antibody that is unable to bind with avidity would exhibit an MNR of 2, because the IgG has twice the amount of antigen-binding capacity as the Fab. MNRs greater than 2 suggest avidity effects resulting from the IgG cross-linking epitopes on the virus. Results from published studies showed high MNRs for antibodies against respiratory syncytial virus and influenza (Edwards and Dimmock, 2001; Schofield et al., 1997; Wu et al., 2005), suggesting that antibodies can take advantage of avidity effects to bind to enveloped viruses other than HIV-1. However, a compilation of the highest reported MNRs for antibodies against HIV showed that neutralizing antibodies yielded relatively low MNRs (Klein and Bjorkman, 2010).

Although the $(Fab)_2$ unit of monomeric 2G12 interacts with at least three high-mannose glycans, the binding surface is a single unit, and thus the 2G12 monomer does not have the capacity to bind antigen with avidity as it is conventionally defined. However, 2G12 dimer can be up to 2500-fold more potent in neutralization than monomeric 2G12 on a molar basis (West et al., 2009); thus, the high MNRs for 2G12 dimer compared to its monomeric form are similar to the large effects seen for conventional IgGs against non-HIV viruses (Klein and Bjorkman, 2010). The discovery

that 2G12 dimer is a flexible molecule that behaves like an oversized version of a conventional IgG antibody now allows us to postulate that avidity effects, rather than simply doubling the surface area of a single combining site, account for the mechanism by which 2G12 dimer achieves its greater potency compared with 2G12 monomer.

The 2G12 dimer structure, taken together with what is known about the 2G12 epitope, permits speculation as to its mode of binding with avidity to HIV spike trimers. 2G12 has been reported to bind to a specific high-mannose patch on gp120 that has been called "intrinsic" due to its conserved and unusual avoidance of a-mannosidase processing while being trafficked through the ER and Golgi (Bonomelli et al., 2011). We propose that one of the $(Fab)_2$ units of 2G12 dimer first tethers with high affinity to the intrinsic mannose patch before sampling the abundant high-mannose landscape in the surrounding glycan shield for a second binding opportunity. Because the intrinsic mannose patch on an adjacent gp120 monomer within a spike trimer would be too far away to be reached by the second $(Fab)_2$ unit of 2G12 dimer, we believe that the second 2G12 "epitope" would be a suboptimal glycan cluster distinct from the intrinsic mannose patch. The finding that 2G12 dimer binds monovalently to immobilized gp120 coupled at low density suggests that two $(Fab)_2$ units cannot bind simultaneously to a single gp120, and thus the suboptimal second epitope would likely be on an adjacent gp120 within a spike trimer.

Our studies provide important information for therapeutic anti-HIV efforts in that they provide a direct demonstration of the importance of avidity in HIV-1 neutralization. Here we show, for the first time, a comparison of the structures of a monomeric and dimeric form of a carbohydrate-only anti-HIV-1 antibody. Unlike anti-HIV-1 antibodies

against protein-only epitopes, the dimeric form of 2G12 can take advantage of avidity to increase its neutralization potency and breadth, and is thus a promising candidate for therapeutic efforts to combat HIV-1. Despite initially discouraging results with less potent antibodies (Poignard et al., 1999), passive delivery of antibodies has been gaining new attention (reviewed in (Klein et al., 2013), with encouraging results from a cocktail of five or three highly effective broadly neutralizing antibodies in humanized mice infected with HIV-1 (Diskin et al., 2013; Klein et al., 2012). 2G12 dimer would be very effectively employed in such a cocktail, as it shares its primary epitope with no other known antibody and it can potentially exploit surrounding glycans as a secondary epitope. Of direct relevance to potential therapeutic use of antibodies for passive immunotherapy, bivalent binding can serve as a buffer against Env mutations (Klein and Bjorkman, 2010); thus, 2G12 dimer is a good candidate for therapeutic efforts against clade A and clade B HIV strains.

EXPERIMENTAL PROCEDURES

Protein expression and purification

2G12 IgG was expressed in transiently transfected HEK293-6E suspension cells as described (West et al., 2009). A mixture of 2G12 monomer and dimer was isolated from harvested supernatants by FcRn affinity chromatography (Huber et al., 1993) using 5 mL of HiTrap NHS-activated resin (GE Healthcare) coupled to 12 mg of rat FcRn. Supernatants were loaded on the FcRn column in 250 mM MES, 150 mM NaCl, 0.02% Sodium azide pH 5.7, and eluted in 250 mM HEPES, 150 mM NaCl, 0.02% NaN_3 pH 8. The eluent was subjected to size-exclusion chromatography in 20 mM Tris pH 8.0, 150 mM NaCl using a Superdex 200 16/60 gel filtration column (GE Healthcare). Fractions corresponding to 2G12 dimer or monomer were pooled and subjected to SEC an additional two times to ensure complete separation of 2G12 species.

Purified monomeric HIV-1 gp120 was a gift from Leo Stamatatos and Zachary Caldwell (Seattle BioMed) (Sharma et al., 2006). Purified 2G12 $(Fab)_2$ was a gift from Zara Fulton and was imaged by Reza Khayat (The Scripps Research Institute). Other reagents, such as control monomeric IgGs and purified soluble rat FcRn (which binds human IgG equally as well as rat IgG (Huber, 1994)) were provided by members of the Bjorkman laboratory, including Paola Marcovecchio, Han Gao, Maria Politzer, and Kathryn Huey Tubman. Protein concentrations were determined spectrophotometrically using extinction coefficients at 280 nm of 200480 M^{-1} cm^{-1} (2G12 monomer), 400960 M^{-1} cm^{-1} (2G12 dimer), 202000 M^{-1} cm^{-1} (conventional monomeric IgG antibodies), 84900

M^{-1} cm^{-1} (rat FcRn), and 146090 M^{-1} cm^{-1} (SF162 gp120). Extinction coefficients were calculated based on amino acid compositions using ProtParam (Artimo et al., 2012).

Crystallization and data collection

Crystals of 2G12 dimer (space group $P6_122$) were grown in hanging drops by mixing equal volumes of 2G12 dimer (11.5 mg/ml) with a solution containing 1.2 M ammonium sulfate, and 100mM HEPES pH 7.0 at 20º C. Crystals were cryopreserved in well solution containing 25-30% glycerol. Data were collected to 7.5 Å resolution at beamline 8.3.1 of the Advanced Light Source (ALS) at Lawrence Berkeley National Laboratory (LBNL), and at beamline 12-2 of the Stanford Synchrotron Radiation Lightsource (SSRL) at the SLAC National Accelerator Laboratory. Over 500 crystals were screened, but all diffracted poorly and were fragile to handle. Experiments to improve the quality of the crystals included seeding, glutaraldehyde crosslinking, recrystallization, additives, exchanging into lithium sulfate, exploring cryoprotectants, and varying drop composition. Tantalum bromide clusters (Jena Biosciences) were soaked into the native crystals, resulting in bright green crystals. SAD data with reflections to 10 Å were collected at beamline 8.3.1 of the ALS at LBNL at a single wavelength of 1.255 Å.

For crystallization of the 2G12 dimer/2G12.1 complex, 2G12.1 peptide (The Polypeptide Group) was mixed with 2G12 dimer (11.5 mg/ml) at a 19:1 molar ratio in 24-well hanging drops of protein and reservoir solution in equal amounts. Clustered hexagonal crystals formed from spherolites by vapor diffusion in 5% Tascimate, 10% PEGMME 5000, and 100 mM HEPES at pH 7.0. Crystals were cryopreserved in the well solution containing 30% PEGMME 5000 and screened at Beamline BL12-2 at the

Stanford Synchrotron Radiation Light Source (SSRL) at SLAC, and the 5 μm microbeam at beamline 23ID-D at the General Medical Sciences and Cancer Institutes Structural Biology Facility (GM/CAT) at the Advanced Photon Source (APS). Upon handling, the clustered crystals sometimes disintegrated into smaller, more singular pieces, which were also cryoprotected and screened. We also collected usable data sets from large crystals (0.3 mm diameter) that contained singular patches.

Data processing and structure determination

Data were processed using XDS (Kabsch, 2010) or HKL2000 (Otwinowski and Minor, 1997) and were indexed, integrated, and scaled using POINTLESS and SCALA. We used a combination of CC1/2 in the range of 90% (Karplus and Diederichs, 2012) and I/s > 1.5 in the highest resolution shell to determine the resolution cutoffs for our data sets. Data for 2G12 dimer were corrected for anisotropy using the UCLA-MBI Anisotropy Server (Strong et al., 2006). Molecular replacement was carried out using Phaser-MR (McCoy et al., 2007; Winn et al., 2011) and Molrep (Lebedev et al., 2008; Vagin and Teplyakov, 2010; Winn et al., 2011). All molecular replacement solutions in space group $P6_122$ yielded higher translation function Z-scores (10 and above for initial placement of three $(Fab)_2$ units) as well as lower initial *R* factors (0.54 versus over 0.60) than solutions in the enantiomeric space group $P6_522$. Model validation calculations using derivative crystals were performed using software in the CCP4 Software Suite (Winn et al., 2011) via the ccp4i graphical user interface (Potterton et al., 2003): cad (Winn et al., 2011), scaleit (Winn et al., 2011), fft (Read, 1988), followed by Phenix.autosol (Adams et al., 2010), and Phenix.emma (Adams et al., 2010). Native Patterson calculations were done using

POLARRFN (Winn et al., 2011) in the the UCLA-MBI Self Rotation Function Server, sfall (Winn et al., 2011) and Patterson (Winn et al., 2011). Rigid body refinement and domain B-factor refinement were carried out using CNS (Brunger, 2007; Brunger et al., 1998) or Phenix.refine (Adams et al., 2010). Model and electron density visualization were done using COOT (Emsley et al., 2010) and PyMol (Schroedinger, LLC). Map truncation was done using Phenix.map_box (Adams et al., 2010). Structure figures were prepared using PyMol. Globular structures in Figures 3, 4, and S4 were prepared by conversion of coordinate files into 25 Å mrc map volumes using pdb2mrc in the EMAN2.0 suite (Tang et al., 2007), which were then rendered in UCSF Chimera (Pettersen et al., 2004).

Electron Microscopy (EM)

2G12 species purified via SEC were analyzed by negative stain EM. A 3 µL aliquot of 1–2.5 µg/ml of 2G12 $(Fab)_2$ or 2G12 monomer, dimer, or trimer was applied to a freshly glow discharged carbon coated 400 Cu mesh grid and stained with 2% uranyl formate for 20 s. Grids were imaged using a FEI Tecnai T12 electron microscope operating at 120 kV at 52,000 x magnification and electron dose of 25 $e^-/Å^2$, which resulted in a pixel size of 2.05 Å at the specimen plane. Images were acquired with a Tietz 4k x 4k CCD camera using LEGINON (Suloway et al., 2005) at a defocus range of 700 to 1000 nm.

Particles were picked automatically using DoG Picker and put into a particle stack using the Appion software package (Lander et al., 2009; Voss et al., 2009). Initial reference-free 2D class averages were calculated using unbinned particles via the Xmipp

Clustering 2D Alignment and sorted into classes (Sorzano et al., 2010). Particles corresponding to only 2G12 species were selected into a substack and another round of reference-free alignment was carried out using Xmipp Clustering 2D alignment and IMAGIC softwares to generate 64 classes (van Heel et al., 1996). A total of 6583, 10341, and 4230 particles went into the final 2D classes of the monomer, dimer, and trimer, respectively. Back projections of 2G12 IgG dimer A were calculated using EMAN software (Tang et al., 2007) as follows: the X-ray coordinates were converted from PDB to MRC format using pdb2mrc, low pass filtered to 25 Å resolution to generate a density map, and the map was projected at 20° Euler angle increments using project3d and displayed in e2display.

Small angle X-ray scattering (SAXS)

Samples for SAXS were concentrated to 17 mg/ml (2G12 monomer), 13 mg/ml (2G12 dimer), and 21 mg/ml (Rituximab) and filtered through 0.22 μm membranes. Dialysis to buffer exchange each protein into Phosphate Buffered Saline was performed overnight, and samples were diluted for a concentration series of 0.25 mg/ml, 0.5 mg/ml, 0.75 mg/ml, 1.0 mg/ml, 2.5 mg/ml, 5.0 mg/ml, and 7.5 mg/ml, along with 1-3% glycerol to minimize aggregation caused by radiation damage. Data were collected at SSRL beam line 4-2 using a Rayonix MX225-HE detector at a distance of 2500 mm, using 1.13 Å wavelength X-rays. For each concentration of each sample, 15 exposures of 1 second were collected, covering a momentum transfer (q) range of 0.0047–0.375 1/Å. The scattering profile for the buffer was obtained in the same manner and subtracted from the protein profiles. The detector images were integrated, background subtracted, and

screened for radiation damage using SasTool (Smolsky, 2007). Extrapolation to infinite dilution was done with PRIMUS (Konarev, 2003). Guinier analysis was performed using AutoRG, distance distribution functions were determined with GNOM (Svergun, 1992), and ab initio reconstructions were performed using DAMMIF (Franke, 2009) and DAMAVER (Volkov, 2003) in the ATSAS package (Petoukhov et al., 2012).

Biosensor studies of 2G12 interactions with gp120

A Biacore T200 biosensor system (GE Healthcare) was used to evaluate the interactions of 2G12 monomer, 2G12 dimer, and control anti-gp120 antibodies NIH45-46^{G54W} (Diskin et al., 2011) and 2909 (Gorny et al., 2005) with recombinant gp120 from the strain SF162 (gift of Leo Stamatatos, Seattle Biomed). Response units (RUs) of gp120 ranging from fewer than 10 to approximately 100 were covalently immobilized on flow cells of CM5 biosensor chips using standard primary amine coupling chemistry (Biacore T200 manual, GE Healthcare). A concentration series of either 2G12 monomer, dimer, or control anti-gp120 IgG was injected at 25 °C in 10 mM HEPES with 150 mM NaCl, 3 mM EDTA and 0.005% (v/v) surfactant P20 at pH 7.4. Sensor chips were regenerated using 10 nM glycine, pH 2.5. After subtracting the signal from the reference flow cell, we globally fit the kinetic data from each experiment to a 1:1 binding model (Biacore evaluation software). When an obvious refractive index change occurred when switching from the association to the dissociation buffer, the sensorgrams were also fit with a refractive index correction (third row, middle panel of Figures 6 and S6). We evaluated the fit to the 1:1 binding model of each binding interaction by calculating and plotting residuals between the experimental and modeled curves.

Equilibrium gel filtration

Equilibrium gel filtration chromatography (Hummel and Dreyer, 1962) was performed to determine the stoichiometry of the association of 2G12 monomer and 2G12 dimer with FcRn. Briefly, chromatography was performed at a flow rate of 100 μL/min using a SMART micropurification system (Pharmacia) monitoring the absorbance at 280 nm. The experiment was run on a Superdex 200 PC 3.2/30 gel filtration column, which was equilibrated with and run in equilibrium buffer (10 mM PIPES, 0.05% Sodium azide, pH 6.1) containing 5 μM soluble FcRn. All IgG samples and various concentrations of FcRn were buffer exchanged into the PIPES buffer via dialysis prior to injection over the column. 2.5 μM of 2G12 monomer was mixed with equilibration buffer containing 5 μM FcRn plus no additional FcRn, 2.5 uM additional FcRn, 5 μM additional FcRn, or 7.5 μM additional FcRn. 1.25 μM of 2G12 dimer was mixed with equilibration buffer containing 5 μM FcRn plus no additional FcRn, 2.5 uM additional FcRn, 5 μM additional FcRn, or 7.5 μM additional FcRn.

ACKNOWLEDGMENTS

We thank Jost Vielmetter and the Caltech Protein Expression Center for assistance with Biacore studies and protein expression, Jens Kaiser, Pavle Nikolovski, the Caltech Molecular Observatory, the 2012 APS Data Collection Workshop, and the CCP4 School at Argonne National Laboratory for help with crystallographic studies, the staff at SSRL Beamlines 4-2 and 12-2 for assistance with SAXS studies, the staff at Beamlines 12-2 (SSRL) and APS GM/CAT Beamlines 231D-B and 231D-D for assistance with SAXS

and crystallographic data collection, Justin Chartron for help with SAXS and crystallographic data analysis, the developers of PHENIX, CCP4, and XDS software for assistance and advice concerning X-ray crystallography, Leo Stamatatos, Zara Fulton, Reza Khayat, and members of the Bjorkman laboratory for protein reagents, William Lange, Marta Murphy, and Maria Politzer for help making figures and models, and Andrew Davenport and Beth Stadtmueller for critical reading of the manuscript. This work was supported by the National Institutes of Health (2 R37 AI041239-06A1 to P.J.B.) and startup funds from the Scripps Research Institute (A.B.W.).

Accession Numbers

Coordinates and X-ray crystallographic data for 2G12 IgG dimer and 2G12 IgG dimer/2G12.1 peptide will be deposited in the Protein Data Bank.

FIGURE LEGENDS

Figure 1. Schematic IgG structures

Heavy chains (identical polypeptide chains, but colored differently for illustrating domain swapping) are cyan and yellow, light chains are gray, and antigen binding sites are shown as starbursts. (A) Conventional IgG with flexible Fab arms and two antigen binding sites at the V_H/V_L interfaces. (B) 2G12 monomer with domain-swapped $(Fab)_2$ unit and an additional antigen binding site at the V_H/V_H' interface. (C) 2G12 dimer with two domain-swapped $(Fab)_2$ units and six antigen binding sites. See also Figure S1.

Figure 2. Packing in 2G12 dimer crystals

(A) Asymmetric unit of a solvent flattened 8.0 Å resolution $2F_o$-F_o electron density map contoured at 1.5 σ. The asymmetric unit contained three half-dimers, i.e., three Fc regions and three $(Fab)_2$ units from three distinct 2G12 dimers (A, B, and C). Crystal contacts involved the antigen binding sites in the $(Fab)_2$ units (green circles); see also Figure S2. (B) Application of symmetry operators to generate the second half of each 2G12 dimer. Dimer A (cyan) was structurally distinct from Dimers B (magenta) and C (indigo), which exhibited the same conformation. (C) Non-crystallographic six-fold symmetry axis showing a hexamer of Fc regions coincident with the 6_1 screw axis along the crystallographic *c* axis. The asymmetric unit is highlighted in yellow. (D) The three dimers in one layer of the crystal, represented by the cyan, magenta, and indigo dimers A, B, and C (panel B), as they fit into the Fc hexamer ring in panel C; see also Figure S2.

Figure 3. Native Patterson validation of packing in 2G12 dimer crystals

(A,B) Native Patterson maps. Comparison of experimental and calculated Harker sections. (C) Two layers of 2G12 dimer molecules as they are packed into the $P6_122$ crystals. Left: top-down view showing the cyan (dimer A), magenta (dimer B), and indigo (dimer C) 2G12 dimers (Figure 2) in the same layer. The magenta and indigo dimers are conformationally identical and the cyan dimer is distinct. The layer below contains three additional dimers (light green, light pink, and light blue), formed via a rotation and translation along the crystallographic 6_1 axis. Symmetry mates are indicated as a darker and lighter version of the same color. Right: a 90º rotation showing hexamer of Fc regions in the middle layer. See also Figure S3.

Figure 4. Structures of the three distinct 2G12 dimers from two independent crystal structures

Dimer structures are shown as 25 Å electron density envelopes calculated from $(Fab)_2$ and Fc coordinates located by molecular replacement. The approximate distance between the tips of the $(Fab)_2$ units of each dimer is shown on the left. The symmetry of two of the 2G12 dimer conformations, dimer A and the dimer in the 2G12/2G12.1 peptide structure (panels A and C), was point group C2 (the dimer two-fold symmetry axis was coincident with a crystallographic two-fold axis). The dimer B/C conformation (panel B) represented a distortion from C2 symmetry. A 2G12 dimer could also have point group D2 symmetry with the $(Fab)_2$ units in a similar position as in a C2 dimer except with their internal two-fold axes coincident, and with the Fcs above and below the plane of the $(Fab)_2$ units with the Fc two-fold axes coincident with each other and perpendicular to the

$(Fab)_2$ two-fold axes. Although the D2 conformation appeared plausible, it was not observed in our structures. To interconvert these forms would require one $(Fab)_2$ unit to rotate 180˚. (A) Dimer A, one of two conformationally-distinct 2G12 dimers in the $P6_122$ 2G12 dimer structure. Middle and Right: Heavy chains are cyan and yellow, light chains are transparent gray. Middle: Top-down view of the 2G12 dimer with Fc regions pointing into the page. Right: Two rotated views showing the large distance between $(Fab)_2$ units and Fc regions and an angle of 180º between $(Fab)_2$ arms. (B) Dimers B and C, the second of the two distinct 2G12 dimers in the $P6_122$ 2G12 dimer structure. Middle and Right: Heavy chains are magenta, indigo, light pink, or light blue; light chains are transparent gray. Middle: Top-down view of the 2G12 dimer molecule with Fc regions pointing into the page. Right: Two rotated views showing an obtuse angle between $(Fab)_2$ units. (C) 2G12 dimer in crystals of 2G12 bound to the 2G12.1 peptide. Middle and Right: Heavy chains are orange, green, light orange, or light green; light chains are light gray. Middle: Top-down view. The two $(Fab)_2$ units are extended at 180° with respect to each other, as are the two Fc regions (not seen in this view). Right: Two rotated views showing the Fc regions under the $(Fab)_2$ units. See also Figure S4.

Figure 5. Negative stain EM of 2G12 oligomers

Representative two-dimensional class averages (left) and false-colored images (right) of 2G12 $(Fab)_2$, 2G12 monomer, 2G12 dimer, and 2G12 trimer showing the orientations of the domain-exchanged $(Fab)_2$ units and the Fc regions. Fabs are colored in cyan and Fcs in yellow. Bar = 10 nm. (B-D) 2D class averages of 2G12 oligomers analyzed by negative stain EM. Bar = 10 nm. Panels of 64 class averages of the (B) 2G12 monomer,

(C) 2G12 dimer, and (D) 2G12 trimer generated using reference-free Xmipp Clustering 2D alignment. (E) Back projections sampled at 20˚ Euler angles of the low-pass filtered 2G12 Dimer A crystal structure. Bar = 10 nm. Many of the back projections resembled the reference-free class averages of the 2G12 IgG dimer in panel C. See also Figure S5 for SAXS data supporting the EM and crystallographic results.

Figure 6. Surface plasmon resonance-based binding studies

Sensorgrams were derived from binding experiments in which 2G12 monomer, 2G12 dimer or a conventional monomeric anti-gp120 IgG was injected over immobilized gp120 from HIV-1 strain SF162. Experimental data (colored lines) were fit to a 1:1 binding model (black lines). Residual plots are shown in Figure S6. (A) 2G12 monomer, 2G12 dimer, and a conventional anti-gp120 IgG (NIH45-46^{G54W}) injected over gp120 immobilized at high coupling density (~100 RU). 2G12 monomer, but not 2G12 dimer or the conventional IgG, could be fit to a 1:1 binding model. (B) 2G12 monomer, 2G12 dimer, and a conventional anti-gp120 IgG (NIH45-46^{G54W}) injected over gp120 immobilized at medium coupling density (~50 RU). 2G12 monomer, but not 2G12 dimer or the conventional IgG, could be fit to a 1:1 binding model. (C) 2G12 monomer, 2G12 dimer, and a conventional anti-gp120 IgG (2909) injected over gp120 immobilized at low coupling density (<10 RU). All could be fit to a 1:1 binding model.

Figure 7. Equilibrium gel filtration analyses of FcRn-2G12 complexes

(A) FcRn was incubated with 2.5 μM 2G12 monomer in the presence of 0, 1, 2, or 3 (additional) equivalents of FcRn in a buffer containing 5 μM FcRn (equilibration buffer).

Samples were then injected onto a column equilibrated in the equilibration buffer. The peak that eluted first corresponded to an FcRn-2G12 monomer complex. The second peak or trough was at the elution volume of free FcRn. (B) FcRn was incubated with 1.25 μM 2G12 dimer in the presence of 0, 2, 4, or 6 (additional) equivalents of FcRn in a buffer containing 5 μM FcRn (equilibration buffer). Samples were then injected onto a column equilibrated in the equilibration buffer. The peak that eluted first corresponds to an FcRn-2G12 dimer complex. The second peak or trough was at the elution volume of free FcRn.

References

Adams, P.D., Afonine, P.V., Bunkoczi, G., Chen, V.B., Davis, I.W., Echols, N., Headd, J.J., Hung, L.W., Kapral, G.J., Grosse-Kunstleve, R.W.*, et al.* (2010). PHENIX: a comprehensive Python-based system for macromolecular structure solution. Acta crystallographica Section D, Biological crystallography *66*, 213-221.

Artimo, P., Jonnalagedda, M., Arnold, K., Baratin, D., Csardi, G., de Castro, E., Duvaud, S., Flegel, V., Fortier, A., Gasteiger, E.*, et al.* (2012). ExPASy: SIB bioinformatics resource portal. Nucleic acids research *40*, W597-603.

Bonomelli, C., Doores, K.J., Dunlop, D.C., Thaney, V., Dwek, R.A., Burton, D.R., Crispin, M., and Scanlan, C.N. (2011). The glycan shield of HIV is predominantly oligomannose independently of production system or viral clade. PloS one *6*, e23521.

Botos, I., and Wlodawer, A. (2005). Proteins that bind high-mannose sugars of the HIV envelope. Progress in biophysics and molecular biology *88*, 233-282.

Brunger, A.T. (2007). Version 1.2 of the Crystallography and NMR system. Nature protocols *2*, 2728-2733.

Brunger, A.T., Adams, P.D., Clore, G.M., DeLano, W.L., Gros, P., Grosse-Kunstleve, R.W., Jiang, J.S., Kuszewski, J., Nilges, M., Pannu, N.S.*, et al.* (1998). Crystallography & NMR system: A new software suite for macromolecular structure determination. Acta crystallographica Section D, Biological crystallography *54*, 905-921.

Burmeister, W.P., Huber, A.H., and Bjorkman, P.J. (1994). Crystal structure of the complex of rat neonatal Fc receptor with Fc. Nature *372*, 379-383.

Calarese, D.A., Lee, H.K., Huang, C.Y., Best, M.D., Astronomo, R.D., Stanfield, R.L., Katinger, H., Burton, D.R., Wong, C.H., and Wilson, I.A. (2005). Dissection of the carbohydrate specificity of the broadly neutralizing anti-HIV-1 antibody 2G12. Proceedings of the National Academy of Sciences of the United States of America *102*, 13372-13377.

Calarese, D.A., Scanlan, C.N., Zwick, M.B., Deechongkit, S., Mimura, Y., Kunert, R., Zhu, P., Wormald, M.R., Stanfield, R.L., Roux, K.H.*, et al.* (2003). Antibody domain exchange is an immunological solution to carbohydrate cluster recognition. Science *300*, 2065-2071.

DeLano, W.L., Ultsch, M.H., de Vos, A.M., and Wells, J.A. (2000). Convergent solutions to binding at a protein-protein interface. Science *287*, 1279-1283.

Diskin, R., Klein, F., Horwitz, J.A., Halper-Stromberg, A., Sather, D.N., Marcovecchio, P.M., Lee, T., West, A.P., Jr., Gao, H., Seaman, M.S.*, et al.* (2013). Restricting HIV-1 pathways for escape using rationally designed anti-HIV-1 antibodies. The Journal of experimental medicine *210*, 1235-1249.

Diskin, R., Scheid, J.F., Marcovecchio, P.M., West, A.P., Jr., Klein, F., Gao, H., Gnanapragasam, P.N., Abadir, A., Seaman, M.S., Nussenzweig, M.C.*, et al.* (2011). Increasing the potency and breadth of an HIV antibody by using structure-based rational design. Science *334*, 1289-1293.

Edwards, M.J., and Dimmock, N.J. (2001). Hemagglutinin 1-specific immunoglobulin G and Fab molecules mediate postattachment neutralization of influenza A virus by inhibition of an early fusion event. Journal of virology *75*, 10208-10218.

Emsley, P., Lohkamp, B., Scott, W.G., and Cowtan, K. (2010). Features and development of Coot. Acta crystallographica Section D, Biological crystallography *66*, 486-501.

Franke, D.S., D. I. (2009). DAMMIF, a program for rapid ab-initio shape determination in small-angle scattering. J Appl Cryst *42*, 342-346.

Gorny, M.K., Stamatatos, L., Volsky, B., Revesz, K., Williams, C., Wang, X.H., Cohen, S., Staudinger, R., and Zolla-Pazner, S. (2005). Identification of a new quaternary neutralizing epitope on human immunodeficiency virus type 1 virus particles. Journal of virology *79*, 5232-5237.

Guddat, L.W., Herron, J.N., and Edmundson, A.B. (1993). Three-dimensional structure of a human immunoglobulin with a hinge deletion. Proceedings of the National Academy of Sciences of the United States of America *90*, 4271-4275.

Harris, L.J., Larson, S.B., Hasel, K.W., and McPherson, A. (1997). Refined structure of an intact IgG2a monoclonal antibody. Biochemistry *36*, 1581-1597.

Harris, L.J., Skaletsky, E., and McPherson, A. (1998). Crystallographic structure of an intact IgG1 monoclonal antibody. Journal of molecular biology *275*, 861-872.

Huber, A.H. (1994). Biochemical and Structural Characterization of Drosophila Neuroglian. In Division of Biology (Pasadena, CA: California Institute of Technology).

Huber, A.H., Kelley, R.F., Gastinel, L.N., and Bjorkman, P.J. (1993). Crystallization and stoichiometry of binding of a complex between a rat intestinal Fc receptor and Fc. Journal of molecular biology *230*, 1077-1083.

Hummel, J.P., and Dreyer, W.J. (1962). Measurement of protein-binding phenomena by gel filtration. Biochimica et biophysica acta *63*, 530-532.

Kabsch, W. (2010). XDS. Acta Crystallogr D Biol Crystallogr *66*, 125-132.

Karplus, P.A., and Diederichs, K. (2012). Linking crystallographic model and data quality. Science *336*, 1030-1033.

Klein, F., Halper-Stromberg, A., Horwitz, J.A., Gruell, H., Scheid, J.F., Bournazos, S., Mouquet, H., Spatz, L.A., Diskin, R., Abadir, A.*, et al.* (2012). HIV therapy by a combination of broadly neutralizing antibodies in humanized mice. Nature *492*, 118-122.

Klein, F., Mouquet, H., Dosenovic, P., Scheid, J.F., Scharf, L., and Nussenzweig, M.C. (2013). Antibodies in HIV-1 vaccine development and therapy. Science *341*, 1199-1204.

Klein, J.S., and Bjorkman, P.J. (2010). Few and far between: how HIV may be evading antibody avidity. PLoS pathogens *6*, e1000908.

Klein, J.S., Webster, A., Gnanapragasam, P.N., Galimidi, R.P., and Bjorkman, P.J. (2010). A dimeric form of the HIV-1 antibody 2G12 elicits potent antibody-dependent cellular cytotoxicity. AIDS (London, England) *24*, 1633-1640.

Konarev, P.V., Volkov, V. V, Sokolava, A. V., Koch, M. H. J., and Svergun, D. I. (2003). PRIMUS - a Windows-PC based system for small-angle scattering data analysis. . J Appl Cryst *36*, 1277-1282.

Krapp, S., Mimura, Y., Jefferis, R., Huber, R., and Sondermann, P. (2003). Structural analysis of human IgG-Fc glycoforms reveals a correlation between glycosylation and structural integrity. Journal of molecular biology *325*, 979-989.

Kratzin, H.D., Palm, W., Stangel, M., Schmidt, W.E., Friedrich, J., and Hilschmann, N. (1989). [The primary structure of crystallizable monoclonal immunoglobulin IgG1 Kol. II. Amino acid sequence of the L-chain, gamma-type, subgroup I]. Biological chemistry Hoppe-Seyler *370*, 263-272.

Kwong, P.D., Doyle, M.L., Casper, D.J., Cicala, C., Leavitt, S.A., Majeed, S., Steenbeke, T.D., Venturi, M., Chaiken, I., Fung, M.*, et al.* (2002). HIV-1 evades antibody-mediated neutralization through conformational masking of receptor-binding sites. Nature *420*, 678-682.

Kwong, P.D., and Mascola, J.R. (2012). Human antibodies that neutralize HIV-1: identification, structures, and B cell ontogenies. Immunity *37*, 412-425.

Lander, G.C., Stagg, S.M., Voss, N.R., Cheng, A., Fellmann, D., Pulokas, J., Yoshioka, C., Irving, C., Mulder, A., Lau, P.W.*, et al.* (2009). Appion: an integrated, database-driven pipeline to facilitate EM image processing. Journal of structural biology *166*, 95-102.

Lebedev, A.A., Vagin, A.A., and Murshudov, G.N. (2008). Model preparation in MOLREP and examples of model improvement using X-ray data. Acta crystallographica Section D, Biological crystallography *64*, 33-39.

Liu, Y., and Eisenberg, D. (2002). 3D domain swapping: as domains continue to swap. Protein science : a publication of the Protein Society *11*, 1285-1299.

Luo, X.M., Lei, M.Y., Feidi, R.A., West, A.P., Jr., Balazs, A.B., Bjorkman, P.J., Yang, L., and Baltimore, D. (2010). Dimeric 2G12 as a potent protection against HIV-1. PLoS pathogens *6*, e1001225.

Mascola, J.R., and Haynes, B.F. (2013). HIV-1 neutralizing antibodies: understanding nature's pathways. Immunological reviews *254*, 225-244.

McCoy, A.J., Grosse-Kunstleve, R.W., Adams, P.D., Winn, M.D., Storoni, L.C., and Read, R.J. (2007). Phaser crystallographic software. Journal of applied crystallography *40*, 658-674.

Menendez, A., Calarese, D.A., Stanfield, R.L., Chow, K.C., Scanlan, C.N., Kunert, R., Katinger, H., Burton, D.R., Wilson, I.A., and Scott, J.K. (2008). A peptide inhibitor of HIV-1 neutralizing antibody 2G12 is not a structural mimic of the natural carbohydrate epitope on gp120. FASEB journal : official publication of the Federation of American Societies for Experimental Biology *22*, 1380-1392.

Otwinowski, Z., and Minor, W. (1997). Processing of X-ray diffraction data. Methods in enzymology *276*, 307-326.

Petoukhov, M.V., Franke, D., Shkumatov, A.V., Tria, G., Kikhney, A.G., Gajda, M., Gorba, C., Mertens, H.D.T., Konarev, P.V., and Svergun, D.I. (2012). New developments in the ATSAS program package for small-angle scattering data analysis. Journal of applied crystallography *45*, 342-350.

Pettersen, E.F., Goddard, T.D., Huang, C.C., Couch, G.S., Greenblatt, D.M., Meng, E.C., and Ferrin, T.E. (2004). UCSF Chimera--a visualization system for exploratory research and analysis. Journal of computational chemistry *25*, 1605-1612.

Poignard, P., Sabbe, R., Picchio, G.R., Wang, M., Gulizia, R.J., Katinger, H., Parren, P.W., Mosier, D.E., and Burton, D.R. (1999). Neutralizing antibodies have limited effects on the control of established HIV-1 infection in vivo. Immunity *10*, 431-438.

Poignard, P., Saphire, E.O., Parren, P.W., and Burton, D.R. (2001). gp120: Biologic aspects of structural features. Annual review of immunology *19*, 253-274.

Potterton, E., Briggs, P., Turkenburg, M., and Dodson, E. (2003). A graphical user interface to the CCP4 program suite. Acta crystallographica Section D, Biological crystallography *59*, 1131-1137.

Read, R.J.S., A. J. (1988). A phased translation function. J Appl Cryst *21*, 490-495.

Roux, K.H. (1999). Immunoglobulin structure and function as revealed by electron microscopy. Int Arch Allergy Imm *120*, 85-99.

Rupp, B. (2010). Biomolecular crystallography : principles, practice, and application to structural biology (New York: Garland Science).

Sanchez, L.M., Penny, D.M., and Bjorkman, P.J. (1999). Stoichiometry of the interaction between the major histocompatibility complex-related Fc receptor and its Fc ligand. Biochemistry *38*, 9471-9476.

Sanders, R.W., Venturi, M., Schiffner, L., Kalyanaraman, R., Katinger, H., Lloyd, K.O., Kwong, P.D., and Moore, J.P. (2002). The mannose-dependent epitope for neutralizing antibody 2G12 on human immunodeficiency virus type 1 glycoprotein gp120. Journal of virology *76*, 7293-7305.

Saphire, E.O., Parren, P.W., Pantophlet, R., Zwick, M.B., Morris, G.M., Rudd, P.M., Dwek, R.A., Stanfield, R.L., Burton, D.R., and Wilson, I.A. (2001). Crystal structure of a

neutralizing human IGG against HIV-1: a template for vaccine design. Science *293*, 1155-1159.

Scanlan, C.N., Pantophlet, R., Wormald, M.R., Ollmann Saphire, E., Stanfield, R., Wilson, I.A., Katinger, H., Dwek, R.A., Rudd, P.M., and Burton, D.R. (2002). The broadly neutralizing anti-human immunodeficiency virus type 1 antibody 2G12 recognizes a cluster of alpha1-->2 mannose residues on the outer face of gp120. J Virol *76*, 7306-7321.

Schofield, D.J., Stephenson, J.R., and Dimmock, N.J. (1997). Variations in the neutralizing and haemagglutination-inhibiting activities of five influenza A virus-specific IgGs and their antibody fragments. The Journal of general virology *78 (Pt 10)*, 2431-2439.

Sharma, V.A., Kan, E., Sun, Y., Lian, Y., Cisto, J., Frasca, V., Hilt, S., Stamatatos, L., Donnelly, J.J., Ulmer, J.B.*, et al.* (2006). Structural characteristics correlate with immune responses induced by HIV envelope glycoprotein vaccines. Virology *352*, 131-144.

Smolsky, I., Liu, P., Niebuhr, M., Ito, K., Weiss, T. M., Tsuruta, H. (2007). Biological small-angle X-ray scattering facility at the Stanford Synchrotron Radiation Laboratory. J Appl Cryst *40*, 453-458.

Sondermann, P., Huber, R., Oosthuizen, V., and Jacob, U. (2000). The 3.2-A crystal structure of the human IgG1 Fc fragment-Fc gammaRIII complex. Nature *406*, 267-273.

Sorzano, C.O., Bilbao-Castro, J.R., Shkolnisky, Y., Alcorlo, M., Melero, R., Caffarena-Fernandez, G., Li, M., Xu, G., Marabini, R., and Carazo, J.M. (2010). A clustering approach to multireference alignment of single-particle projections in electron microscopy. Journal of structural biology *171*, 197-206.

Starcich, B.R., Hahn, B.H., Shaw, G.M., McNeely, P.D., Modrow, S., Wolf, H., Parks, E.S., Parks, W.P., Josephs, S.F., Gallo, R.C., *et al.* (1986). Identification and characterization of conserved and variable regions in the envelope gene of HTLV-III/LAV, the retrovirus of AIDS. Cell *45*, 637-648.

Strong, M., Sawaya, M.R., Wang, S., Phillips, M., Cascio, D., and Eisenberg, D. (2006). Toward the structural genomics of complexes: crystal structure of a PE/PPE protein complex from Mycobacterium tuberculosis. Proceedings of the National Academy of Sciences of the United States of America *103*, 8060-8065.

Suloway, C., Pulokas, J., Fellmann, D., Cheng, A., Guerra, F., Quispe, J., Stagg, S., Potter, C.S., and Carragher, B. (2005). Automated molecular microscopy: the new Leginon system. Journal of structural biology *151*, 41-60.

Svergun, D.I. (1992). Determination of the regularization parameter in indirect-transform methods using perceptual criteria J Appl Cryst *25*, 495-503.

Tang, G., Peng, L., Baldwin, P.R., Mann, D.S., Jiang, W., Rees, I., and Ludtke, S.J. (2007). EMAN2: an extensible image processing suite for electron microscopy. Journal of structural biology *157*, 38-46.

Trkola, A., Purtscher, M., Muster, T., Ballaun, C., Buchacher, A., Sullivan, N., Srinivasan, K., Sodroski, J., Moore, J.P., and Katinger, H. (1996). Human monoclonal antibody 2G12 defines a distinctive neutralization epitope on the gp120 glycoprotein of human immunodeficiency virus type 1. Journal of virology *70*, 1100-1108.

Vagin, A., and Teplyakov, A. (2010). Molecular replacement with MOLREP. Acta crystallographica Section D, Biological crystallography *66*, 22-25.

van Heel, M., Harauz, G., Orlova, E.V., Schmidt, R., and Schatz, M. (1996). A new generation of the IMAGIC image processing system. Journal of structural biology *116*, 17-24.

Volkov, V.S., D. (2003). Uniqueness of ab-initio shape determination in small-angle scattering. J Appl Cryst *36*, 860-864.

Voss, N.R., Yoshioka, C.K., Radermacher, M., Potter, C.S., and Carragher, B. (2009). DoG Picker and TiltPicker: software tools to facilitate particle selection in single particle electron microscopy. Journal of structural biology *166*, 205-213.

West, A.P., Jr., and Bjorkman, P.J. (2000). Crystal structure and immunoglobulin G binding properties of the human major histocompatibility complex-related Fc receptor(,). Biochemistry *39*, 9698-9708.

West, A.P., Jr., Galimidi, R.P., Foglesong, C.P., Gnanapragasam, P.N., Huey-Tubman, K.E., Klein, J.S., Suzuki, M.D., Tiangco, N.E., Vielmetter, J., and Bjorkman, P.J. (2009). Design and expression of a dimeric form of human immunodeficiency virus type 1 antibody 2G12 with increased neutralization potency. J Virol *83*, 98-104.

Winn, M.D., Ballard, C.C., Cowtan, K.D., Dodson, E.J., Emsley, P., Evans, P.R., Keegan, R.M., Krissinel, E.B., Leslie, A.G., McCoy, A.*, et al.* (2011). Overview of the CCP4 suite and current developments. Acta crystallographica Section D, Biological crystallography *67*, 235-242.

Wu, H., Pfarr, D.S., Tang, Y., An, L.L., Patel, N.K., Watkins, J.D., Huse, W.D., Kiener, P.A., and Young, J.F. (2005). Ultra-potent antibodies against respiratory syncytial virus: effects of binding kinetics and binding valence on viral neutralization. Journal of molecular biology *350*, 126-144.

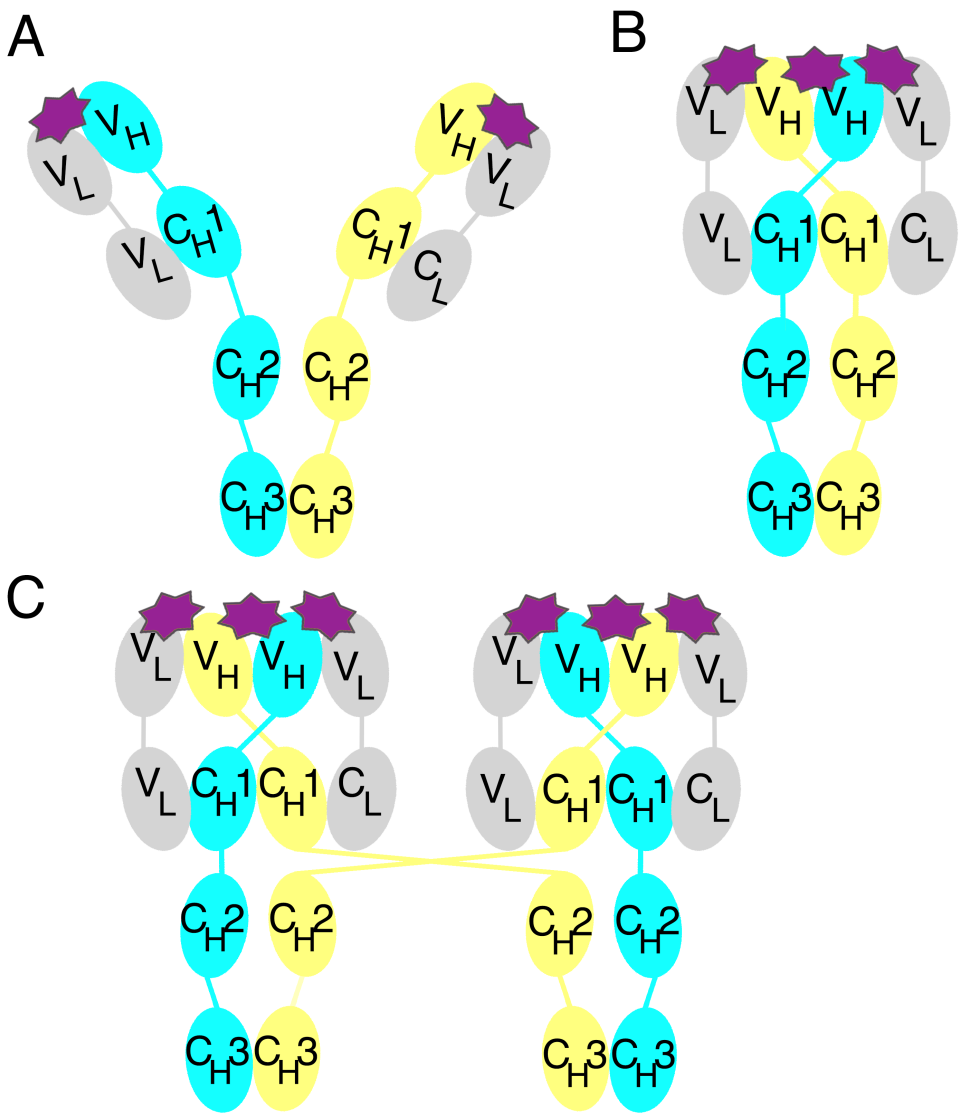

Figure 1

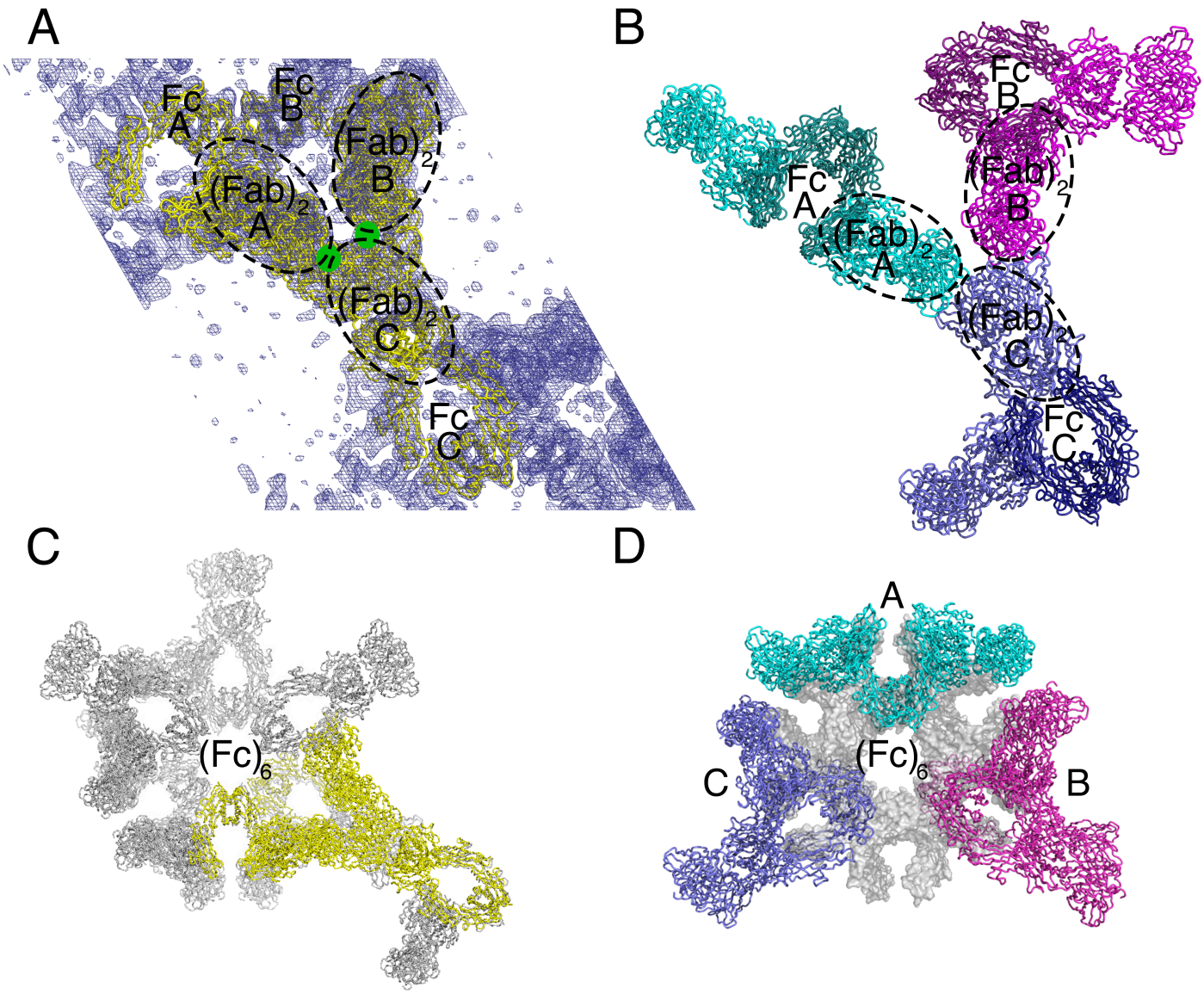
A
Fc
A
Fc
B
(Fab)2
B
(Fab)2
A
(Fab)2
C
Fc
C
B
Fc
B
(Fab)2
B
Fc
A
(Fab)2
A
(Fab)2
C
Fc
C
C
(Fc)6
D
A
C
(Fc)6
B

Figure 2

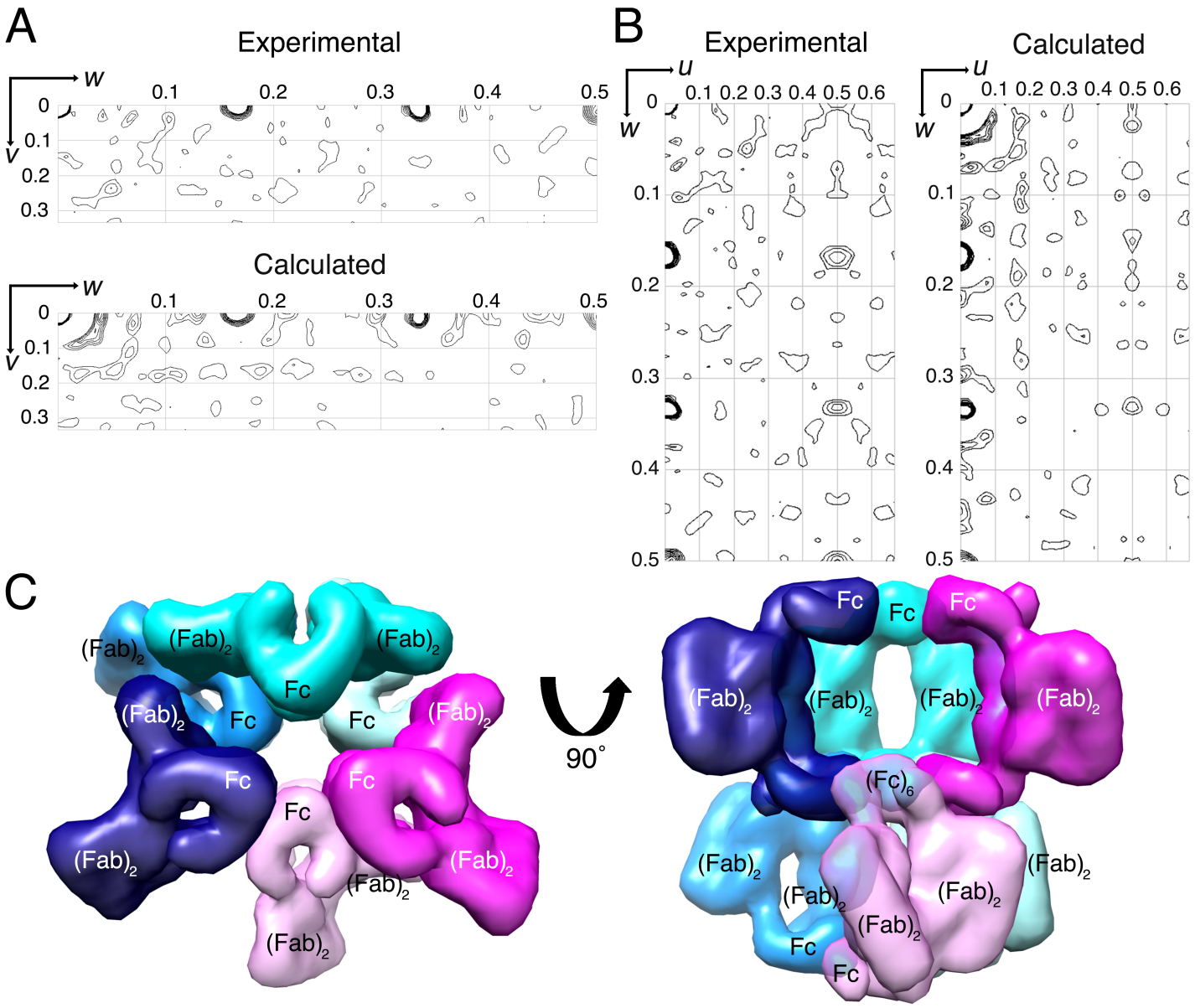
A
Experimental
w
v
0
0.1
0.2
0.3
0.4
0.5
Calculated
B
Experimental
Calculated
u
w
0.6
C
(Fab)2
Fc
90˚
(Fc)6

Figure 3

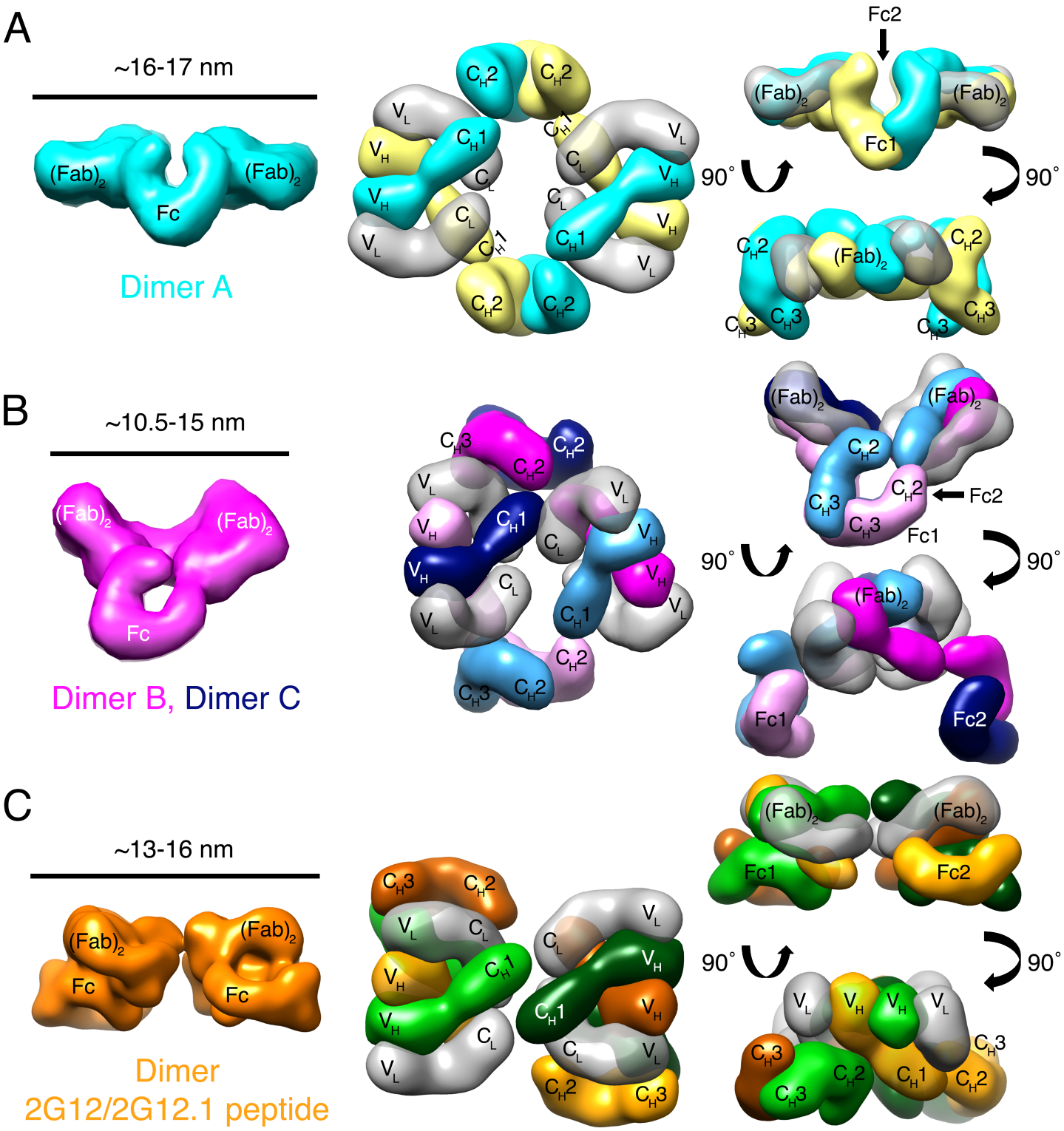
A
~16-17 nm
(Fab)2
Fc
(Fab)2
Dimer A
Fc2
(Fab)2
(Fab)2
Fc1
90˚
90˚
B
~10.5-15 nm
(Fab)2
(Fab)2
Fc
Dimer B, Dimer C
Fc2
Fc1
90˚
90˚
(Fab)2
Fc1
Fc2
C
~13-16 nm
(Fab)2
(Fab)2
Fc
Fc
Dimer
2G12/2G12.1 peptide
(Fab)2
(Fab)2
Fc1
Fc2
90˚
90˚

Figure 4

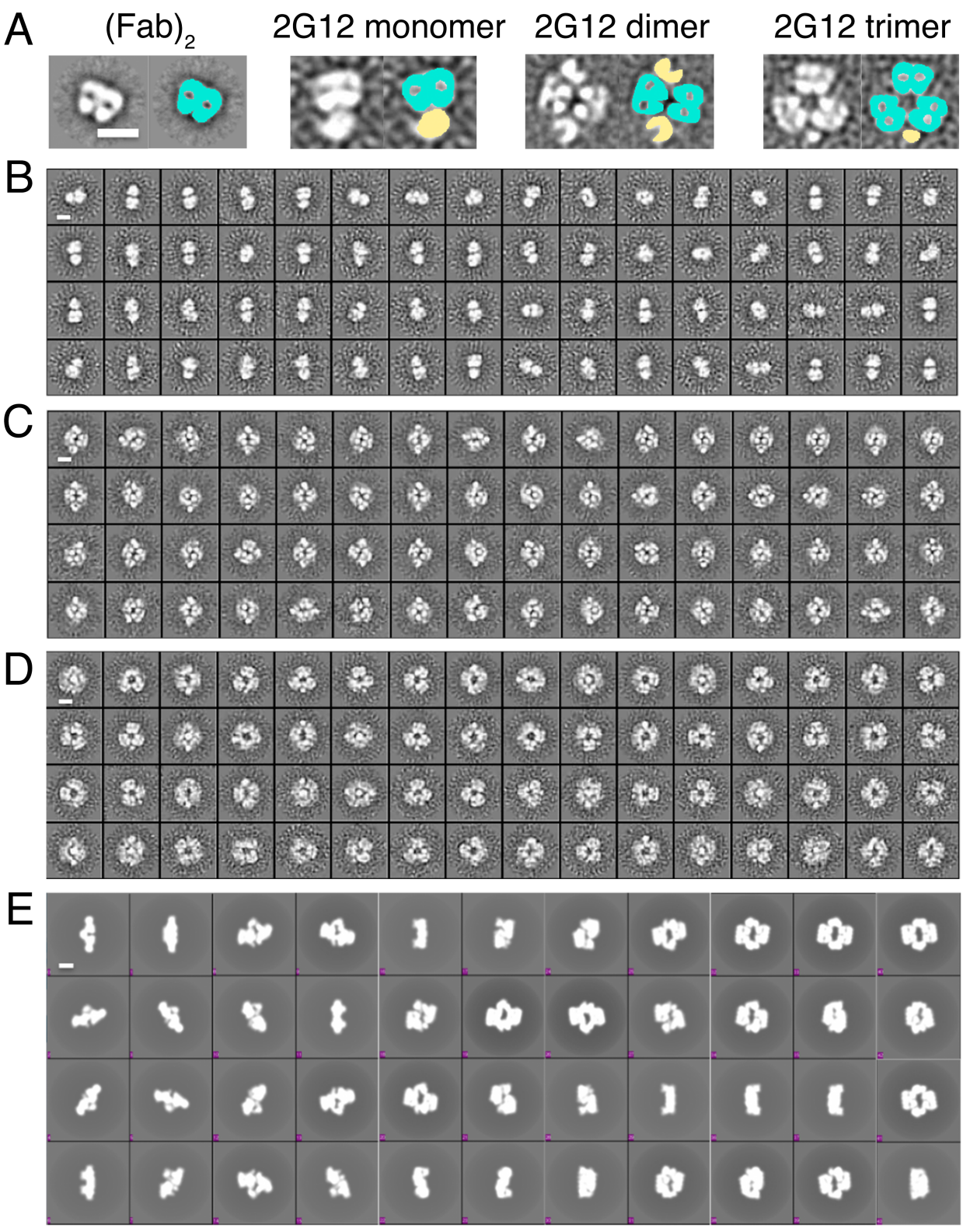

Figure 5

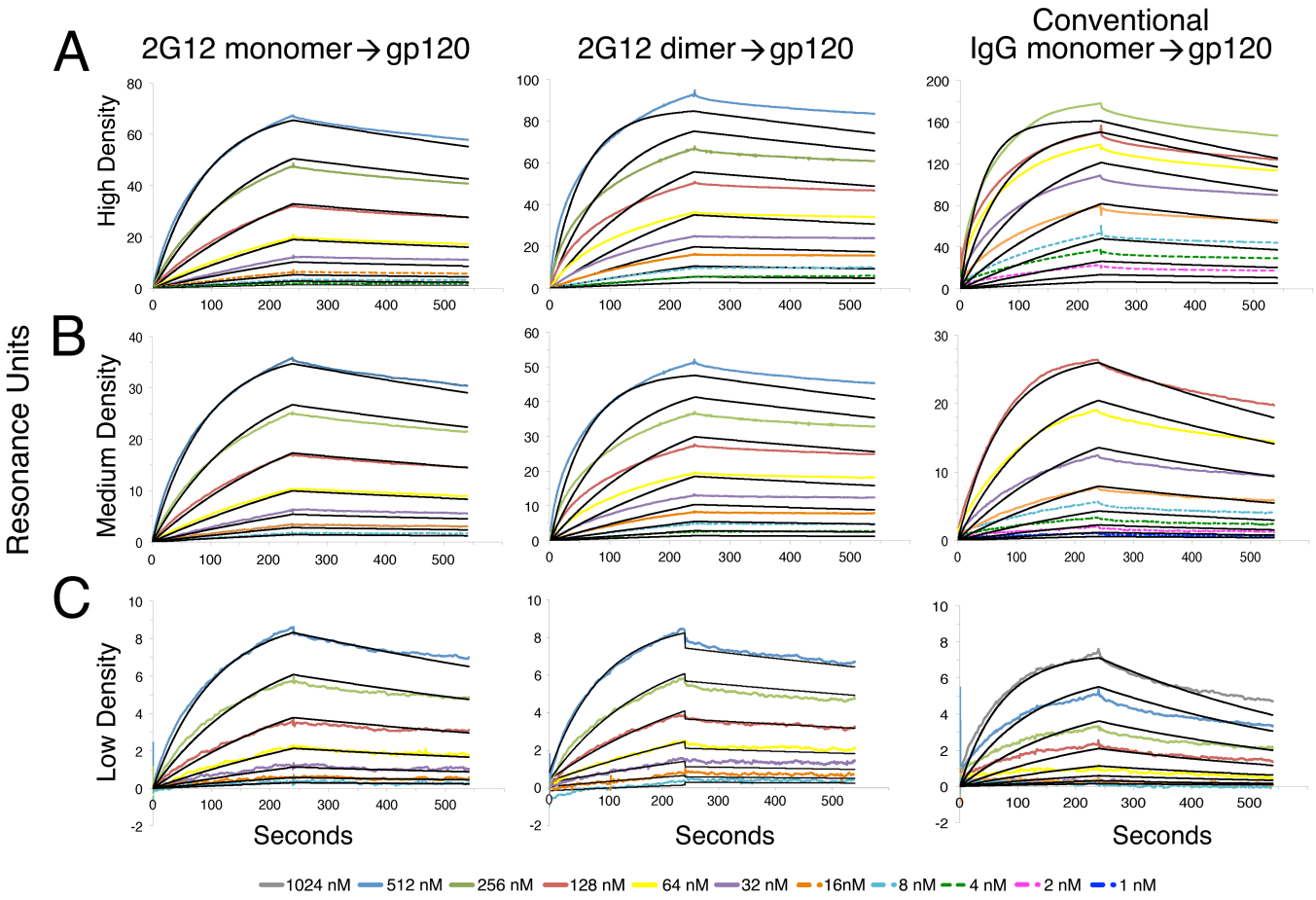
A
2G12 monomer→gp120
2G12 dimer→gp120
Conventional IgG monomer→gp120
High Density
B
Medium Density
C
Low Density
Resonance Units
Seconds
1024 nM
512 nM
256 nM
128 nM
64 nM
32 nM
16nM
8 nM
4 nM
2 nM
1 nM

Figure 6

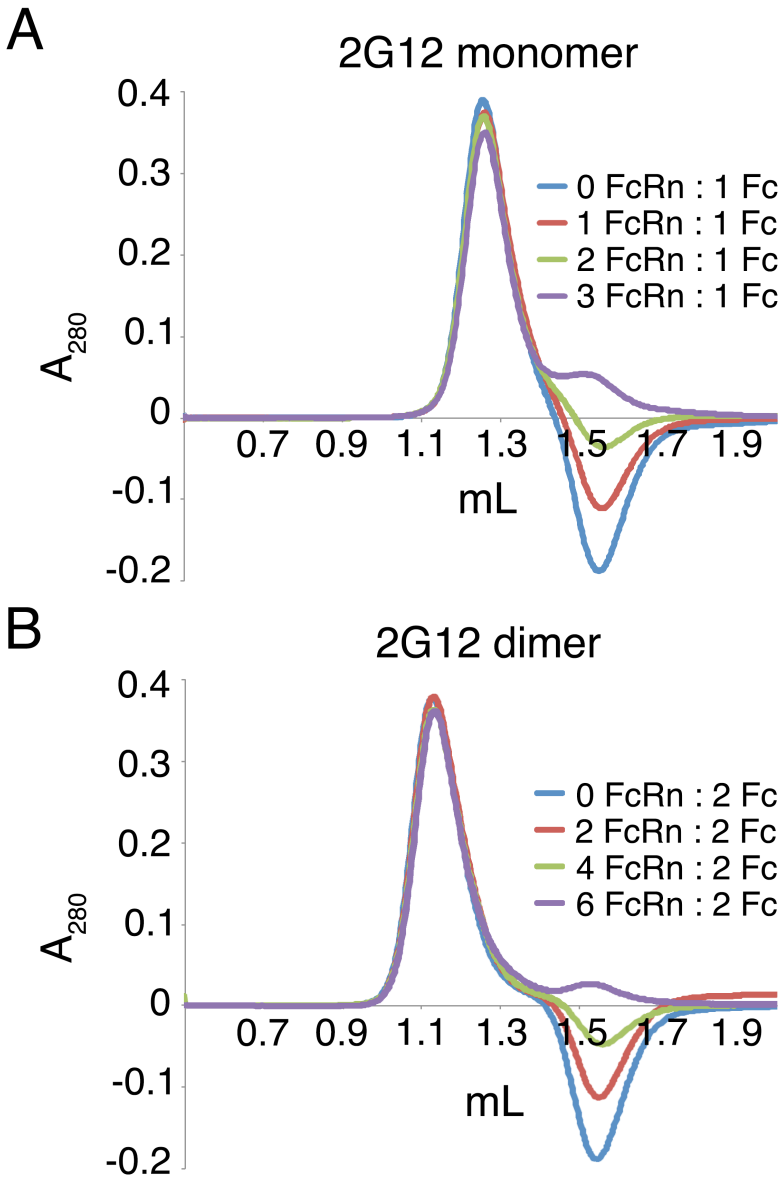
A
2G12 monomer
0.4
0.3
0.2
0.1
0
-0.1
-0.2
A280
0.7 0.9 1.1 1.3 1.5 1.7 1.9
mL
0 FcRn : 1 Fc
1 FcRn : 1 Fc
2 FcRn : 1 Fc
3 FcRn : 1 Fc
B
2G12 dimer
0.4
0.3
0.2
0.1
0
-0.1
-0.2
A280
0.7 0.9 1.1 1.3 1.5 1.7 1.9
mL
0 FcRn : 2 Fc
2 FcRn : 2 Fc
4 FcRn : 2 Fc
6 FcRn : 2 Fc

Figure 7

Supplemental Information

for

Structural basis for enhanced neutralization of HIV-1 by a dimeric IgG form of the glycan-recognizing antibody 2G12

SUPPLEMENTAL RESULTS

Calculation of interchain distances for connectivity model for 2G12 dimer/2G12.1 peptide complex

Nineteen residues within the 2G12 hinge region were missing from the $(Fab)_2$ (pdb ID 1OP3) and Fc (pdb ID 1H3X) structures used as search models for molecular replacement. Distances from the N-termini of the four Fc polypeptide chains to the C-termini of the four $(Fab)_2$ heavy chains were measured using coordinates for high resolution models placed into the 2G12 dimer/2G12.1 structure for residues Pro-238 (N-terminus of Fc) and Lys-228 (C-terminus of the $(Fab)_2$ heavy chain) (residue numbering based on the structures of 2G12 $(Fab)_2$ (pdb ID 1OP3) and Fc (pdb ID 1H3X)).

Solution studies of 2G12 monomer and 2G12 dimer

Small-angle X-ray scattering (SAXS) can be used to derive *ab initio* information about the size, shape, and flexibility of proteins in solution (Putnam et al., 2007). To obtain independent structural information for 2G12 dimer, we used SAXS to investigate the conformational range of 2G12 dimer (Figure S5). We obtained X-ray scattering profiles (Figure S5E) from solutions of purified 2G12 monomer, 2G12 dimer, and Rituximab, a conventional monomeric human IgG (Anderson et al., 1997). For each protein, we generated 10 *ab initio* models (Figure S5A-C) using DAMMIF (Franke, 2009), which were superposed, averaged, and filtered using DAMAVER (Volkov, 2003). Models filled with dummy atoms showed 2G12 monomer as a relatively rigid "slab" with potential flexibility only at the hinge region between the $(Fab)_2$ unit and the Fc (Figure S5A). In

contrast, models of 2G12 dimer showed a larger molecule with increased conformational flexibility (Figure S5B). Rituximab models showed a thinner but conformationally similar molecule to 2G12 dimer (Figure S5C).

The distance distribution function *P(r)* was derived through an indirect Fourier transform of the scattering curve using GNOM (Svergun, 1992). *P(r)* was monomodal for 2G12 monomer and 2G12 dimer (Figure S5D), corresponding to the profile for a globular protein. *P(r)* for Rituximab exhibited a smaller second peak, suggesting the presence of more elongated domains in solution (Figure S5D) (Putnam et al., 2007). *P(r)* functions for all three proteins converged smoothly to zero at D_{max}, which corresponded to the maximum linear dimension of the scattering particles: 162 Å for 2G12 monomer, 178 Å for Rituximab, and 193 Å for 2G12 dimer. The differences in apparent size in solution corroborated our findings from the crystal structures of 2G12 dimer: as predicted, the gyration space that 2G12 dimer occupied in solution was larger than that of both 2G12 monomer and Rituximab. 2G12 monomer, which should exhibit limited mobility due to the $(Fab)_2$ domain exchange, indeed had a lower R_g than both conventional IgG and 2G12 dimer (Guinier analysis yielded R_g values of 46 ± 0.42 Å, 52 ± 2.3 Å, and 59 ± 0.67 Å, for 2G12 monomer, Rituximab, and 2G12 dimer, respectively; see Figure S5D). Rituximab also exhibited a broader R_g distribution in Guinier analysis than both 2G12 monomer and dimer, suggesting that the conventional IgG was more flexible in solution than 2G12 dimer. 2G12 dimer was in turn more flexible than 2G12 monomer, which exhibited the narrowest R_g distribution. The reference model chosen by DAMAVER produced a .fir file in DAMMIF, which was used to calculate a back-transform of the final averaged models (Figure S5E). Simulated scattering from the averaged models fit

the experimental scattering data well, with χ^2 of fit values between I_{exp} and I_{sim} of 1.347, 1.202, and 1.218 for 2G12 monomer, 2G12 dimer, and control IgG Rituximab, respectively (Figure S5E).

SUPPLEMENTAL EXPERIMENTAL METHODS

Protein expression and purification

Purified monomeric HIV-1 gp120 was a gift from Leo Stamatatos and Zachary Caldwell (Seattle BioMed) (Sharma et al., 2006). Purified 2G12 $(Fab)_2$ was a gift from Zara Fulton and was imaged by Reza Khayat (The Scripps Research Institute). Other reagents, such as control monomeric IgGs and purified soluble rat FcRn (which binds human IgG equally as well as rat IgG (Huber, 1994)) were provided by members of the Bjorkman laboratory, including Paola Marcovecchio, Han Gao, Maria Politzer, and Kathryn Huey Tubman. Protein concentrations were determined spectrophotometrically using extinction coefficients at 280 nm of 200480 M^{-1} cm^{-1} (2G12 monomer), 400960 M^{-1} cm^{-1} (2G12 dimer), 202000 M^{-1} cm^{-1} (conventional monomeric IgG antibodies), 84900 M^{-1} cm^{-1} (rat FcRn), and 146090 M^{-1} cm^{-1} (SF162 gp120). Extinction coefficients were calculated based on amino acid compositions using ProtParam (Artimo et al., 2012).

Crystallization and data collection

Crystals of 2G12 dimer (space group $P6_122$) were grown in hanging drops by mixing equal volumes of 2G12 dimer (11.5 mg/ml) with a solution containing 1.2 M ammonium sulfate, and 100 mM HEPES pH 7.0 at 20º C. Crystals were cryopreserved in well solution containing 25-30% glycerol. Data were collected to 7.5 Å resolution at beamline 8.3.1 of the Advanced Light Source (ALS) at Lawrence Berkeley National Laboratory (LBNL), and at beamline 12-2 of the Stanford Synchrotron Radiation Lightsource (SSRL) at the SLAC National Accelerator Laboratory. Over 500 crystals were screened,

but all diffracted poorly and were fragile to handle. Experiments to improve the quality of the crystals included seeding, glutaraldehyde crosslinking, recrystallization, additives, exchanging into lithium sulfate, exploring cryoprotectants, and varying drop composition. Tantalum bromide clusters (Jena Biosciences) were soaked into the native crystals, resulting in bright green crystals. SAD data with reflections to 10 Å were collected at beamline 8.3.1 of the ALS at LBNL at a single wavelength of 1.255 Å.

For crystallization of the 2G12 dimer/2G12.1 complex, 2G12.1 peptide (the Polypeptide Group) was mixed with 2G12 dimer (11.5 mg/ml) at a 19:1 molar ratio in 24-well hanging drops of protein and reservoir solution in equal amounts. Clustered hexagonal crystals formed from spherolites by vapor diffusion in 5% Tascimate, 10% PEGMME 5000, and 100 mM HEPES at pH 7.0. Crystals were cryopreserved in the well solution containing 30% PEGMME 5000 and screened at beamline BL12-2 at the SSRL at SLAC, and the 5 μm microbeam at beamline 23ID-D at the General Medical Sciences and Cancer Institutes Structural Biology Facility (GM/CAT) at the Advanced Photon Source (APS). Upon handling, the clustered crystals occasionally disintegrated into smaller, more singular pieces, which were also cryoprotected and screened. We also collected usable data sets from large crystals (0.3 mm diameter) that contained singular patches.

Model validation calculations

Calculations using derivative crystals were performed using software in the CCP4 Software Suite (Winn et al., 2011) via the ccp4i graphical user interface (Potterton et al.,

2003): cad (Winn et al., 2011), scaleit (Winn et al., 2011), fft (Read, 1988), followed by Phenix.autosol (Adams et al., 2010), and Phenix.emma (Adams et al., 2010).

Small angle X-ray scattering (SAXS)

Samples for SAXS were concentrated to 17 mg/ml (2G12 monomer), 13 mg/ml (2G12 dimer), and 21 mg/ml (Rituximab) and filtered through 0.22 μm membranes. Dialysis to buffer exchange each protein into Phosphate Buffered Saline was performed overnight, and samples were diluted for a concentration series of 0.25 mg/ml, 0.5 mg/ml, 0.75 mg/ml, 1.0 mg/ml, 2.5 mg/ml, 5.0 mg/ml, and 7.5 mg/ml, along with 1-3% glycerol to minimize aggregation caused by radiation damage. Data were collected at SSRL beamline 4-2 using a Rayonix MX225-HE detector at a distance of 2500 mm, using 1.13 Å wavelength X-rays. For each concentration of each sample, 15 exposures of 1 second were collected, covering a momentum transfer (q) range of 0.0047–0.375 1/Å. The scattering profile for the buffer was obtained in the same manner and subtracted from the protein profiles. The detector images were integrated, background subtracted, and screened for radiation damage using SasTool (Smolsky, 2007). Extrapolation to infinite dilution was done with PRIMUS (Konarev, 2003). Guinier analysis was performed using AutoRG, distance distribution functions determined with GNOM (Svergun, 1992), and *ab initio* reconstructions were performed using DAMMIF (Franke, 2009) and DAMAVER (Volkov, 2003) in the ATSAS package (Petoukhov et al., 2012).

Supplemental Table

Table S1. Data Collection and Refinement Statistics

	2G12 dimer	2G12 dimer with $(Ta_6Br_{12})^{2+}$	2G12/2G12.1 peptide
Data Collection			
Resolution (Å)	39.8-8.0 (8.3-8.0)	35.0-10.0 (10.34-10.0)	64.9-6.5 (6.7-6.5)
Space group	$P6_12\ 2$	$P6_12\ 2$	P6
Unit cell	$a = b = 246$ Å $c = 657$ Å $\alpha = \beta = 90°$ $\gamma = 120°$	$a = b = 250$ Å $c = 652$ Å $\alpha = \beta = 90°$ $\gamma = 120°$	$a = b = 375$ Å $c = 64$ Å $\alpha = \beta = 90°$ $\gamma = 120°$
Total reflections	26016 (2520)	90570	113124 (11045)
Unique reflections	12654 (1260)	11087 (483)	10665 (1022)
Completeness (%)	96.95 (71.03)	99.0 (89.6)	99.96 (100.00)
Mean I/σ(I)	6.51 (1.72)	7.6 (1.3)	7.84 (1.51)
R_{merge}	0.088 (0.46)	0.33 (0.78)	0.28 (2.1)
CC½	0.99 (0.80)		1.0 (0.83)
CC*	1.0 (0.94)		1.0 (0.95)
R_{anom}		0.22 (0.87)	
Anomalous completeness		74.6 (74.4)	
Anomalous multipicity		4.6 (4.7)	
f'		-26.4	
f''		17.0	
Refinement			
R_{work}	0.35 (0.35)		0.38 (0.44)
R_{free}	0.37 (0.36)		0.36 (0.39)
Number of atoms	29250		28984
Protein residues	3795		3750
RMS bonds (Å)	0.018		0.037
RMS angles (°)	1.62		1.78
Average B-factor (Å^2)	159.0		481.0

*Statistics for the highest-resolution shell are shown in parentheses.

Supplemental Figure Legends

Figure S1. Proposed connectivities of 2G12 dimer and 2G12 trimer, related to Figure 1

(A,B) Schematic diagrams illustrating how intermolecular domain swapping could lead to 2G12 dimer (A) and 2G12 trimer (B). The connectivity model allows for the formation of higher order multimers, including tetramers (panel C). (C) Size exclusion chromatography profile for 2G12 proteins after elution from an FcRn affinity column. Peaks labeled as monomer and dimer were identified using in-line static light scattering to determine their molecular masses (West et al., 2009). Peaks migrating at higher apparent molecular weights are labeled as trimer and tetramer.

Figure S2. Heavy atom validation of molecular replacement phases, related to Figure 2

Data were collected from crystals of 2G12 dimer soaked with tantalum bromide clusters to 10 Å resolution at a wavelength of 1.255 Å, chosen to maximize the anomalous diffraction signal of tantalum. Using phases derived from the molecular replacement model, we calculated both anomalous and isomorphous difference Fourier maps, which each yielded a set of peaks, seven of which were common to both maps. We checked the top five potential heavy atom sites by iteratively omitting one site, calculating phases with the remaining sites, and then examining difference Fourier maps to see if the omitted site was found. Two of the five potential sites, iteratively omitted in this way, were independently reproduced. In each calculation of an isomorphous difference Fourier

map during cross-phasing, three additional sites were consistently and independently produced. One site was reproduced in the calculations of anomalous difference Fourier maps during cross-phasing. We concluded that the three sites that survived the cross-phasing process after appearing consistently in both isomorphous and anomalous difference Fourier maps corresponded to tantalum bromide clusters. The putative tantalum bromide sites corresponded to locations on the surface of the 2G12 dimer model. (A) Heavy atom sites (colored spheres) on dimer B/C from Figure 2. (B) Heavy atom sites on dimer A from Figure 2.

Figure S3. Packing of 2G12/2G12.1 peptide crystals, related to Figure 3

Half of a unit cell containing three copies of the asymmetric unit in space group P6 is shown. The asymmetric unit contains one intact 2G12 dimer (two $(Fab)_2$ units and two Fcs; yellow Ca trace) and half of a second 2G12 dimer (one $(Fab)_2$ unit and one Fc; magenta Ca trace). Rotation around a crystallographic two-fold axis creates the second half of the magenta dimer, which is conformationally the same as the yellow dimer. (A) Green circles show locations of antigen binding sites, which do not contact each other in the P6 crystals. Addition of 2G12.1 peptide to 2G12 dimer disrupted the crystal contacts at the antigen binding sites in the $P6_122$ 2G12 dimer crystals (Figure 2A). (B) Blue circles highlight crystal contacts between Fc regions. Similar crystal contacts were found in the $P6_122$ 2G12 dimer crystals (Figures 2C, 3C). (C) 2G12/2G12.1 structure shown as a volume representation (Figure 4C) superimposed on the locations of the yellow dimers (left) and magenta dimers (right).

Figure S4. Distinct 2G12 dimer structures, related to Figure 4

Dimer structures are shown as 25 Å electron density envelopes calculated from $(Fab)_2$ and Fc coordinates located by molecular replacement calculations. Side indicates dimers shown with side views of $(Fab)_2$ units, top indicates a view in which Fc regions point into the page, and bottom indicates a view in which Fc regions point out of the page. (A) Dimer A from Figure 2 (cyan) (Figure 4A). (B) Dimers B and C from Figure 2 (magenta and indigo) (Figure 4B). (C) Dimer from 2G12/2G12.1 peptide structure (Figure 4C). The symmetry of two of the 2G12 dimer conformations, dimer A and the dimer in the 2G12/2G12.1 peptide structure (panels A and C), was point group C2 (the dimer two-fold symmetry axis was coincident with a crystallographic two-fold axis). The dimer B/C conformation (panel B) represented a distortion from C2 symmetry. A 2G12 dimer could also have point group D2 symmetry with the $(Fab)_2$ units in a similar position as in a C2 dimer except with their internal two-fold axes coincident, and with the Fcs above and below the plane of the $(Fab)_2$ units with the Fc two-fold axes coincident with each other and perpendicular to the $(Fab)_2$ two-fold axes. Although the D2 conformation appeared plausible, it was not observed in our structures. To interconvert these forms would require one $(Fab)_2$ unit to rotate 180˚.

Figure S5. SAXS Data for 2G12 monomer, dimer, and a conventional IgG monomer, related to Figure 5

Ab initio models filled with dummy atoms revealing size and shape of (A) 2G12 monomer, (B) 2G12 dimer, and (C) Rituximab, a conventional IgG monomer. (D) Pair-

distribution functions and Guinier plots from 2G12 monomer, dimer, and Rituximab. Guinier plots calculated from low *q* ranges behaved linearly, indicating minimal aggregation (Hammel, 2012; Mertens and Svergun, 2010). Differences in D_{max} calculated from *P(r)* were consistent with 2G12 monomer's comparatively smaller range of motion and Rituximab's more freely mobile domains compared to 2G12 dimer. (E) Data analyses. Left: Scattering profiles of 2G12 monomer, 2G12 dimer, and Rituximab, plotted as log(I) vs. *q*. Profiles from all concentrations of each protein were superimposable when scaled by concentration, indicating low inter-particle forces, properly folded species, and ideal sample quality. Accordingly, one representative scattering profile was chosen from the concentration series for each individual protein, and merging of multiple scattering profiles was not required. Second from left: Traditional Kratky analysis used for detecting conformational flexibility via visual inspection (Putnam et al., 2007). Bimodal profiles for 2G12 dimer and Rituximab revealed behavior similar to that of a heterogeneous mixture of species. 2G12 dimer exhibited a slowly increasing curve at large *q* values, suggesting an elongated species when compared to Rituximab and 2G12 monomer. Third from left: Analysis of samples using Porod-Debye law revealed a loss of plateau in Rituximab when compared with 2G12 monomer, indicating increased flexibility. 2G12 dimer exhibited a divergent curve at large *q* values, characteristic of an elongated species (Hammel, 2012). Right: Simulated scattering from DAMAVER averaged models (red, green, or blue) fit to the experimental scattering data (gray), plotted as log(I) vs. *q*.

Figure S6. SPR sensorgrams containing residuals of 1:1 binding model fits, related to Figure 6

Sensorgrams were derived from binding experiments in which 2G12 monomer, 2G12 dimer, or a conventional monomeric anti-gp120 IgG was injected over immobilized gp120 from HIV-1 strain SF162. Experimental data (colored lines) were fit to a 1:1 binding model (black lines). Residual plots are shown in Figure S6. (A) 2G12 monomer, 2G12 dimer, and a conventional anti-gp120 IgG (NIH45-46^{G54W}) injected over gp120 immobilized at high coupling density (~100 RU). 2G12 monomer, but not 2G12 dimer or the conventional IgG, could be fit to a 1:1 binding model. (B) 2G12 monomer, 2G12 dimer, and a conventional anti-gp120 IgG (NIH45-46^{G54W}) injected over gp120 immobilized at medium coupling density (~50 RU). 2G12 monomer, but not 2G12 dimer or the conventional IgG, could be fit to a 1:1 binding model. (C) 2G12 monomer, 2G12 dimer, and a conventional anti-gp120 IgG (2909) injected over gp120 immobilized at low coupling density (<10 RU). All could be fit to a 1:1 binding model.

Supplemental References

Adams, P.D., Afonine, P.V., Bunkoczi, G., Chen, V.B., Davis, I.W., Echols, N., Headd, J.J., Hung, L.W., Kapral, G.J., Grosse-Kunstleve, R.W.*, et al.* (2010). PHENIX: a comprehensive Python-based system for macromolecular structure solution. Acta crystallographica Section D, Biological crystallography *66*, 213-221.

Anderson, D.R., Grillo-Lopez, A., Varns, C., Chambers, K.S., and Hanna, N. (1997). Targeted anti-cancer therapy using rituximab, a chimaeric anti-CD20 antibody (IDEC-C2B8) in the treatment of non-Hodgkin's B-cell lymphoma. Biochemical Society transactions *25*, 705-708.

Artimo, P., Jonnalagedda, M., Arnold, K., Baratin, D., Csardi, G., de Castro, E., Duvaud, S., Flegel, V., Fortier, A., Gasteiger, E.*, et al.* (2012). ExPASy: SIB bioinformatics resource portal. Nucleic acids research *40*, W597-603.

Burmeister, W.P., Huber, A.H., and Bjorkman, P.J. (1994). Crystal structure of the complex of rat neonatal Fc receptor with Fc. Nature *372*, 379-383.

Franke, D.S., D. I. (2009). DAMMIF, a program for rapid ab-initio shape determination in small-angle scattering. J Appl Cryst *42*, 342-346.

Hammel, M. (2012). Validation of macromolecular flexibility in solution by small-angle X-ray scattering (SAXS). European biophysics journal : EBJ *41*, 789-799.

Huber, A.H. (1994). Biochemical and Structural Characterization of Drosophila Neuroglian. In Division of Biology (Pasadena, CA: California Institute of Technology).

Huber, A.H., Kelley, R.F., Gastinel, L.N., and Bjorkman, P.J. (1993). Crystallization and stoichiometry of binding of a complex between a rat intestinal Fc receptor and Fc. Journal of molecular biology *230*, 1077-1083.

Hummel, J.P., and Dreyer, W.J. (1962). Measurement of protein-binding phenomena by gel filtration. Biochimica et biophysica acta *63*, 530-532.

Konarev, P.V., Volkov, V. V, Sokolava, A. V., Koch, M. H. J., and Svergun, D. I. (2003). PRIMUS - a Windows-PC based system for small-angle scattering data analysis. . J Appl Cryst *36*, 1277-1282.

Mertens, H.D., and Svergun, D.I. (2010). Structural characterization of proteins and complexes using small-angle X-ray solution scattering. Journal of structural biology *172*, 128-141.

Petoukhov, M.V., Franke, D., Shkumatov, A.V., Tria, G., Kikhney, A.G., Gajda, M., Gorba, C., Mertens, H.D.T., Konarev, P.V., and Svergun, D.I. (2012). New developments in the ATSAS program package for small-angle scattering data analysis. Journal of applied crystallography *45*, 342-350.

Potterton, E., Briggs, P., Turkenburg, M., and Dodson, E. (2003). A graphical user interface to the CCP4 program suite. Acta crystallographica Section D, Biological crystallography *59*, 1131-1137.

Putnam, C.D., Hammel, M., Hura, G.L., and Tainer, J.A. (2007). X-ray solution scattering (SAXS) combined with crystallography and computation: defining accurate macromolecular structures, conformations and assemblies in solution. Quarterly reviews of biophysics *40*, 191-285.

Read, R.J.S., A. J. (1988). A phased translation function. J Appl Cryst *21*, 490-495.

Sanchez, L.M., Penny, D.M., and Bjorkman, P.J. (1999). Stoichiometry of the interaction between the major histocompatibility complex-related Fc receptor and its Fc ligand. Biochemistry *38*, 9471-9476.

Sharma, V.A., Kan, E., Sun, Y., Lian, Y., Cisto, J., Frasca, V., Hilt, S., Stamatatos, L., Donnelly, J.J., Ulmer, J.B.*, et al.* (2006). Structural characteristics correlate with immune responses induced by HIV envelope glycoprotein vaccines. Virology *352*, 131-144.

Smolsky, I., Liu, P., Niebuhr, M., Ito, K., Weiss, T. M., Tsuruta, H. (2007). Biological small-angle X-ray scattering facility at the Stanford Synchrotron Radiation Laboratory. J Appl Cryst *40*, 453-458.

Svergun, D.I. (1992). Determination of the regularization parameter in indirect-transform methods using perceptual criteria J Appl Cryst *25*, 495-503.

Volkov, V.S., D. (2003). Uniqueness of ab-initio shape determination in small-angle scattering. J Appl Cryst *36*, 860-864.

West, A.P., Jr., and Bjorkman, P.J. (2000). Crystal structure and immunoglobulin G binding properties of the human major histocompatibility complex-related Fc receptor(,). Biochemistry *39*, 9698-9708.

West, A.P., Jr., Galimidi, R.P., Foglesong, C.P., Gnanapragasam, P.N., Huey-Tubman, K.E., Klein, J.S., Suzuki, M.D., Tiangco, N.E., Vielmetter, J., and Bjorkman, P.J. (2009). Design and expression of a dimeric form of human immunodeficiency virus type 1 antibody 2G12 with increased neutralization potency. Journal of virology *83*, 98-104.

Winn, M.D., Ballard, C.C., Cowtan, K.D., Dodson, E.J., Emsley, P., Evans, P.R., Keegan, R.M., Krissinel, E.B., Leslie, A.G., McCoy, A.*, et al.* (2011). Overview of the CCP4 suite and current developments. Acta crystallographica Section D, Biological crystallography *67*, 235-242.

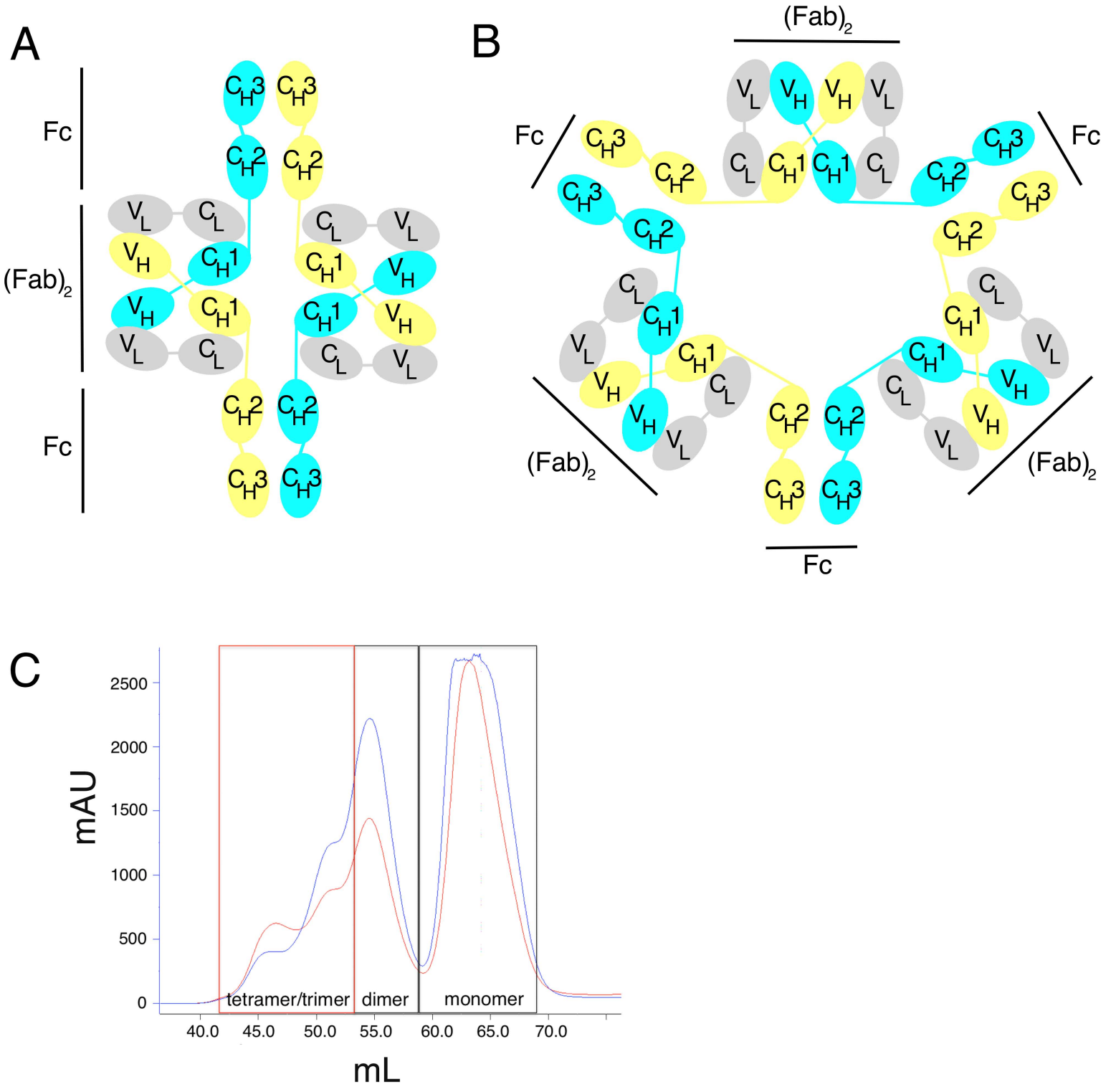

Figure S1, related to Figure 1

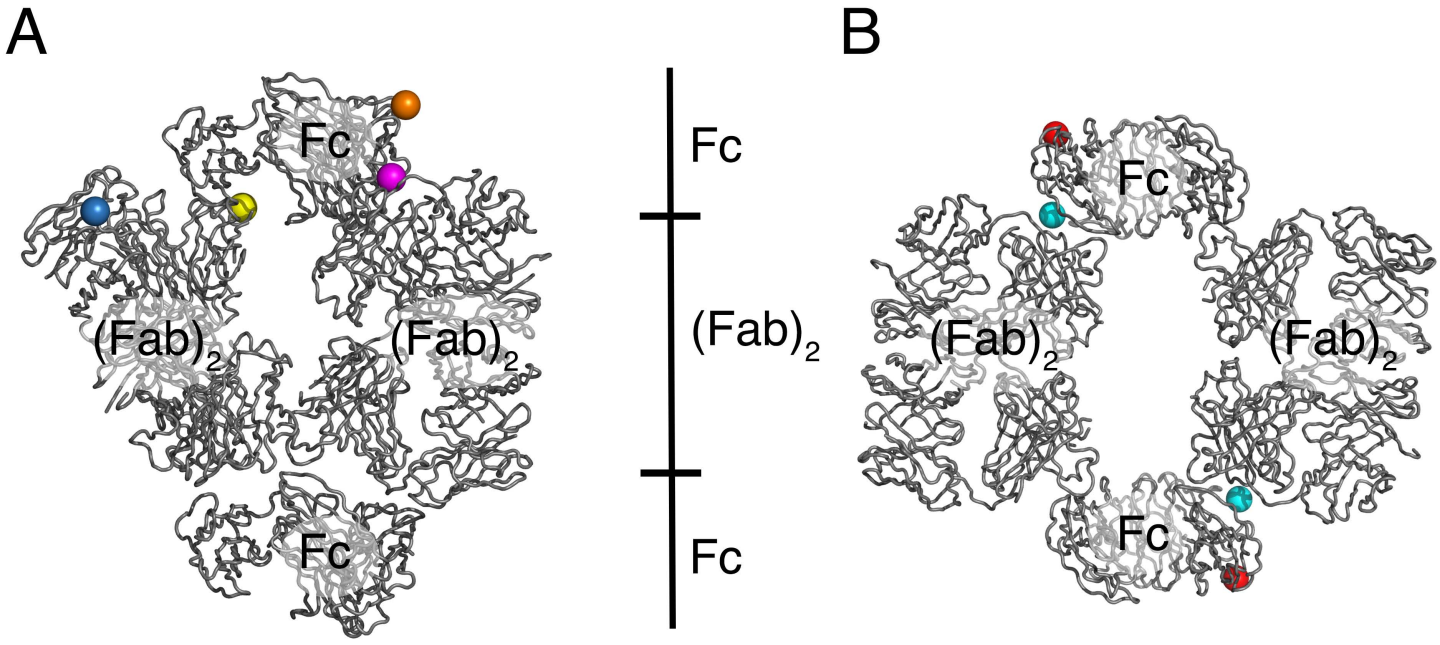

Figure S2, related to Figure 2

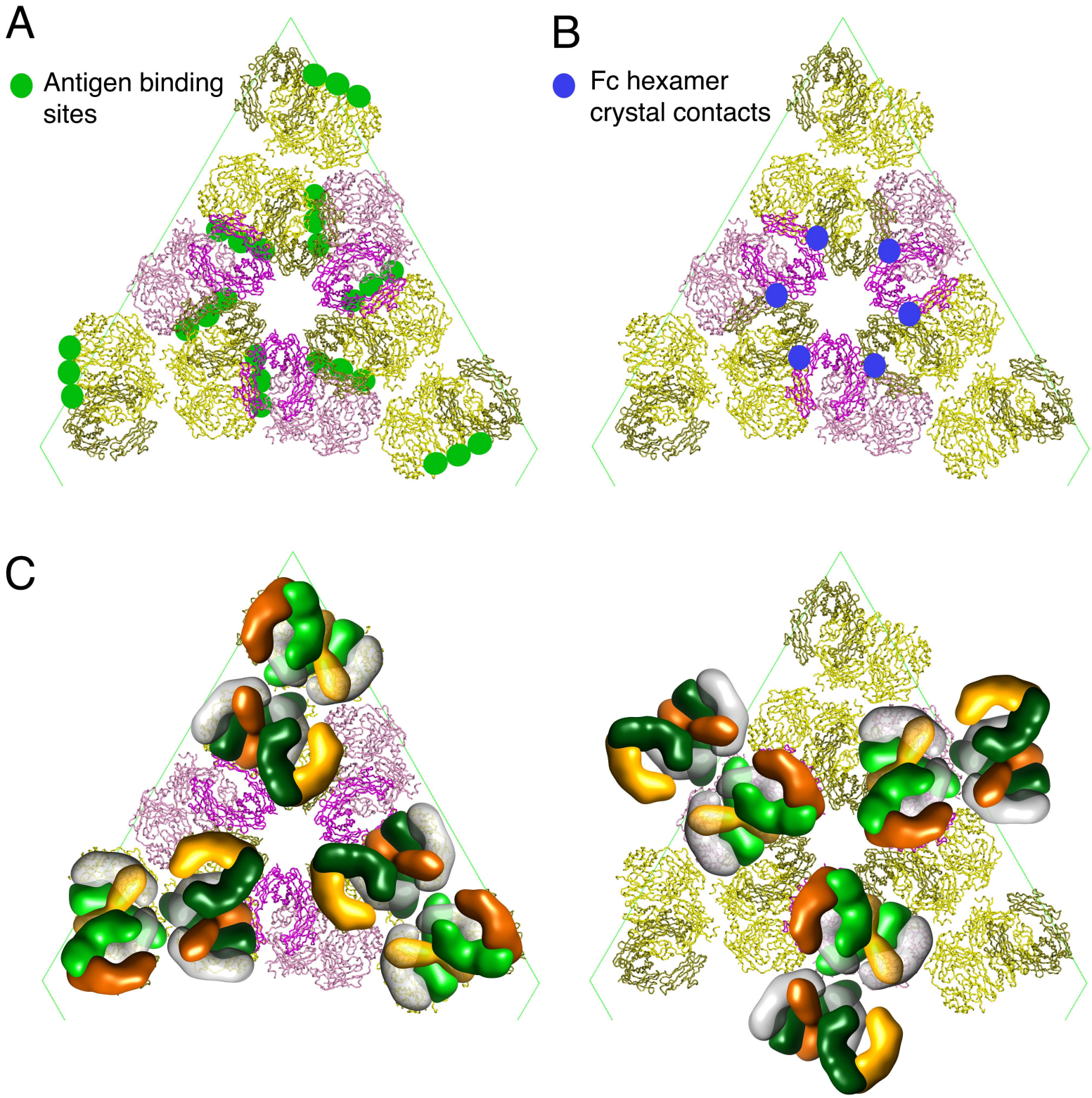

Figure S3, related to Figure 3

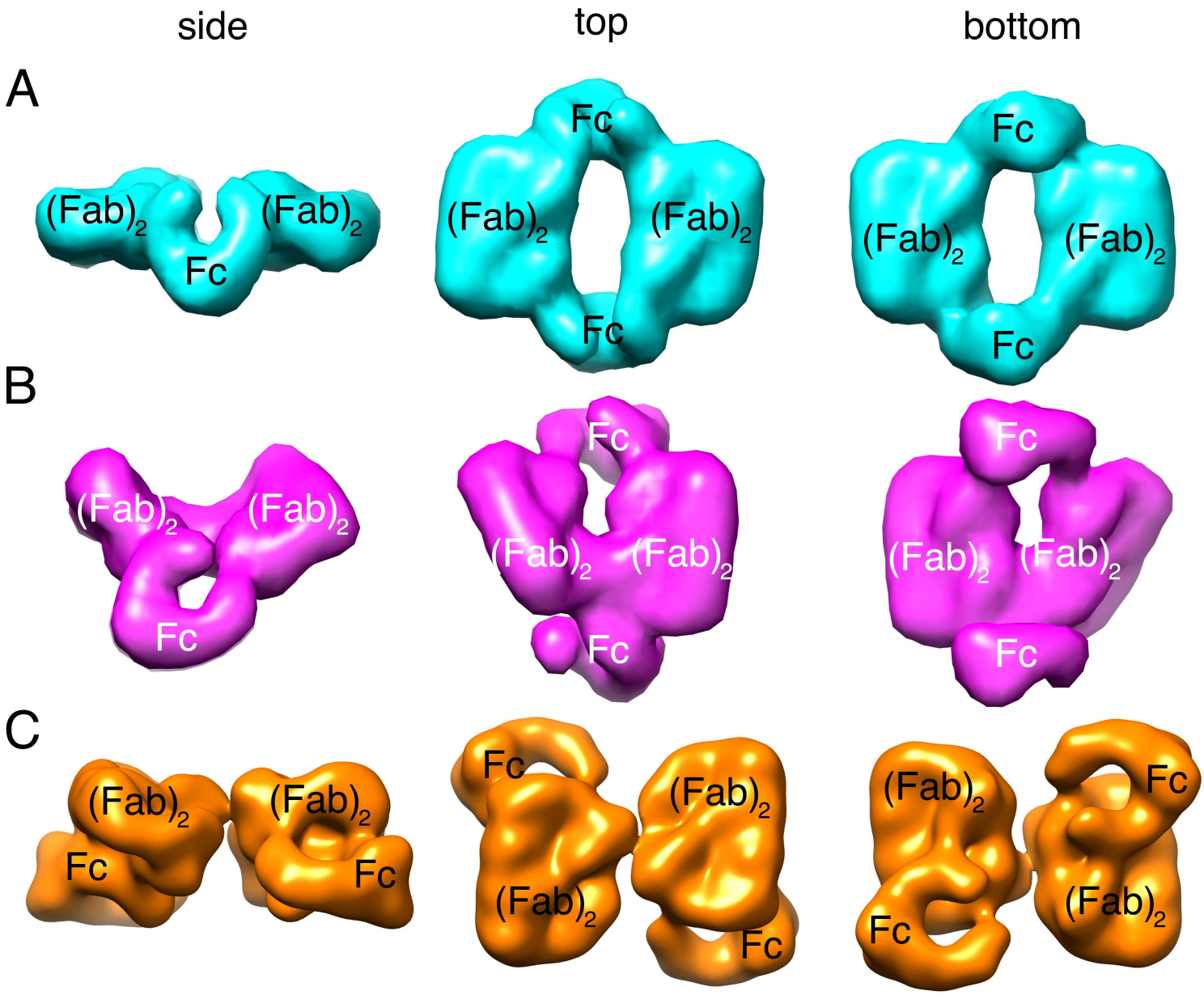

Figure S4, related to Figure 4

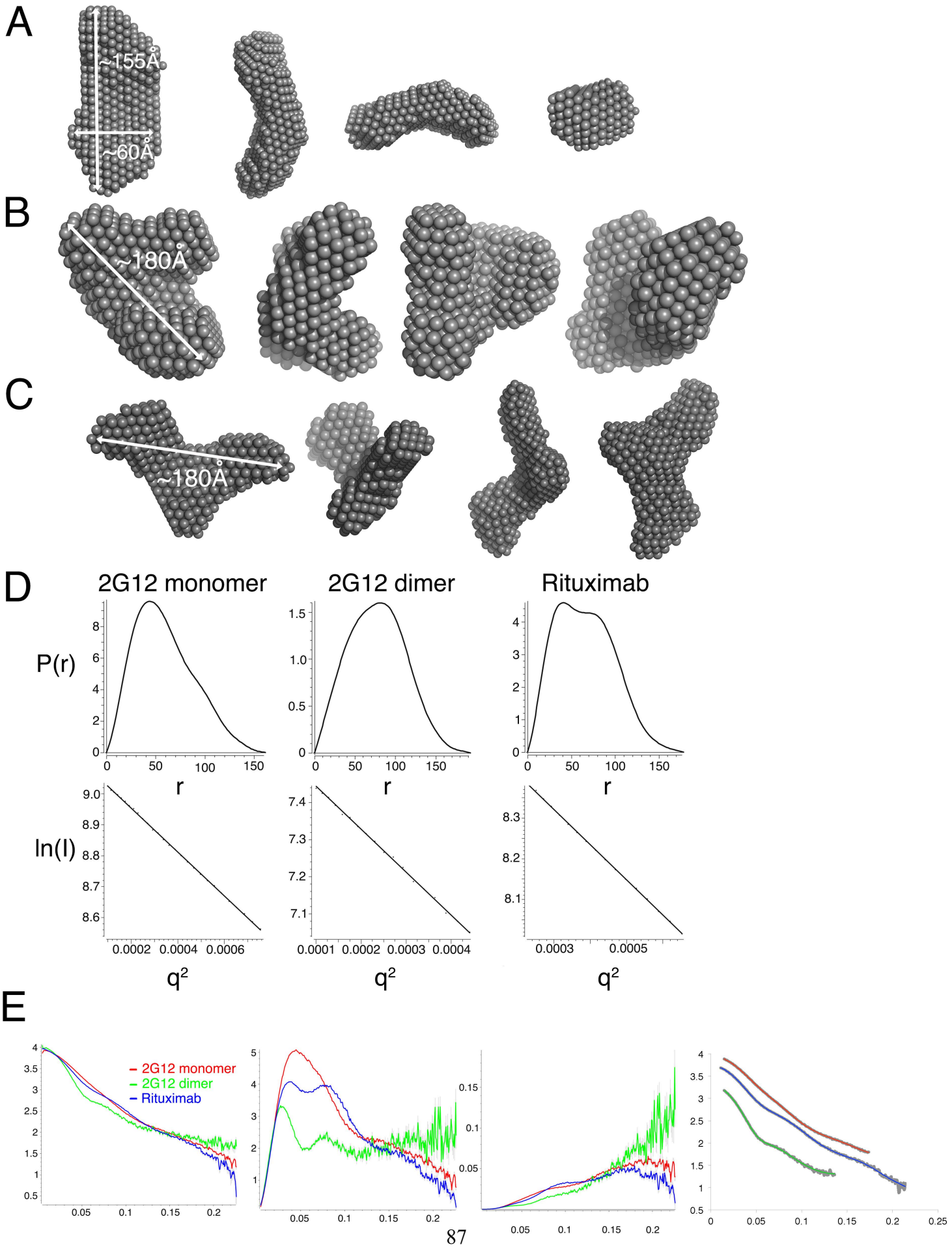

Figure S5, related to Figure 5

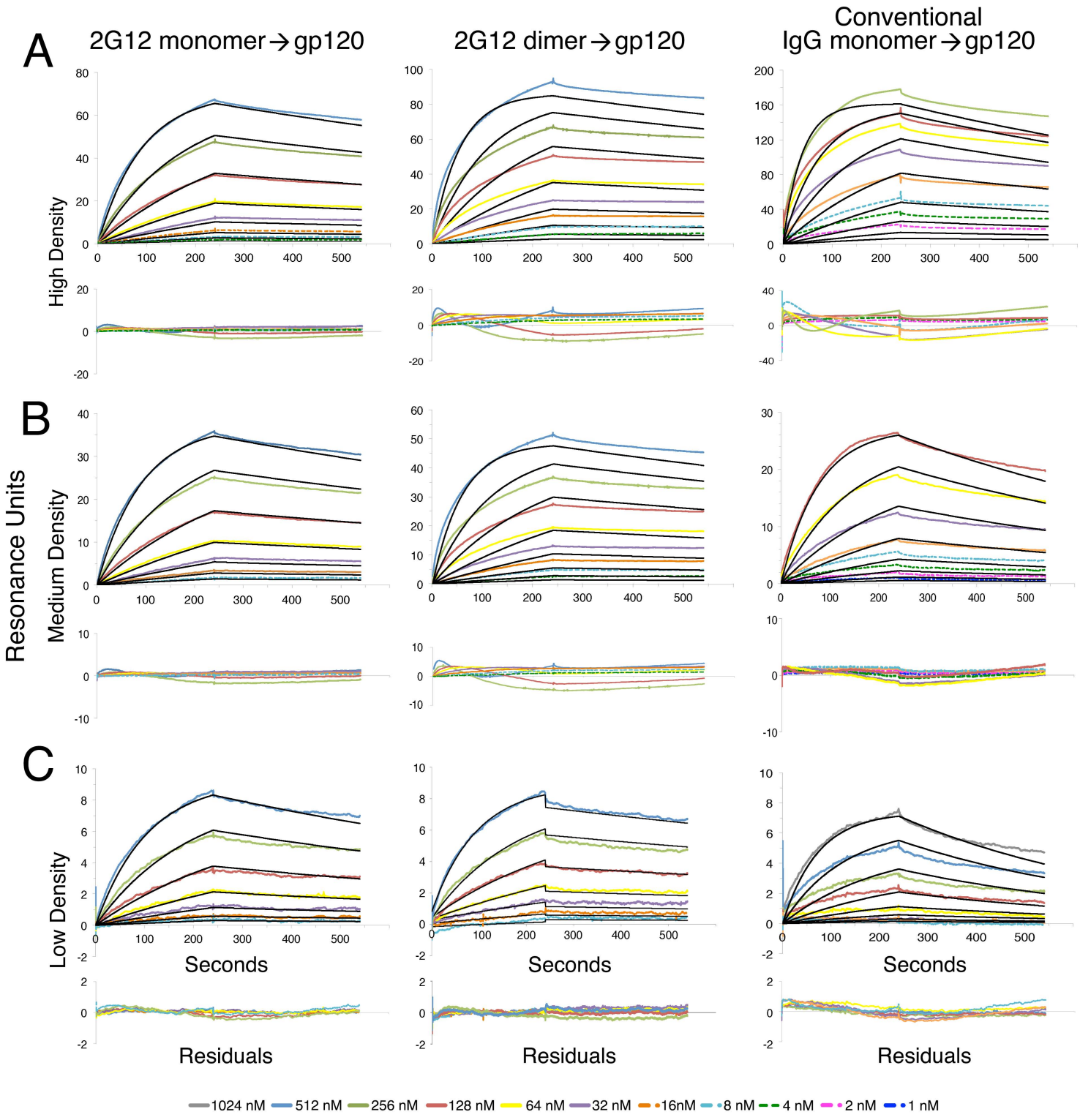

Figure S6, related to Figure 6

Ringe, R.P., Sanders, R.W., Yasmeen, A., Kim, H.J., Lee, J.H., Cupo, A., Korzun, J., Derking, R., van Montfort, T., Julien, J.P., *et al.* (2013). Cleavage strongly influences whether soluble HIV-1 envelope glycoprotein trimers adopt a native-like conformation. Proceedings of the National Academy of Sciences of the United States of America *110*, 18256-18261.

Sanders, R.W., Derking, R., Cupo, A., Julien, J.P., Yasmeen, A., de Val, N., Kim, H.J., Blattner, C., de la Pena, A.T., Korzun, J., *et al.* (2013). A next-generation cleaved, soluble HIV-1 Env trimer, BG505 SOSIP.664 gp140, expresses multiple epitopes for broadly neutralizing but not non-neutralizing antibodies. PLoS pathogens *9*, e1003618.

Sanders, R.W., Vesanen, M., Schuelke, N., Master, A., Schiffner, L., Kalyanaraman, R., Paluch, M., Berkhout, B., Maddon, P.J., Olson, W.C., *et al.* (2002). Stabilization of the soluble, cleaved, trimeric form of the envelope glycoprotein complex of human immunodeficiency virus type 1. Journal of virology *76*, 8875-8889.

Scharf, L., Scheid, J.F., Lee, J.H., West, A.P., Jr., Chen, C., Gao, H., Gnanapragasam, P.N., Mares, R., Seaman, M.S., Ward, A.B., *et al.* (2014). Antibody 8ANC195 reveals a site of broad vulnerability on the HIV-1 envelope spike. Cell reports *7*, 785-795.

Zhang, C.W., Chishti, Y., Hussey, R.E., and Reinherz, E.L. (2001). Expression, purification, and characterization of recombinant HIV gp140. The gp41 ectodomain of HIV or simian immunodeficiency virus is sufficient to maintain the retroviral envelope glycoprotein as a trimer. The Journal of biological chemistry *276*, 39577-39585.

Chapter 3

Structure of an HIV-2 gp120 envelope glycoprotein in complex with CD4

Introduction

Human immunodeficiency virus type 1 (HIV-1) remains a threat to global public health. With no vaccine available, it disproportionately causes acquired immunodeficiency syndrome (AIDS) in the developing world. While the related virus HIV-2 is still capable of causing full-blown AIDS, infection rates are more localized and on the decline (de Silva et al., 2008; Kong et al., 2012a; Kong et al., 2012b). In contrast to patients infected with HIV-1, the majority of HIV-2 patients remain asymptomatic with low plasma viral loads and normal CD4+ T cell counts (Berry et al., 1998; Jaffar et al., 1997; van der Loeff et al., 2010). HIV-2 is a robust immunogen in natural infection, and patients generally make high titer, broadly reactive, and very strongly neutralizing antibodies against primary strains – something rarely seen in HIV-1 infection (de Silva et al., 2008; Kong et al., 2012a; Kong et al., 2012b). In addition, neutralizing antibodies emerge readily after HIV-2 infection, whereas this process in HIV-1 can take many years (Kong et al., 2012a; Kong et al., 2012b). In spite of the presence of a robust immune response, HIV-2 appears slower to evolve the neutralization-resistant variants so commonly found in HIV-1 infections (de Silva et al., 2008; MacNeil et al., 2007). For cohorts in the same population, vertical transmission of HIV-2 via breastfeeding from mother to child without antiretroviral therapy (ART) is less than 4%, compared with over 24% for HIV-1 (O'Donovan et al., 2000).

The bulk of current investigative efforts in the HIV field are focused on HIV-1 due to its high virulence and transmissibility. However, the immune response in the context of HIV-2 infection may provide a natural model of effective HIV control. While HIV-2 is not an attenuated virus, infected patients seem to naturally exhibit characteristics of a desired response to an effective therapy against HIV-1. Therefore, a deeper understanding of the immune response against HIV-2 should reveal insight into the missing pieces required to elicit a similar response against HIV-1. While the features of an "ideal" immune response remain unclear, a study of patient serum dually infected with HIV-1 and -2 (HIV-D) found that neutralizing activity existed only against HIV-2 (Schim van der Loeff et al., 2002). This suggests the presence of distinct and divergent immune responses against these related viruses. In addition, HIV-2 is more closely related to Simian Immunodeficiency Virus (~80% amino acid identity in envelope glycoprotein) than it is to HIV-1. Therefore, knowledge about HIV-2 pathogenicity in the context of an immune response can inform our understanding of ongoing studies using SIV and simian-human immunodeficiency virus (SHIV)-macaque infection models (Kong et al., 2012b).

HIV-1 and HIV-2 share 30% sequence identity and 40% amino acid identity in their envelope glycoprotein (env) gp160 (Kong et al., 2012a; Kong et al., 2012b; Kwong et al., 1998). Much has been uncovered over the last 30 years about the role of the HIV-1 env as an antigen, with a wealth of recent insight from its sensitivity to broadly-neutralizing antibodies. Env is the only known target of such antibodies, and understanding its interactions with the immune system is invaluable for rational immunogen and prophylactic design. Infected patients have the capability to make

antibodies against many epitopes on gp120: the variable loops, the conserved CD4 binding site, the CD4i or co-receptor binding site, various glycans, and the membrane proximal region of gp41, among others (Kwong and Mascola, 2012). 10-20% of these HIV-1 infected subjects are able to make broadly neutralizing antibodies in low titers, and these have been the subject of intense study, structural and otherwise. Despite the high sequence identity between HIV-1 and HIV-2, neutralizing antibodies generally do not cross-react between the two viruses outside of a few highly conserved epitopes (Decker et al., 2005; Kong et al., 2012a).

Despite the growing collection of HIV-1 gp120 and gp140 trimer structures from X-ray crystallography and electron microscopy, no structures of HIV-2 gp120 exist. To investigate possible explanations for its decreased pathogenicity and increased immunogenicity compared with HIV-1, we solved the structure of a HIV-2 gp120 core from the ST strain in complex with the first two domains of the CD4 host receptor. ST gp120 exhibits only ~35% sequence identity with HIV-1 gp120 strains, and we compared it here to known HIV-1 gp120 core crystal structures with or without CD4 bound. It is our hope that this represents the first of many structural studies of HIV-2 envelope glycoprotein, as insights gained from this natural form of HIV viral control may inform therapy and immunogen design for HIV-1.

Results

Crystallization of the HIV-2 gp120 core with sCD4 D1D2

Sequences for gp120 from strains HIV-2_{UC1}, HIV-2_{ST}, HIV-$2_{7312A\text{-}0303}$, and HIV-$2_{7312A\text{-}9217}$ were obtained from the Los Alamos National Laboratory HIV Sequence Database (http://www.hiv.lanl.gov/). These strains were chosen based on availability and completeness of sequences as well as demonstrated sensitivity to newly isolated anti-HIV-2 gp120 monoclonal antibodies with known epitopes. As no previous structures of HIV-2 gp120 exist, we attempted to create crystallization constructs adapted from the HIV-1 gp120 core convention: deletions of the V1/V2 and V3 variable loops as well as a portion of the C-terminus (Kwong et al., 1998). While the HIV-2 sequences align unambiguously with HIV-1 gp120, we have no information about the importance of glycans attached to potential *N*-linked glycosylation sites in the folding process of HIV-2 gp120. Therefore, we only mutated one conserved site (T89I) distal from predicted binding interfaces.

After screening several combinations of anti-HIV-2 and anti-HIV-1 antibody Fab fragments, CD4 N-terminal domains D1 and D2 (sCD4 D1D2), and HIV-2 gp120 cores from different strains, we obtained crystals of HIV-2 gp120 core from the ST strain in complex with sCD4 D1D2. Co-crystals of gp120/CD4 diffracted to 2.5 Å resolution at the SSRL beamline 12-2, with collected data usable up to 3.0 Å as indicated by the CC½ statistic (Karplus and Diederichs, 2012). Data were processed using XDS, and crystals were in space group $C222_1$ with unit cell dimensions of a=94.276, b=100.223, c=199.139 (Table 1). Using high-resolution structures for sCD4 D1D2 (pdb ID 2NXY, 100% sequence identity) and core HIV-1 gp120 CAP210 (pdb ID 3LQA, 36% sequence

identity) as search models, Phaser (McCoy et al., 2007) successfully placed gp120 by molecular replacement. Upon fixing this partial solution, sCD4 was placed at the expected location for engaging gp120, with one gp120/sCD4 complex in the asymmetric unit. Prior to rebuilding, initial refinement of the molecular replacement model resulted in R_{work}/R_{free} values of 42%/48%, indicative of significant discrepancies between the search model and data. Many rounds of manual rebuilding and refinement were performed, which were complicated by low data quality and poor electron density maps in various regions. In all, 46 out of 339 residues in the HIV-2 gp120 core and 31 out of 181 residues in sCD4 D1D2 were disordered. The D2 domain of sCD4 exhibited especially poor density, as it lacked stabilizing crystal contacts. Manual rebuilding was guided by a simulated annealing composite omit map to minimize model bias (Brunger and Rice, 1997), and the final structure was refined to R_{work}/R_{free} values of 24.5%/29.8% (Table 1).

	$gp120_{ST}$/CD4
Data Collection	
Resolution (Å)	99.6-3.0 (3.1-3.0)
Space group	$C222_1$
Unit cell	$a = 94.3$ Å $b = 100$ Å $c = 200$ Å $\alpha = \beta = \gamma = 90°$
Total reflections	85946 (8705)
Unique reflections	19116 (1901)
Completeness (%)	99.2 (99.7)
Mean I/σ(I)	12.8 (2.3)
R_{merge}	0.081 (0.82)
CC½	1.0 (0.84)
CC*	1.0 (0.96)
Refinement	
R_{work} (%)	24.5 (36.6)
R_{free} (%)	29.8 (44.2)
Number of atoms	3672
Protein residues	437
RMS bonds (Å)	0.03
RMS angles (°)	1.8
Ramachandran favored (%)	91.7
Ramachandran outliers (%)	1.0
Average B-factor (Å²)	100.6

*Statistics for the highest-resolution shell are shown in parentheses.

Table 1. Data collection and refinement statistics.

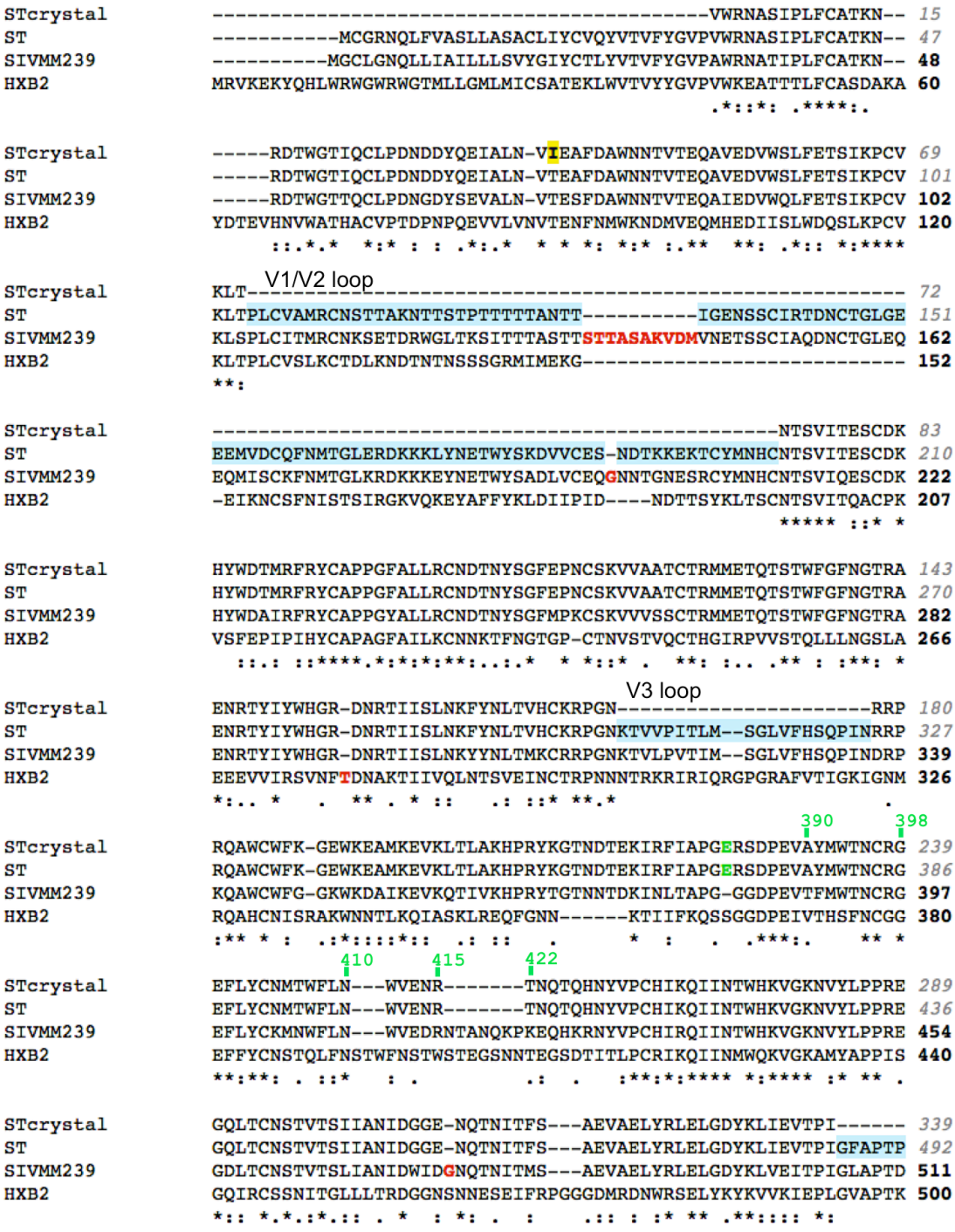

Figure 1. Sequence alignment showing numbering convention for gp120$_{ST}$. ST numbering is according to SIVMM239 convention (Calef, et al, 2001, Los Alamos HIV Sequence Compendium) except where indicated in green. Insertions in SIVMM239 relative to ST are shown in red. Insertion in ST relative to SIVMM239 is shown in green. Blue highlighting indicates crystallographic truncations. HXB2 is included for reference.

Structural overview of HIV-2 gp120 core

The core HIV-2 ST gp120 structure comprises 23 β-strands (β1-23), four a-helices (α1-4), five loop regions A-E, truncated variable loops V1-3, and disordered V4 and V5 loops. Six conserved disulfide bonds were clearly visible in electron density and superimposed well with disulfides in other HIV-1 gp120 core structures. Nine putative *N*-linked glycosylation sites (ST numbering according to SIVMAC239 convention, see Figure 1) – N212, N244, N278, N284, N295, N306, N404, N460, and N479 (N197, N229, N263, N269, N280, N291, N389, N446, and N464 in HXB2 numbering, respectively) showed visible density for sugar residues (Figure 2). Only two of these ($N263_{HXB2}$ and $N389_{HXB2}$) are also glycosylation sites in 93TH057 gp120. The overall architecture of ST gp120 was nearly identical to that of other HIV-1 gp120s. Superposition with HIV-1 gp120s resulted in Cα backbone R.M.S.D. values between 1.5-1.6 Å. Inner and outer domains could be unambiguously assigned (Figure 2). There were no notable global conformational or secondary structure deviations from existing HIV-1 gp120 structures, though potentially significant local differences exist.

Beginning with the inner domain (Figure 2), no visible density was seen for the first seven residues of the N-terminus, and a short seven-residue region (Figure 2, yellow) of the β-2 strand was placed into density by unambiguous superposition with 93TH057 gp120 from pdb 3U7Y (corresponding to residues 51-57 in 93TH057/HXB2). The intact trace begins at residue $D63_{ST}$ ($D81_{HXB2}$), three residues earlier than the start of the original HxBc2 gp120 core structure (Kwong 1998). β-strands 1-8 and α-1 helix were well aligned to HIV-1 gp120, with some discrepancy between ST and 93TH057 at the

stumps of the truncated V1/V2 loop. The loop region between β-3 and β-4 in ST corresponding to the putative position of the disordered α-0 helix clashed with the loop regions around the position of α-0 helix in 93TH057 gp120, indicating a possible alternative conformation for this helix in ST gp120.

In the outer domain (Figure 2, mint green), secondary structure elements remained well aligned to HIV-1 gp120. Loops C and D were both slightly offset from their counterparts in 93TH057. It has been postulated that HIV-2 has a more open V3 loop conformation than HIV-1 due to HIV-2 having fewer potential N-linked glycosylation sites (Shi et al., 2005).

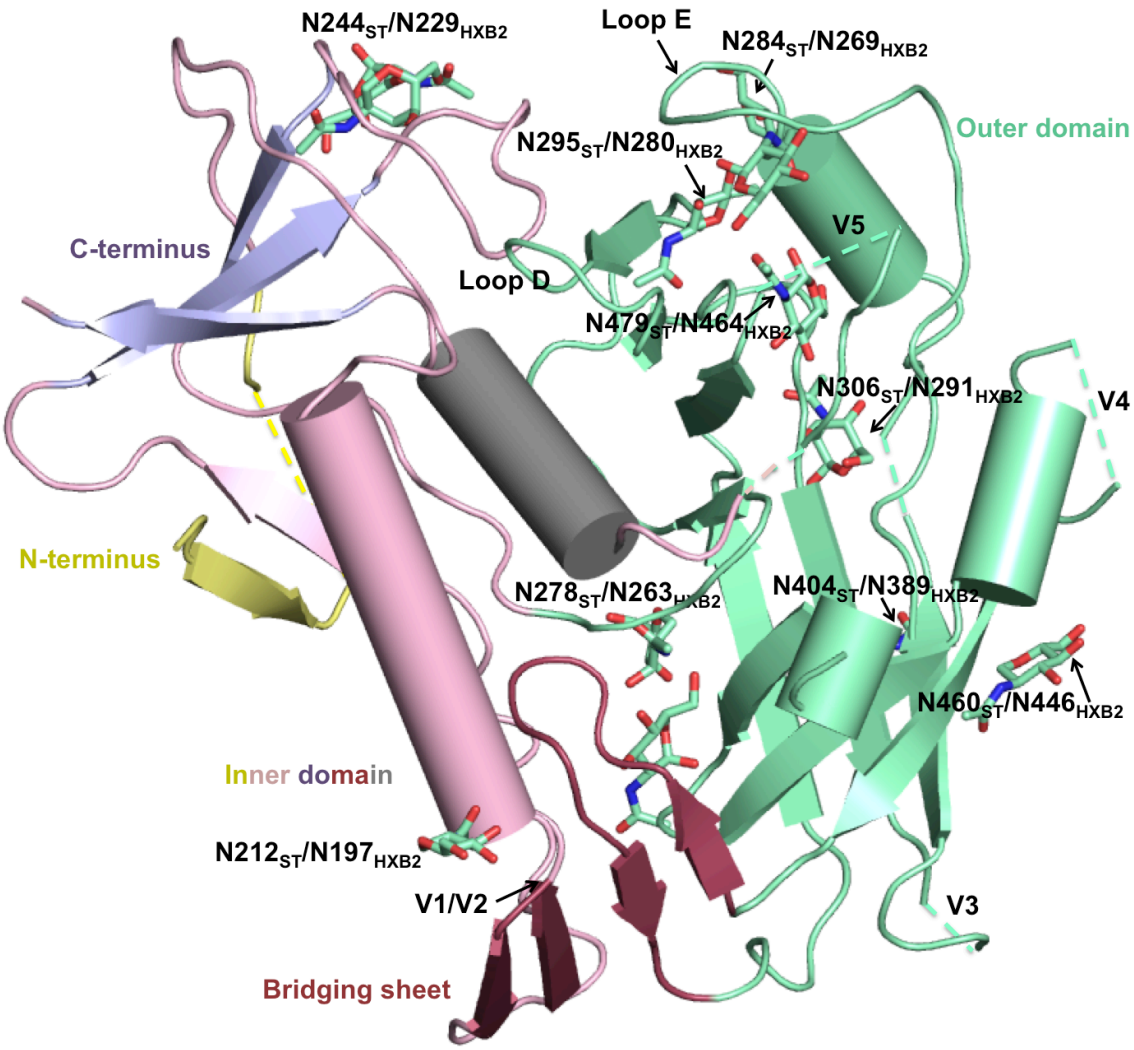

Figure 2. Structural overview of HIV-2 gp120 in cartoon representation, with modeled glycans as sticks. Outer domain is in mint green, inner domain is in yellow, pink, lavender, raspberry, and gray. Disordered loops are represented by dashed lines. Glycan residues are shown in ball-and-stick representation and numbered according to ST and HXB2 convention.

However, the ST structure has a truncated V3 stem with the same number of residues as 93TH057 from pdb 3U7Y and ten more residues than the original HxBc2 gp120 structure from pdb 2NXY. The ST and 93TH057 V3 stems of equal length superimpose with RMSD = 0.46 Å, so the discovery of any differences between HIV-1 and HIV-2 would require future comparison of structures with an intact V3 loop. Loop E in HIV-2 gp120 is three to five residues longer than in HIV-1, and features a turn not seen in HIV-1 gp120 structures. The V4 and V5 loops in the ST structure, which in HIV-2 are shorter and less glycosylated than in HIV-1, were completely disordered.

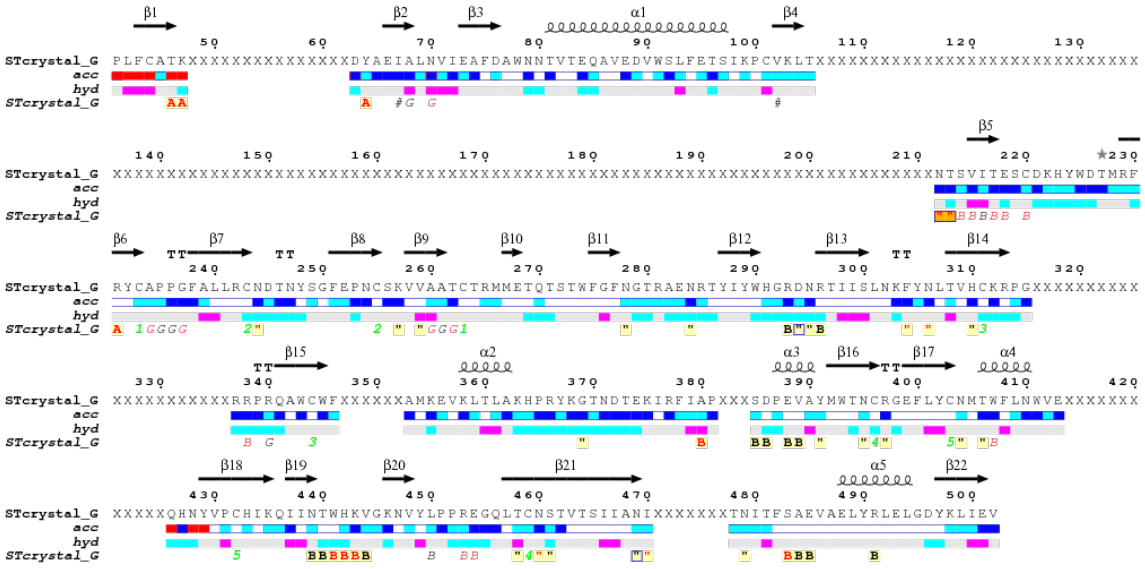

<u>Figure 3.</u> Sequence of ST gp120 crystal structure showing only ordered residues. Secondary structure (shown above sequence) and contacts with CD4 (indicated below bars by black or red letter "B" on yellow background, non-italicized). Disordered residues are shown as "X" in the sequence. Relative accessibility "acc" is indicated in the bar directly below the sequence: white is buried, cyan is intermediate, and blue is accessible. Hydropathy "hyd" is indicated in the lowermost bar below the sequence: pink is hydrophic, gray is intermediate, and cyan is hydrophilic.

Comparison to CD4-bound and unbound HIV-1 gp120 structures

The ST gp120/CD4 structure superimposed with HIV-1 gp120/CD4 structures using sequence-based alignment in PyMOL (The PyMOL Molecular Graphics System, Schrödinger, LLC) with RMSD between 1.5-1.6 Å (Figure 5). ST gp120 contacted CD4 at the residues expected from HIV-1 gp120/CD4 co-crystal structures (specifically, residues 278-281$_{HXB2}$, 365-6$_{HXB2}$, 370-371$_{HXB2}$, 373-374$_{HXB2}$, 425-430$_{HXB2}$, 455-456$_{HXB2}$, 472-474$_{HXB2}$, and 480$_{HXB2}$ (Figure 3).

Analysis of structural and sequence conservation between ST gp120 and the top seven most similar HIV-1 gp120 core structures in the PDB (4DVR, 3TGR, 1G9N, 3U7Y, 4JM2, 2NY0, 1GC1) using EndScript (Robert and Gouet, 2014) showed high degrees of sequence similarity (75 identical residues) and structural conservation in most regions except for structured loops (Figure 4A and 4B). Loops V3, V4, V5, and E exhibit especially high sequence and structural variation.

A comparison of the ST/CD4 structure to three HIV-1 gp120/CD4 structures revealed no notable difference in the molecular interfaces of CD4 binding to HIV-2 gp120 (Ca backbone R.M.S.D. values ~1.6 Å) (Figure 5A). Loop D in HIV-2, which makes close contacts with CD4, is shifted and conformationally distinct from loop D in HIV-1 (Figure 5B). Notably, position 280$_{HXB2}$/295$_{ST}$ in all HIV-1 and HIV-2 features a conserved asparagine, but position 297$_{ST}$/282$_{HXB2}$ in HIV-2 is a threonine, making N295$_{ST}$/N280$_{HXB2}$ a potential *N*-linked glycosylation site. Figure 5C shows the position of N280 in aligned HIV gp120 structures, showing that N280 in ST is in a shifted

location relative to HIV-1. There was no appreciable difference between the loop D of the CD4-bound (pdb 4P9H) or unbound (pdb 3U7Y) versions of 93TH057 gp120.

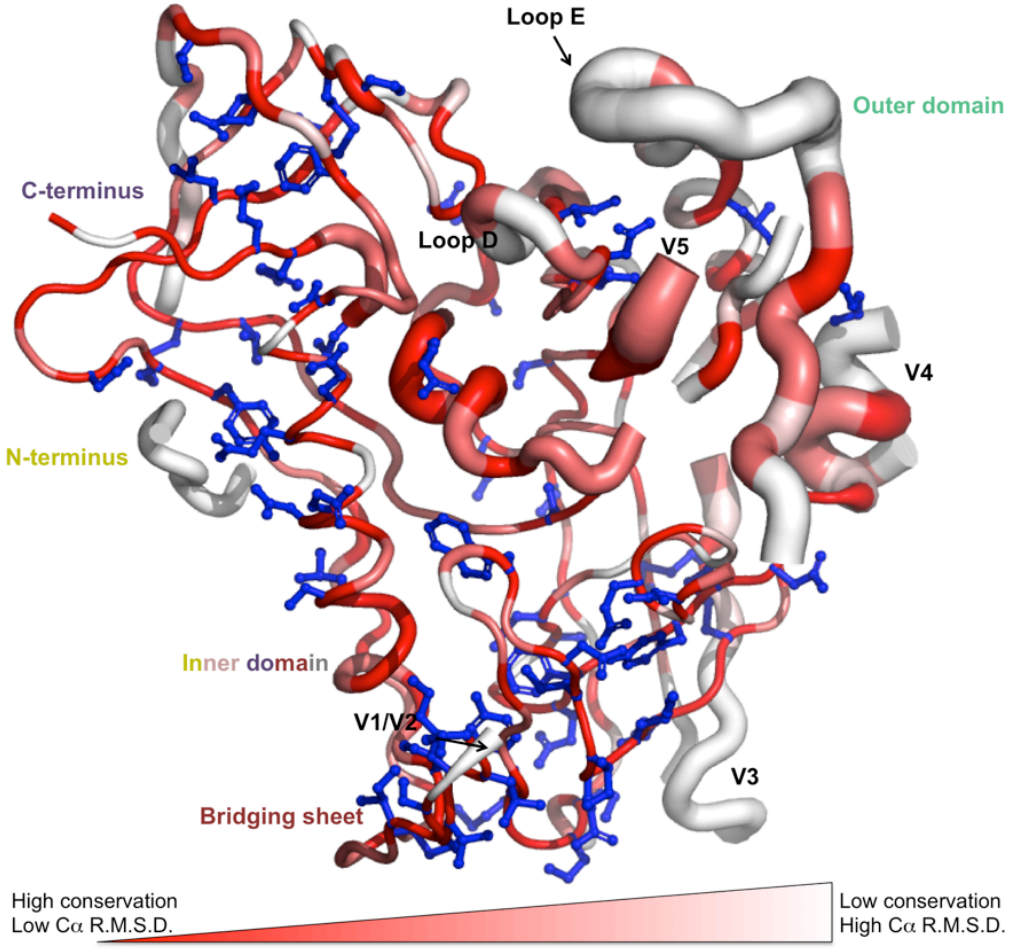

Figure 4A. Analysis of structural and sequence conservation. ST gp120 compared to seven gp120 cores in the Protein Data Bank of highest sequence similarity to ST. Thin sausage indicates high structural similarity, and thick sausage indicates high structural deviation. Red indicates high sequence conservation (identity), and white indicates high sequence variation (lower limit 0.7% equivalent, see Endscript). Identical residues between all eight gp120s are shown in blue stick representation. Sequence alignment from EndScript (Robert and Gouet, 2014) using all eight gp120s is shown below in Figure 4B.

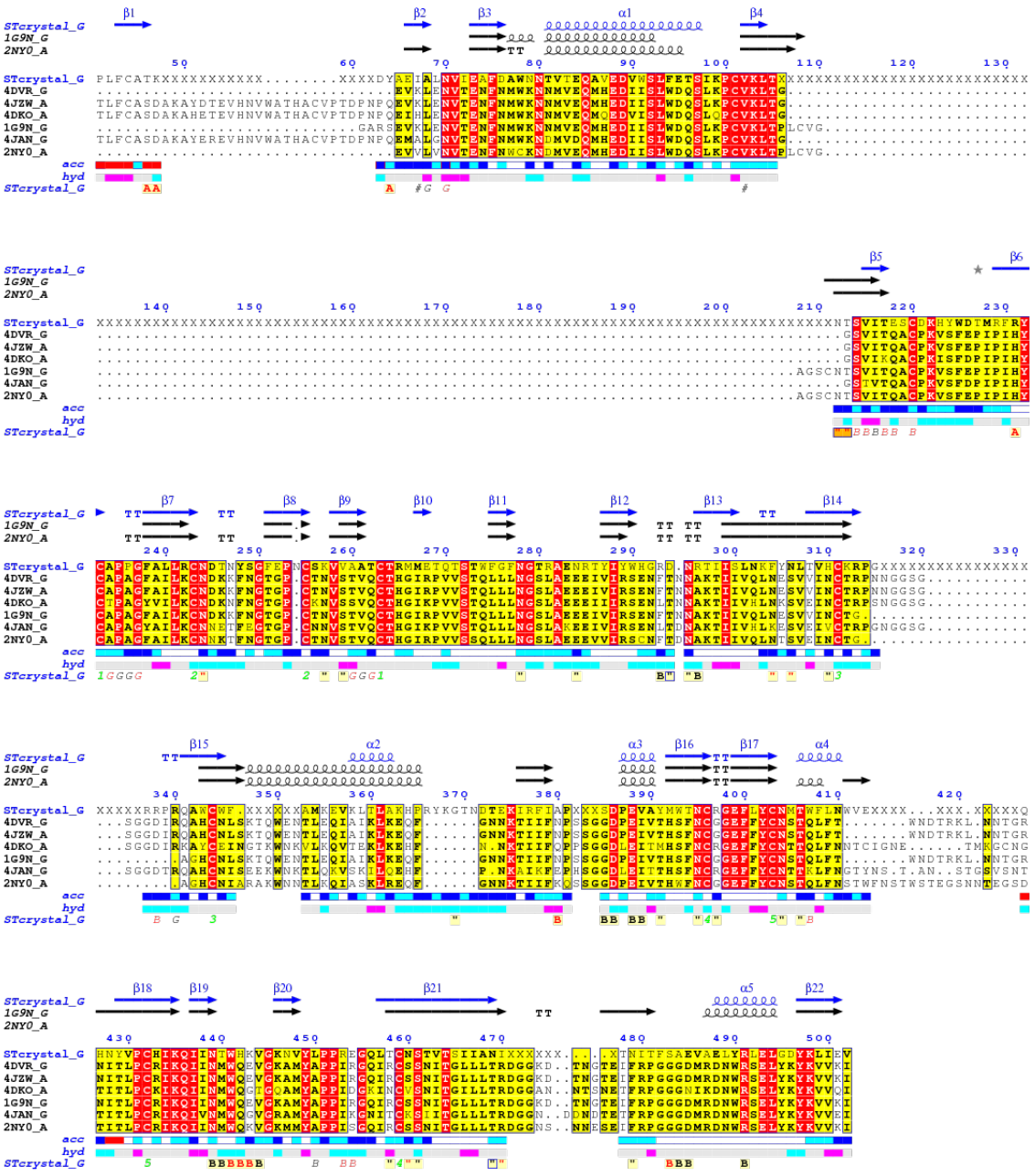

Figure 4B. Sequence alignment of ordered residues in ST gp120 core crystal structure to seven HIV-1 gp120 cores. Identical residues are in red, similar residues in yellow. ST numbering according to SIVMAC239 convention.

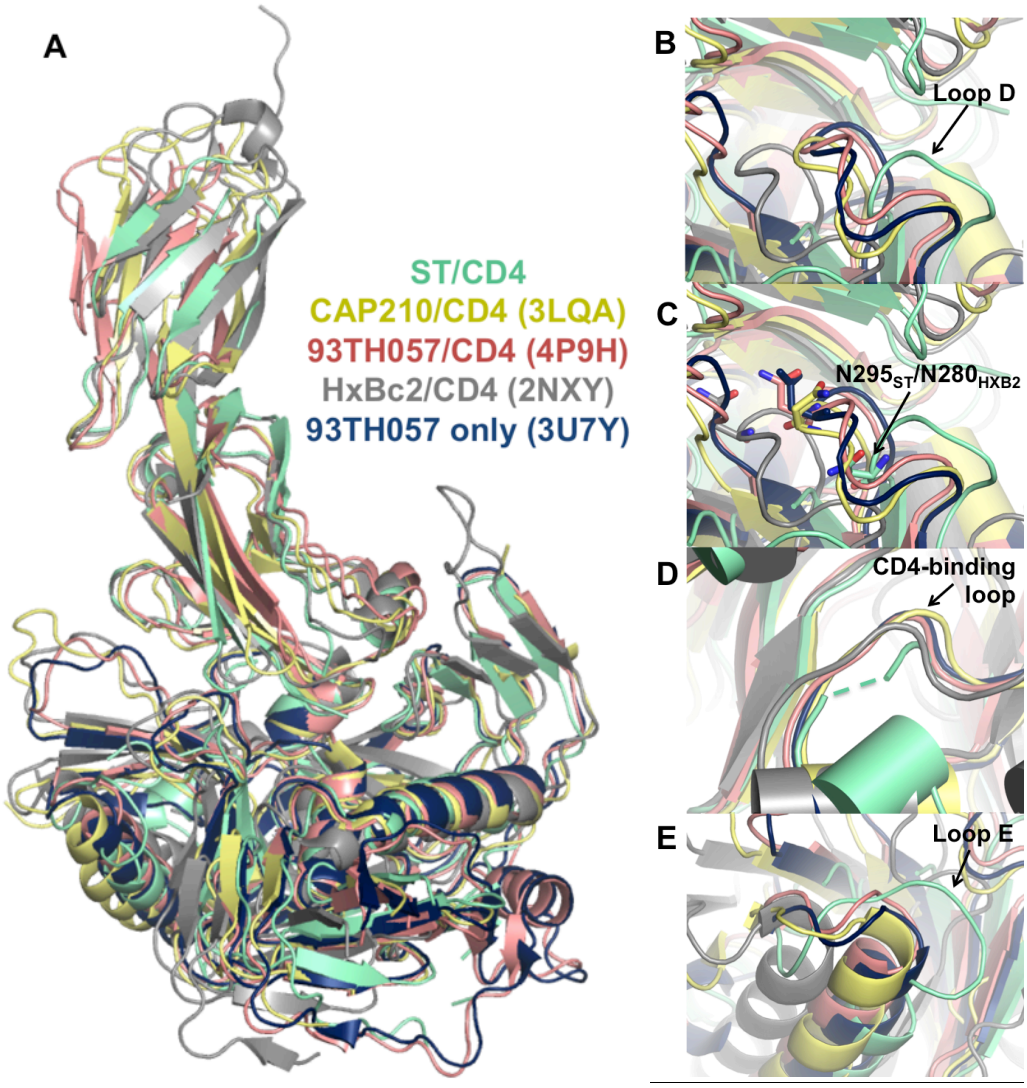

Figure 5. Overlays of gp120s and gp120/CD4 structures. (A) Alignment of ST/CD4 with three HIV-1 gp120/CD4 complex structures and one free gp120 structure. (B) ST loop D is slightly shifted from most HIV-1 loop Ds, especially when oriented by the position of conserved residue $N280_{HXB2}$ (C). (D) The ST CD4-binding loop with a portion represented as dashes due to structural disorder. (E) ST loop E is three to five residues longer in HIV-2 than in HIV-1.

The CD4-binding loop in ST gp120 was partially disordered, but alignment of ordered residues with HIV-1 CD4-binding loops suggested a similar conformation (Figure 5D). As expected from these observations, the side chain of residue F43 on CD4 fits into a hydrophobic pocket on HIV-2 gp120 (Figure 6A), as observed for the "Phe43" pocket in HIV-1 gp120 structures (Kwong et al., 1998). Key residues important for CD4 binding are intact and identical to those in HIV-1 gp120/CD4 complex structures (Figure 6B).

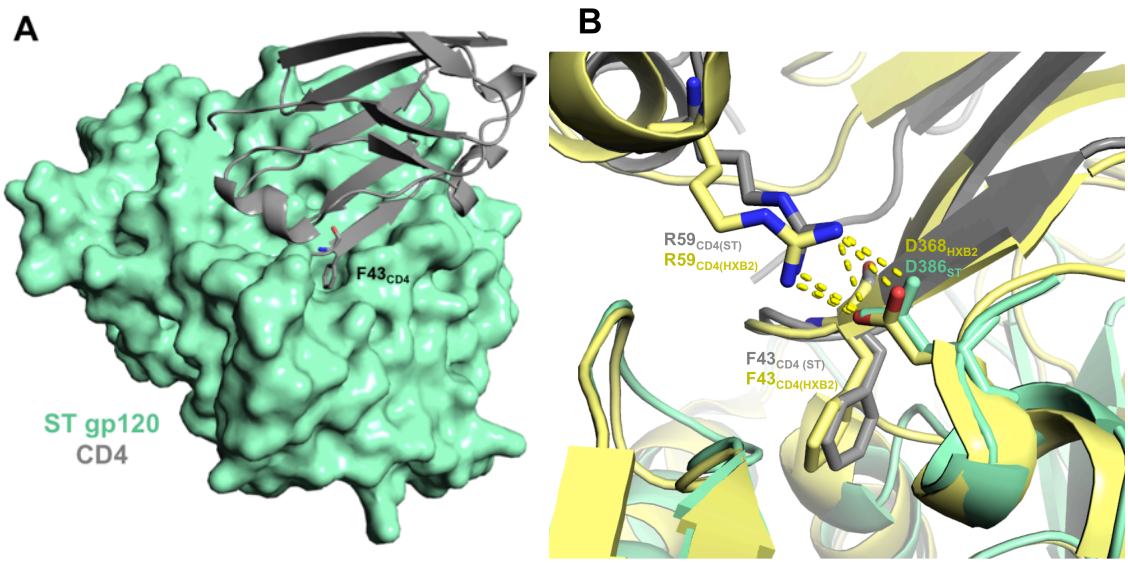

Figure 6. CD4 binding site on ST gp120. (A) The side chain of CD4 F43 (gray cartoon representation) inserts itself into a hydrophobic pocket of gp120 (mint surface representation), identical to CD4 binding in HIV-1 gp120. (B) Key residues in CD4 binding to HIV-2 gp120 are conserved and nearly identical to those for binding to HIV-1 gp120. Aligned with HXB2/CD4 from pdb 2NXY (RMSD = 1.503 Å).

One of the most distinct structural differences between HIV-2 and HIV-1 gp120 is the extended Loop E of HIV-2 gp120. Loop E is three to five residues longer in HIV-2 and originates from the junction between the α-2 helix and β-14 strand in the ST/CD4 structure. In alignments with Loop E from HIV-1 gp120 (Figure 5E), Loop E from ST was longer and potentially more flexible, bending down toward the rest of the gp120 rather than adopting an extended conformation.

Some HIV-2 isolates have been shown to enter cells in a CD4-independent manner (Thomas et al., 2003), leading to the hypothesis that HIV-2 may have a more open co-receptor binding domain (de Silva et al., 2008). At least for the CD4-bound state, the co-receptor binding footprint of ST gp120 is virtually identical to that of other HIV-1 gp120s (Figure 7).

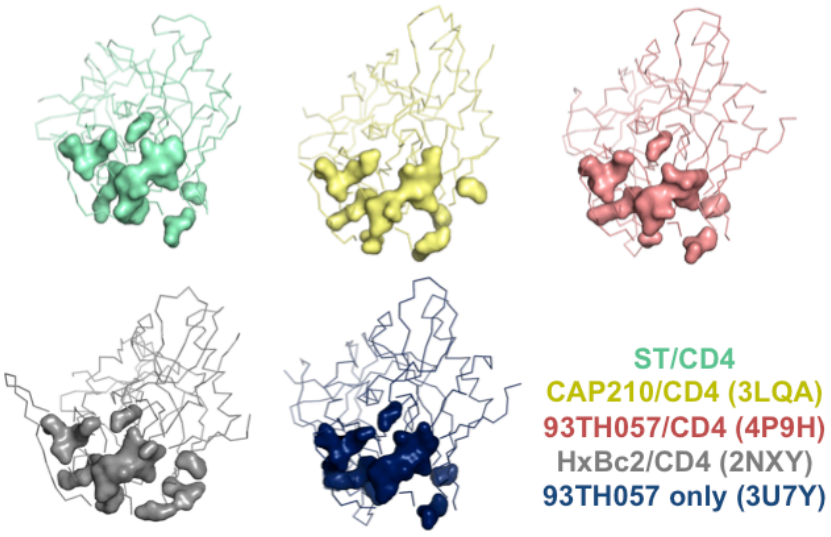

Figure 7. Co-receptor binding footprint in ST gp120 and HIV-1 gp120 structures. gp120 backbone trace in ribbon representation, co-receptor footprint in surface representation, Key residues from (Decker et al., 2005).

Comparison with unliganded SIV gp120 structure

Full-length ST gp120 has 72% sequence identity with SIVmac32H gp120, the strain whose unliganded crystal structure was previously solved (Chen et al., 2005a, b). The sequence alignment of both crystal structures is shown in Figure 8B. Despite the high level of conservation between SIV and HIV-2 full length gp120s (Figure 9), ST gp120 aligned poorly with the unliganded SIV gp120 structure (RMSD = 5.2 Å for 863 backbone Ca atoms), and molecular replacement using the unliganded SIV gp120 structure as a search model yielded no solutions. The β-strands that compose the bridging sheet are shifted by ~13-25 Å with the V1/V2 loops ~ 27 Å apart, potentially due to differences caused by CD4 binding. Helix α-1 is shifted by 15 Å, and the three-stranded β-sheet at the C-terminus is offset by a 90° rotation (Figure 8A).

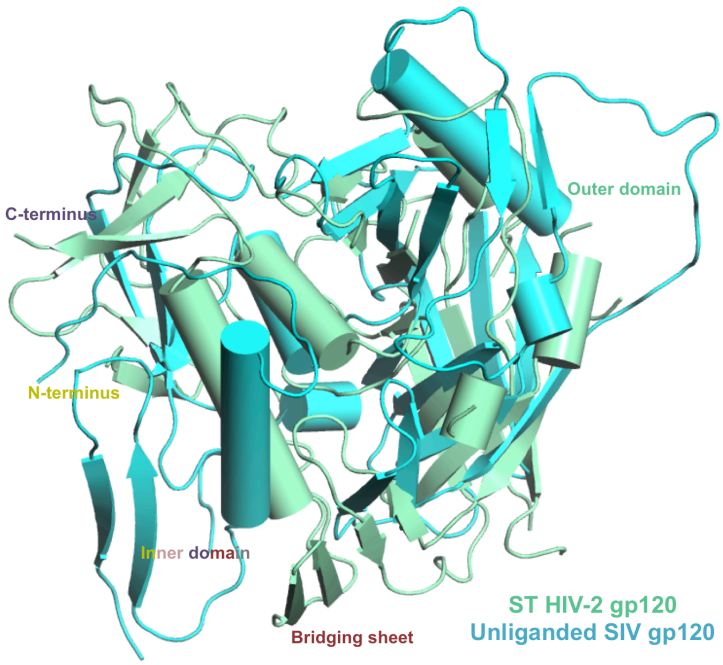

Figure 8A. Sequence based structure alignment of ST gp120 to unliganded SIV gp120 from pdb 2BF1, chain A (RMSD = 5.2 Å).

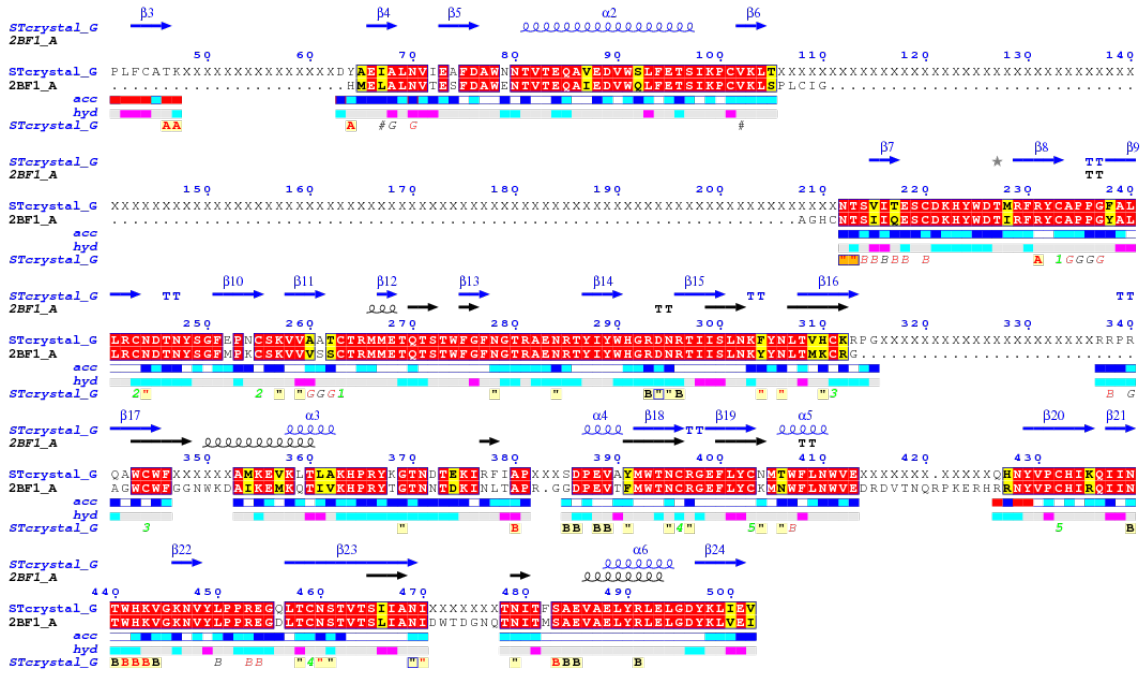

Figure 8B. Alignment of ST crystallization construct and SIV crystallization construct. Conservation, secondary structure, hydropathy, and contacts of ST crystallization construct.

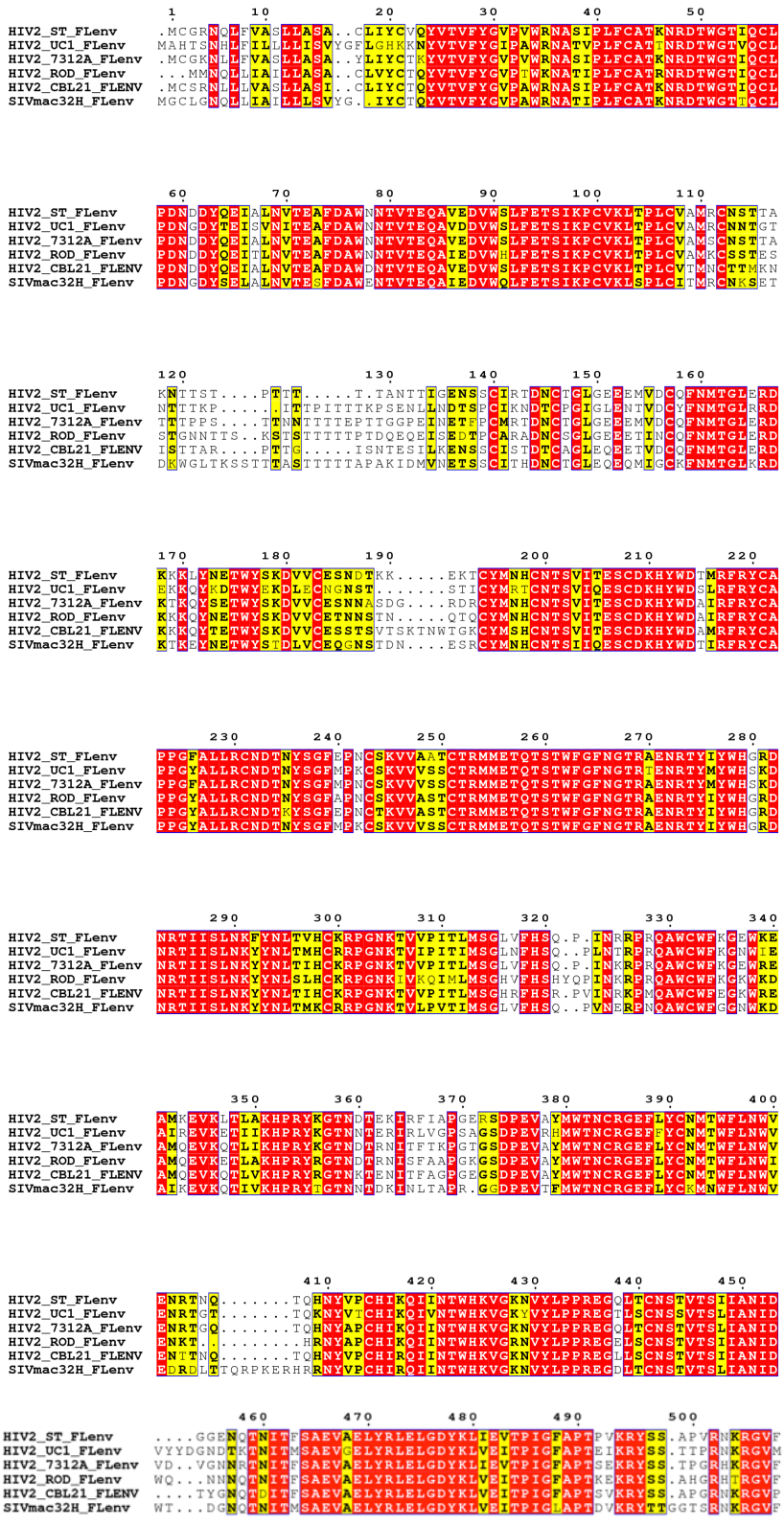

Figure 9. Sequence alignment of HIV-2_{ST} gp120 to other HIV-2 gp120s.

Discussion

The structure of ST gp120 in complex with CD4 represents the first structural characterization of an HIV-2 envelope glycoprotein. While its overall architecture is nearly identical to that of HIV-1 gp120, our observation of differences between the two viruses at the molecular level is the first step toward mechanism-revealing structural studies. In 2013, Shaw and colleagues isolated and mapped the epitopes of 14 new monoclonal antibodies against several epitopes on HIV-2 gp120 (Kong et al., 2012a; Kong et al., 2012b). These antibodies were found to be broadly reactive against the CD4 binding site, CD4i co-receptor site, and the V3 and V4 loops, and can serve as valuable tools for structural studies. Studying the behavior of neutralizing antibodies against HIV-2 and their epitopes on the virus can shed light on HIV-2 as an antigen inciting an effective and appropriate immune response – insights that can also be relevant to efforts to understanding HIV-1 as well as SIV and SHIV models.

Systematic investigations of HIV-2 gp120 in complex with antibody antigen binding fragments (Fabs) are the clear next step. Ideally, a series of co-crystal structures with gp120-Fab complexes will reveal a comprehensive epitope map on the surface of HIV-2 gp120. Co-crystals with CD4i antibodies will provide additional insight into the co-receptor binding site, since the possibility of a more open conformation in that region is intriguing given the ability of some HIV-2 isolates to infect cells without engaging CD4. Concurrent with HIV-2 gp140 trimer studies using negative stain electron microscopy (see Chapter 4), these HIV-2 complex structures can be docked into 3D reconstructions created from gp120-Fab complexes to gain insight into quaternary

epitopes or intermolecular interactions within the spike trimer. HIV-2 native trimer may exhibit differences in overall conformation compared to HIV-1.

Given the difference in pathogenicity between HIV-1 and HIV-2 (de Silva et al., 2008) and the highly distinct unliganded SIV gp120 structure (Chen et al., 2005b), we expected a larger discrepancy between the gp120 structures of the two human viruses. While the observed similarities do not explain the difference in virulence between HIV-1 and HIV-2, they allow us to begin ruling out potential sources. Differential immune activation may result from significant differences in the variable loops, which are truncated or disordered in the current structure. Fewer potential *N*-linked glycans, and thus, decreased glycan shielding, of the V3 and V4 loops in HIV-2 could lead to higher immunogenicity in those areas (Shi et al., 2005). The present crystallization construct could be improved upon with GlySer linkers in place of simple truncations of variable loops. Attempts could also be made to crystallize the gp120 core with variable loops left intact.

Due to the robust neutralizing antibody response to HIV-2, it is likely that the difference in pathogenicity is due, at least in large part, to the role of the envelope glycoprotein. This is encouraging for the potential future growth of HIV-2 knowledge, as the HIV field has long been focused and is well equipped for conducting comprehensive structural studies of the interactions between Env and its binding partners. We still lack basic molecular descriptions of the relationship between HIV-2 and the human immune system, so it is compelling to imagine other possibilities for differences outside of the Env glycoprotein. HIV-2 is a desirable target for investigation to the scientific community, as it represents a model of naturally attenuated HIV infection, a long-pursued

target. Patients infected with HIV-2 benefit from a feedback loop: for unknown reasons, they make effective antibodies against Env, which results in a well-controlled infection and a better-preserved, less-suppressed immune system. This in turn enables a more robust and effective immune response. This suggests that HIV-1 exploits the breakdown of any step in this feedback loop for its own mechanisms of immune evasion, which emphasizes the importance of therapies that interfere with the neutralizing antibody binding step of the immune response. In an unknown fashion, HIV-2 remains a fit virus, able to bring some patients to full-blown AIDS and yet seems to maintain a low mutation rate in the face of neutralizing antibodies. Our lack of understanding of this balance reveals potential holes in our knowledge of basic principles in HIV biology, and further structural studies of HIV-2 will undoubtedly uncover new solutions to this problem.

Experimental methods

Construct design, subcloning, protein expression and purification of recombinant gp120 for crystallization. Sequences for gp120 from strains HIV-2_{UC1}, HIV-2_{ST}, HIV-$2_{7312A-0303}$, and HIV-$2_{7312A-9217}$ were obtained from the Los Alamos National Laboratory HIV Sequence Database. These strains were chosen based on availability and completeness of sequences as well as demonstrated sensitivity to newly isolated anti-HIV-2 gp120 monoclonal antibodies with known epitopes. For each strain, constructs were designed with deletions of the V1/V2 and V3 variable loops, as well as 15 residues from the C-terminus (GFAPTPVKRYSSAPVRNKR). The N-terminus was left intact. We made only one mutation at T89I and left all other glycosylation sites intact. Using gblock (Integrated DNA Technologies) assembly via PCR and restriction enzymes EcoRI and NotI (New England Biolabs), all four genes were subcloned into pTT5-CMV vectors and expressed in N-acetylglucosaminyltransferase I (GnTI) deficient mammalian cells to limit glycan processing. All constructs contained secretion peptide MDAMKRGLCCVLLLCGAVFVSPAGAGS, and secreted gp120 protein was harvested from cell supernatants. Gp120 was purified via Ni-NTA affinity chromatography and further purified via size exclusion chromatography (SEC) on a Superdex200 16/60 column.

Of the four strains, ST and 7312A-9217 exhibited unimodal SEC profiles. Strain 7312A-0303, despite being a closely related variant of 7312A-9217, formed apparent multimers over SEC. Strain UC1 expressed poorly in mammalian cells, and a baculovirus/SF9 expression of full-length UC1 yielded multimers over SEC. As a result, 7312A-9217 and ST gp120 were purified and concentrated by centrifugation to 12-16

mg/ml. As a binding partner to be used in co-crystallization, domains D1 and D2 of soluble CD4 were expressed and purified from baculovirus-infected SF9 cells. At the time, we did not have access to any of the new anti-HIV-2 gp120 monoclonal antibodies. Anti-HIV-1 antibody 21c binds to the co-receptor site on gp120 after the conformational change induced by CD4 engagement. A co-crystal of 21c Fab, sCD4 D1D2, and a core CAP210 gp120 was published by Ron Diskin from our lab in 2009 (Diskin et al., 2010). In his studies, he found that 21c also bound to UC1, an HIV-2 strain. A study (Decker et al., 2005) exploring the conservation of the co-receptor site suggested that many CD4-induced (CD4i) antibodies against HIV-1 gp120, including 21c, were able to neutralize or bind to HIV-2 gp120. While the paper did not explicitly state that 21c interacted with the strain ST, we proceeded to use 21c Fab in co-crystallization trials with sCD4 D1D2 and both ST and 7312A-9217. 21c IgG was expressed in and harvested from supernatants of HEK293-6E mammalian cells and purified via Ni-NTA affinity and size exclusion chromatography. IgG was cleaved into Fab fragments using a Papain cleavage kit (Thermo) while uncleaved IgG was purified away using Protein A beads.

Complex formation, purification, and crystallization of gp120. To form complexes, 2 mg gp120, equimolar sCD4 D1D2, and initially 21c Fab in slight molar excess were combined and allowed to incubate at room temperature for 1 hour. The preps were treated with Endo H for 16 hours at room temperature and purified over a Superdex 200 10/300 size exclusion column. Both ST and 7312A-9217 appeared to form stable complexes with their binding partners over SEC, but ST yielded the highest complex peak and was chosen for crystallization trials after concentration to A_{280} ~ 10-12. A small amount of the 7312A-9217 complex peak was concentrated but was rendered unusable after aggregating

readily. 21c Fab eluted separately during size-exclusion chromatography and did not bind to ST gp120, so it was not included in the crystal screening despite being in the original prep. To check for the presence of any 21c Fab binding to the gp120/CD4 complex, fractions from the SEC trace were run on an SDS-PAGE gel, but as 21c Fab and ST ran at the same position, it was not apparent if 21c was in the complex. ST gp120 ran as a smear consistent with heterogeneous glycosylation. Soluble CD4 D1D2 appeared to be unambiguously present in the complex. Peaks were pooled and concentrated for crystallization trials. Crystals formed via sitting drop vapor diffusion in 3-4 days in 0.15M DL-Malic acid 7.0, 0.1M imidazole 7.0, and 22% PEGMME 550. The crystals were readily reproducible after being scaled up into 600nl + 600nl hanging drop trays. Since a complex with ST and sCD4 D1D2 alone co-purified over SEC yielded the same crystals, it was determined that these were the only two components of the co-crystals.

Data collection, processing, and molecular replacement calculations of gp120/sCD4 D1D2 structure. For data collection, crystals were cryopreserved in either mother liquor containing 30% glycerol or Fomblin oil. The latter resulted in higher resolution diffraction. Crystals diffracted to up to 2.5 Å at the SSRL beamline 12-2, with collected data usable up to 3.0 Å decided by CC1/2. Data were processed using XDS, and crystals were in space group $C222_1$ with unit cell dimensions of a=94.276, b=100.223, c=199.139, a=90, b=90, g=90. Using high resolution structures for sCD4 D1D2 (pdb ID 2NXY) and core HIV-1 gp120 CAP210 (3LQA) as search models in Phaser-MR, molecular replacement yielded no solutions containing both components. Upon fixing partial solutions containing only gp120, sCD4 was placed at the expected location for engaging gp120. Initial refinement of the model resulted in R_{work}/R_{free} values of 0.42/0.48, and 2Fo-

Fc maps for the resultant model containing sCD4 D1D2 and gp120 were generally poor, since the two gp120s share only 35% sequence identity.

Refinement of gp120/sCD4 D1D2 structure. The structure of gp120/sCD4 D1D2 was manually rebuilt in Coot guided by a simulated annealing composite omit map calculated using CNS (Brunger, 2007) or Phenix.autosol (Adams et al., 2010) in conjunction with the $2F_o$-F_c map. Many iterative rounds of refinement were performed using Phenix.refine (Adams et al., 2010), including but not limited to rigid body, group B-factor, TLS, real-space, and Rosetta-guided refinement algorithms (Adams et al., 2013). The final structure was re-refined using Refmac (Murshudov et al., 1997) within the PDB_REDO server (Joosten et al., 2014).

References

Adams, P.D., Afonine, P.V., Bunkoczi, G., Chen, V.B., Davis, I.W., Echols, N., Headd, J.J., Hung, L.W., Kapral, G.J., Grosse-Kunstleve, R.W.*, et al.* (2010). PHENIX: a comprehensive Python-based system for macromolecular structure solution. Acta crystallographica Section D, Biological crystallography *66*, 213-221.

Adams, P.D., Baker, D., Brunger, A.T., Das, R., DiMaio, F., Read, R.J., Richardson, D.C., Richardson, J.S., and Terwilliger, T.C. (2013). Advances, interactions, and future developments in the CNS, Phenix, and Rosetta structural biology software systems. Annual review of biophysics *42*, 265-287.

Berry, N., Ariyoshi, K., Jaffar, S., Sabally, S., Corrah, T., Tedder, R., and Whittle, H. (1998). Low peripheral blood viral HIV-2 RNA in individuals with high CD4 percentage differentiates HIV-2 from HIV-1 infection. Journal of human virology *1*, 457-468.

Brunger, A.T. (2007). Version 1.2 of the Crystallography and NMR system. Nature protocols *2*, 2728-2733.

Brunger, A.T., and Rice, L.M. (1997). Crystallographic refinement by simulated annealing: methods and applications. Methods in enzymology *277*, 243-269.

Chen, B., Vogan, E.M., Gong, H., Skehel, J.J., Wiley, D.C., and Harrison, S.C. (2005a). Determining the structure of an unliganded and fully glycosylated SIV gp120 envelope glycoprotein. Structure *13*, 197-211.

Chen, B., Vogan, E.M., Gong, H., Skehel, J.J., Wiley, D.C., and Harrison, S.C. (2005b). Structure of an unliganded simian immunodeficiency virus gp120 core. Nature *433*, 834-841.

de Silva, T.I., Cotten, M., and Rowland-Jones, S.L. (2008). HIV-2: the forgotten AIDS virus. Trends in microbiology *16*, 588-595.

Decker, J.M., Bibollet-Ruche, F., Wei, X., Wang, S., Levy, D.N., Wang, W., Delaporte, E., Peeters, M., Derdeyn, C.A., Allen, S.*, et al.* (2005). Antigenic conservation and immunogenicity of the HIV coreceptor binding site. The Journal of experimental medicine *201*, 1407-1419.

Diskin, R., Marcovecchio, P.M., and Bjorkman, P.J. (2010). Structure of a clade C HIV-1 gp120 bound to CD4 and CD4-induced antibody reveals anti-CD4 polyreactivity. Nature structural & molecular biology *17*, 608-613.

Jaffar, S., Wilkins, A., Ngom, P.T., Sabally, S., Corrah, T., Bangali, J.E., Rolfe, M., and Whittle, H.C. (1997). Rate of decline of percentage CD4+ cells is faster in HIV-1 than in HIV-2 infection. Journal of acquired immune deficiency syndromes and human retrovirology : official publication of the International Retrovirology Association *16*, 327-332.

Joosten, R.P., Long, F., Murshudov, G.N., and Perrakis, A. (2014). The PDB_REDO server for macromolecular structure model optimization. IUCrJ *1*, 213-220.

Karplus, P.A., and Diederichs, K. (2012). Linking crystallographic model and data quality. Science *336*, 1030-1033.

Kong, R., Li, H., Bibollet-Ruche, F., Decker, J.M., Zheng, N.N., Gottlieb, G.S., Kiviat, N.B., Sow, P.S., Georgiev, I., Hahn, B.H.*, et al.* (2012a). Broad and potent neutralizing antibody responses elicited in natural HIV-2 infection. Journal of virology *86*, 947-960.

Kong, R., Li, H., Georgiev, I., Changela, A., Bibollet-Ruche, F., Decker, J.M., Rowland-Jones, S.L., Jaye, A., Guan, Y., Lewis, G.K., *et al.* (2012b). Epitope mapping of broadly neutralizing HIV-2 human monoclonal antibodies. Journal of virology *86*, 12115-12128.

Kwong, P.D., and Mascola, J.R. (2012). Human antibodies that neutralize HIV-1: identification, structures, and B cell ontogenies. Immunity *37*, 412-425.

Kwong, P.D., Wyatt, R., Robinson, J., Sweet, R.W., Sodroski, J., and Hendrickson, W.A. (1998). Structure of an HIV gp120 envelope glycoprotein in complex with the CD4 receptor and a neutralizing human antibody. Nature *393*, 648-659.

MacNeil, A., Sankale, J.L., Meloni, S.T., Sarr, A.D., Mboup, S., and Kanki, P. (2007). Long-term intrapatient viral evolution during HIV-2 infection. The Journal of infectious diseases *195*, 726-733.

McCoy, A.J., Grosse-Kunstleve, R.W., Adams, P.D., Winn, M.D., Storoni, L.C., and Read, R.J. (2007). Phaser crystallographic software. Journal of applied crystallography *40*, 658-674.

Murshudov, G.N., Vagin, A.A., and Dodson, E.J. (1997). Refinement of macromolecular structures by the maximum-likelihood method. Acta crystallographica Section D, Biological crystallography *53*, 240-255.

O'Donovan, D., Ariyoshi, K., Milligan, P., Ota, M., Yamuah, L., Sarge-Njie, R., and Whittle, H. (2000). Maternal plasma viral RNA levels determine marked differences in mother-to-child transmission rates of HIV-1 and HIV-2 in The Gambia. MRC/Gambia Government/University College London Medical School working group on mother-child transmission of HIV. Aids *14*, 441-448.

Robert, X., and Gouet, P. (2014). Deciphering key features in protein structures with the new ENDscript server. Nucleic acids research *42*, W320-324.

Schim van der Loeff, M.F., Jaffar, S., Aveika, A.A., Sabally, S., Corrah, T., Harding, E., Alabi, A., Bayang, A., Ariyoshi, K., and Whittle, H.C. (2002). Mortality of HIV-1, HIV-2 and HIV-1/HIV-2 dually infected patients in a clinic-based cohort in The Gambia. Aids *16*, 1775-1783.

Shi, Y., Brandin, E., Vincic, E., Jansson, M., Blaxhult, A., Gyllensten, K., Moberg, L., Brostrom, C., Fenyo, E.M., and Albert, J. (2005). Evolution of human immunodeficiency virus type 2 coreceptor usage, autologous neutralization, envelope sequence and glycosylation. The Journal of general virology *86*, 3385-3396.

Thomas, E.R., Shotton, C., Weiss, R.A., Clapham, P.R., and McKnight, A. (2003). CD4-dependent and CD4-independent HIV-2: consequences for neutralization. Aids *17*, 291-300.

van der Loeff, M.F., Larke, N., Kaye, S., Berry, N., Ariyoshi, K., Alabi, A., van Tienen, C., Leligdowicz, A., Sarge-Njie, R., da Silva, Z.*, et al.* (2010). Undetectable plasma viral load predicts normal survival in HIV-2-infected people in a West African village. Retrovirology *7*, 46.

Chapter 4 (Unpublished work in progress)

Making a soluble, cleaved, native-like HIV-2 gp140 trimer

Introduction

Human immunodeficiency virus (HIV) infects host CD4+ T cells via its envelope glycoprotein (Env), which is the key to viral fusion mediated by host receptors CD4 and CCR5/CXCR4. Full length Env glycoprotein gp160 is synthesized and proteolytically cleaved intracellularly into gp120 and gp41 using host machinery, and then trafficked to the viral surface upon maturation. The Env complex comprises a trimer of heterodimers: three gp120-gp41 subunits held together noncovalently after cleavage (Poignard et al., 2001). For many years, structural studies of HIV Env have focused on the gp120 or gp41 core fragments, which can be prepared stably using recombinant methods. These fragments generally corresponded to the CD4-bound, post-fusion state of Env, which is not as informative as the prefusion configuration that initially encounters the immune system. While these studies have revealed details of the interaction between HIV and the immune system, they are lacking in their interrogation of the native trimeric infectious unit. Studies of the trimer could lead to more effective vaccine targets, as many known non-neutralizing monoclonal antibodies against HIV-1 only bind to monomeric Env and not to trimeric Env . It is likely that the immune system reacts differently to trimeric Env versus nonnative, non-intact fragments of the trimer, such as dissociated gp120 or poorly formed gp160 trimers. The latter events likely result in nonproductive interactions in which antibodies are made against epitopes irrelevant for HIV neutralization. For these reasons, an HIV trimer that can mimic the native, cleaved conformation while remaining

stable when expressed recombinantly would be valuable for both structural and immunological studies.

Due to the labile nature of the noncovalent gp120-gp41 interaction, recombinant production of fully posttranslationally processed trimers were problematic for many years (Sanders et al., 2002). An intermolecular disulfide bond (SOS) was introduced with mutations at A501C and T605C in order to covalently link gp120 and the gp41 ectodomain ($gp41_{ECTO}$). Full length gp160 was truncated just before the membrane-proximal region, resulting in gp140. Oligomeric SOS gp140 could be transiently expressed in HEK 293T cells (Sanders et al., 2002), but its purification resulted in gp140 monomers, indicating a loss of integrity at the trimerization interface despite improvement of the gp120-$gp41_{ECTO}$ association. To stabilize the trimerization interface, an isoleucine-to-proline (IP) mutation was introduced at position 559 (Binley et al., 2000; Sanders et al., 2002) to destabilize the post-fusion configuration and therefore enhance stability of the prefusion configuration, which is of highest biological interest given that most existing structures feature the postfusion form of Env. This specific I to P mutation was effective at coercing SOS gp140 to trimerize more reliably in the prefusion form over a number of other mutations at other sites (Sanders et al., 2013; Sanders et al., 2002). This version of Env was dubbed "SOSIP," and it formed native-like, soluble, cleaved, noncovalently associated trimers.

In 2013, a "next-generation" version of SOSIP trimers of subtype A strain BG505 was shown to preferentially bind neutralizing antibodies (Sanders et al., 2013). These stable and native-like trimers featured a truncation at position 664 of the gp41 transmembrane domain (just prior to the MPER) and a cleavage-enhancing mutation of

REKR to RRRRR at the Furin proteolytic site between gp120 and gp41(Sanders et al., 2013). These trimers are generally co-expressed with soluble Furin protease, which performs the cleavage (Sanders et al., 2002). BG505 SOSIP.664 trimer eluted via size-exclusion chromatography with a prominent trimer peak along with a smaller monomer peak. The trimer peak could be re-purified and used for further studies. As a result, crystal and cryo-EM structures of this protein were published to 4.7 Å and 5.8 Å resolution, respectively (Julien et al., 2013; Lyumkis et al., 2013). Both structures were in agreement with respect to the overall architecture of the soluble trimer, and they revealed crucial interactions between gp120 and gp41 as well as between the gp120 subunits. The BG505 SOSIP.664 trimer represents a new, native-like standard for studying the function of the HIV envelope spike during host infection as well as provides crucial insight for immunogen and prophylactic design.

For similar motivations, we sought to create and describe the analogous trimeric envelope glycoprotein from HIV-2. As previously discussed, the formidable body of knowledge that has accumulated surrounding HIV-1 Env does not exist for HIV-2. Therefore, it remains uncertain whether any observed differences in pathogenicity and virulence between the two viruses derive from differences in Env. To obtain a stable, native-like HIV-2 trimer protein analogous to BG505 SOSIP.664 gp140 from HIV-1, we will initially introduce the identical SOSIP modifications to HIV-2 gp140 glycoproteins from various strains. If successful, characterization of this protein with or without binding partners (e.g., CD4, MAbs) via electron microscopy, X-ray crystallography, and other biophysical methods will provide insight into the native behavior of HIV-2 virions in the context of host infection and subsequent immunological response. Comparative studies

between the HIV-1 and HIV-2 versions of soluble, native trimers will further elucidate the differences in their pathogenicities.

Initial design of HIV-2 SOSVP trimers

We first obtained all available full-length HIV-2 gp160 sequences from the Los Alamos HIV Sequence Database (HIV Sequence Compendium 2013). We then chose the most complete sequences that were in agreement with GenBank depositions, resulting in three strains as candidates for creating HIV-2 trimers: 7312A, UC1, and ST (see Figure 3.1 for sequence alignment). We included cysteine mutations to add the engineered SOS disulfide bond between gp120 and gp41, as well as a valine (isoleucine in HIV-1) to proline mutation to promote trimerization. We named these constructs HIV-2 "SOSVP" gp140 trimers (Figure 3.2). The REKR Furin cleavage site (consensus with HIV-1) was initially mutated to RRRR (4R) to enhance proteolytic cleavage (Binley et al., 2002; Sanders et al., 2013). The original BG505 SOSIP.664 constructs contained a mutation to RRRRRR (6R) in lieu of the original Furin cleavage site. Since very little was known about making HIV-2 soluble Env trimers, we sought to be conservative and created both 4R and 6R mutants. The sequence was truncated at position 664 to exclude the transmembrane domain of gp41 (Figure 3.2). The constructs also contained a C-terminal Gly-Ser linker and a His_6 tag to facilitate Ni-NTA affinity purification.

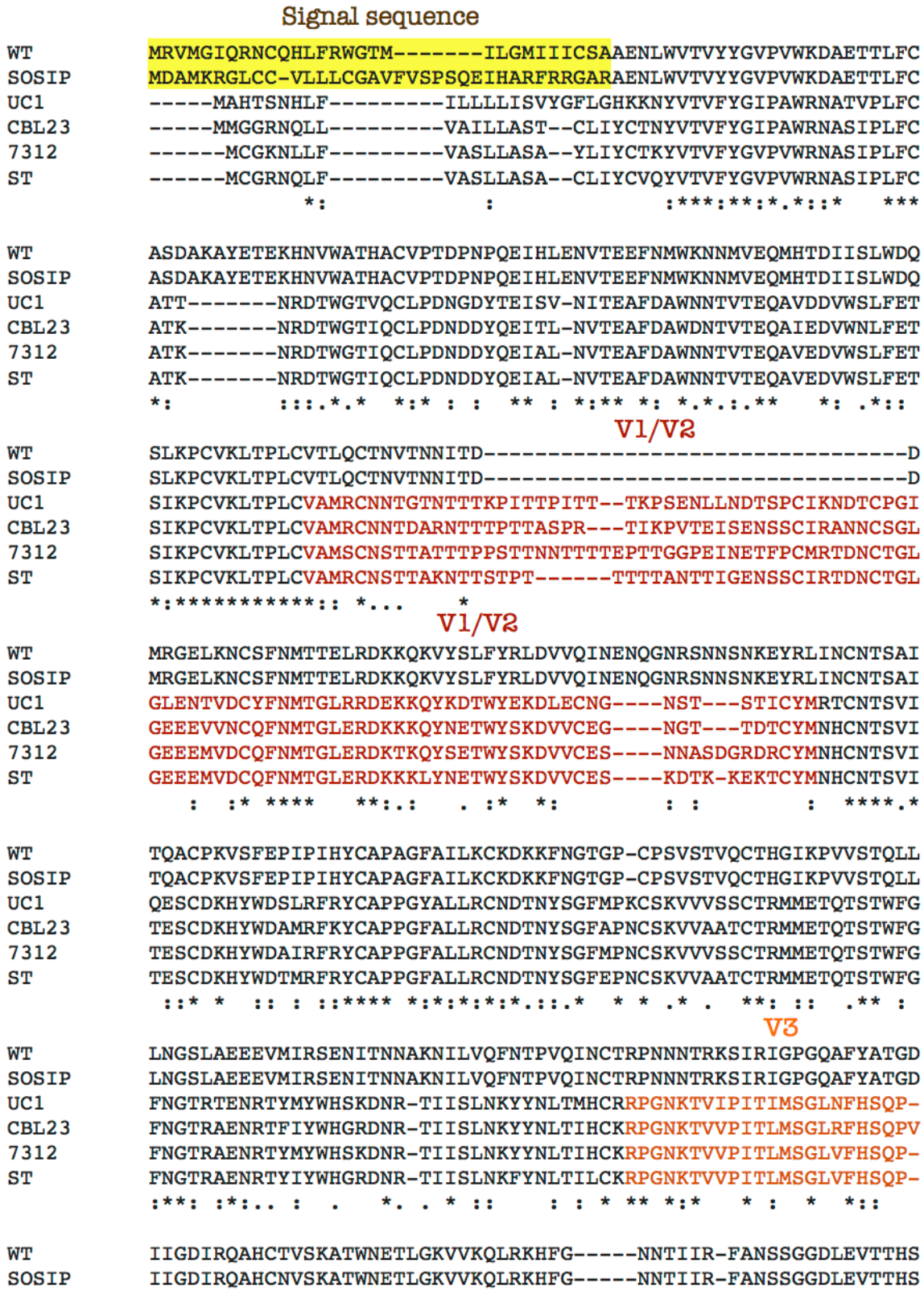

Figure 3.1 Sequence alignment of HIV-1/2 gp160, cont'd on next page.

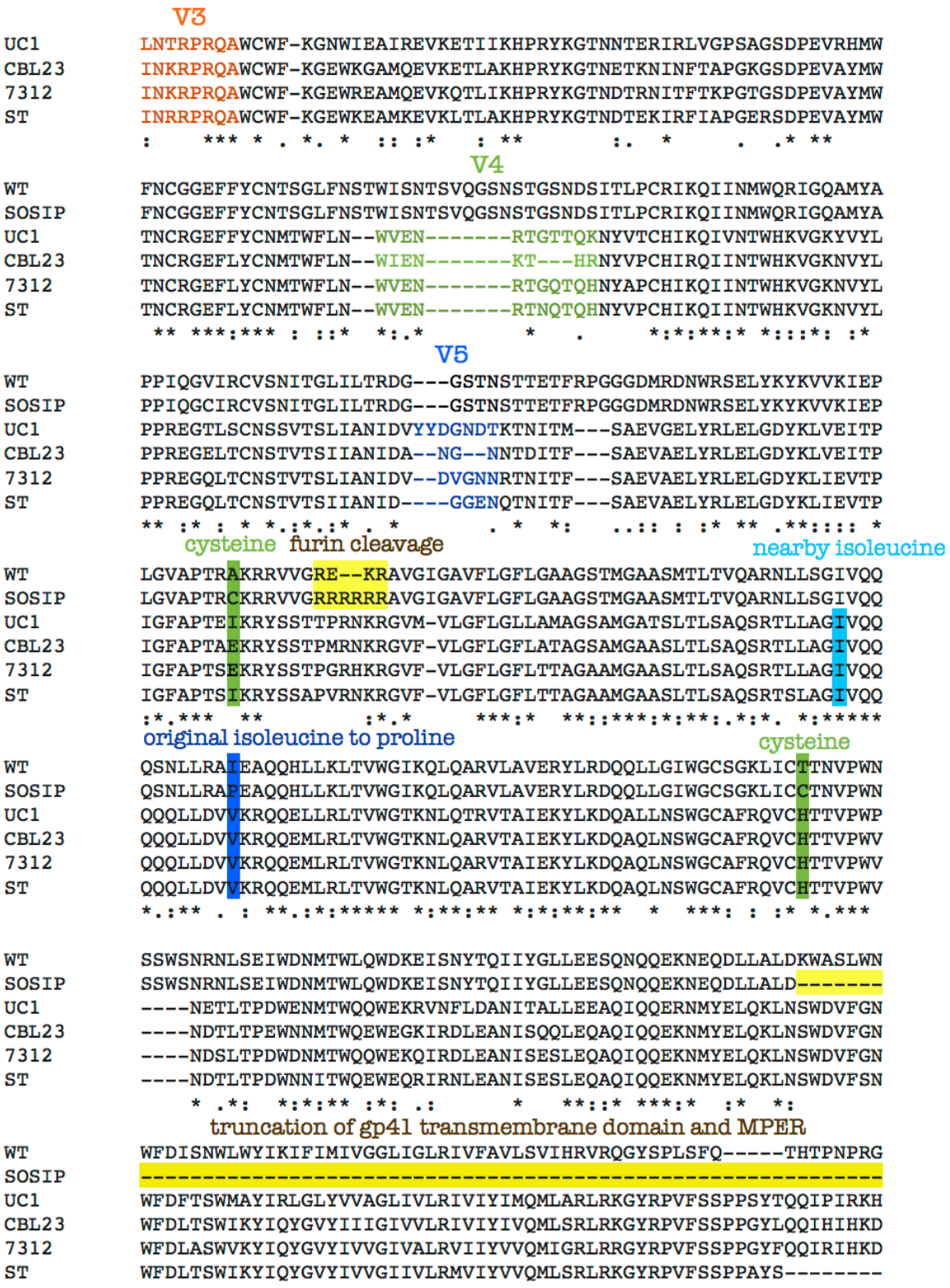

Figure 3.1, cont'd. Annotated alignment of WT BG505, SOSIP BG505, and four WT HIV-2 gp160 sequences (sequence after MPER not shown).

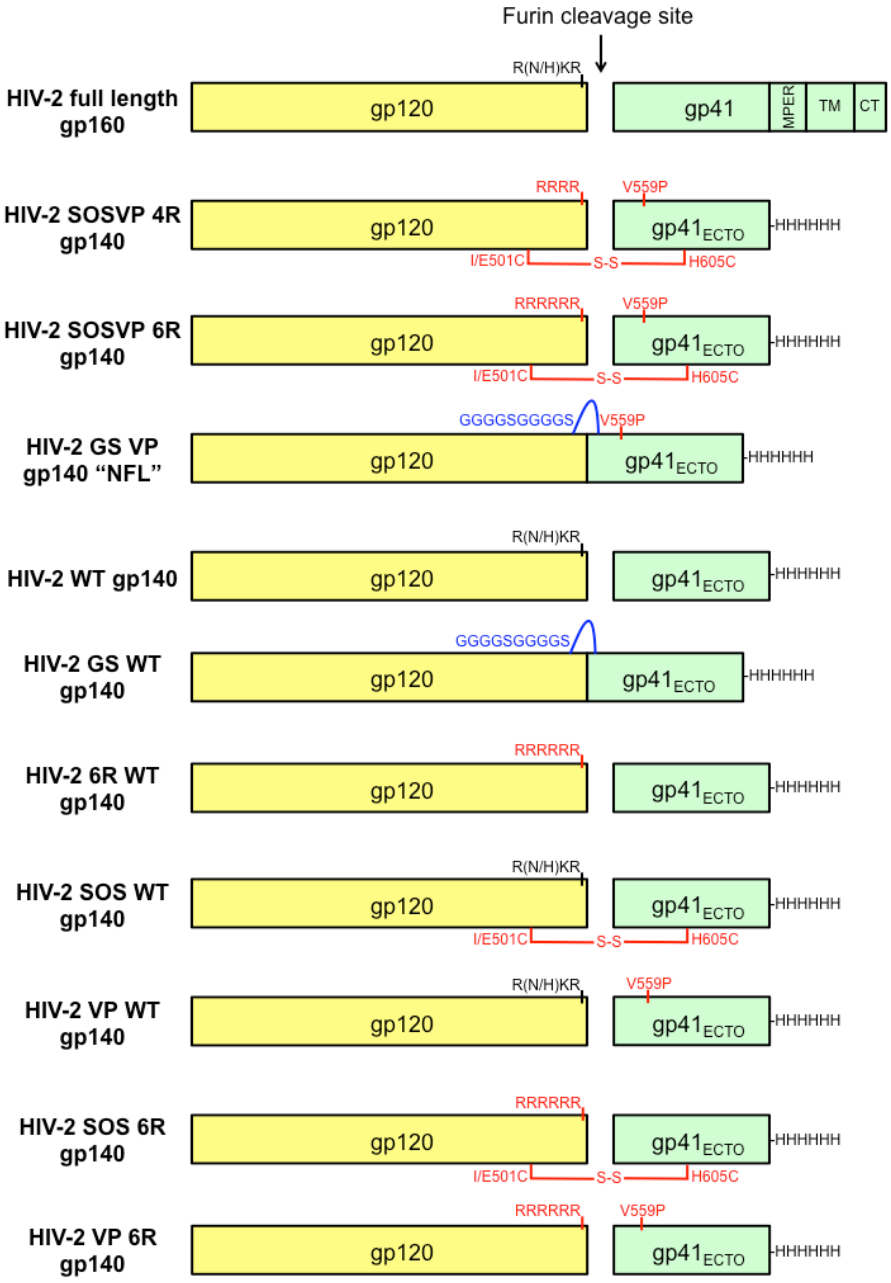

Figure 3.2 Schematic of HIV-2 gp140 Env trimers. Native features are shown in black, and modifications to wild-type are shown in red or blue. R(N/H)KR indicates native Furin cleavage site in HIV-2 gp160, 4R or 6R indicates Furin cleavage enhancing mutations. V559P is analogous to I559P "IP" mutation in HIV-1 SOSIP trimers. Mutations for additional SOS disulfide bond are indicated. G_4S linkers completely substitute for Furin cleavage site in "NFL" or GS trimers. All G_4S-containing trimer constructs were not co-transfected with sFurin.

Biochemical analysis of purified HIV-2 SOSVP protein

Elution fractions from size-exclusion chromatography were initially analyzed via Coomassie blue and silver stained SDS-PAGE gels. The elution profile exhibited peaks for what appeared to be multimeric, trimeric, and monomeric states (Figure 3.3). Coomassie blue stain for both 7312A SOSVP and UC1 SOSVP of boiled, non-reduced fractions revealed that the trimeric state migrated as a single band, indicating that the engineered disulfide bond was behaving properly. However, the non-reduced band ran at an apparent molecular weight greater than 250 kDa, while the boiled, reduced fractions ran at an apparent lower molecular weight, around 140 kDa. This is in contrast to the BG505 SOSIP trimer, which ran at 140 kDa non-reduced and 120 kDa reduced (as expected from the name gp140 and gp120). The $gp41_{ECTO}$ domain, which should run between 25 to 37 kDa for a reduced sample, was not stained by Coomassie blue. We silver stained these samples but saw no evidence of a cleavage product around that size, with the same result for a BG505 SOSIP positive control (data not shown). In addition, we performed a Western blot with anti-His_6 tag antibody to check for the cleavage product, since the His_6 tag should migrate with the gp41 portion on a reducing gel if cleavage occurred as expected and if the SOS disulfide bond was broken under reducing conditions. This Western blot, shown in the top panel of Figure 3.4, suggests that 7312A SOSVP 4R and UC1 SOSVP 4R were not cleaved. In this analysis, BG505 SOSIP $gp41_{ECTO}$ did give a signal between 25 to 37 kDa as a positive control. In an attempt to make the cleaved version of HIV-2 SOSVP trimers, the original RRRR enhanced Furin cleavage site in the 7312A SOSVP and UC1 SOSVP contructs were mutagenized to RRRRRR (6R). The resulting HIV-2 trimers were purified as previously stated. The SEC

profile once again exhibited multimer, trimer, and monomer peaks (Figure 3.3), and the trimer peak was isolated for analysis via SDS-PAGE. For both UC1 SOSVP 4R and 6R proteins, the first elution from Ni-NTA affinity chromatography exhibited a higher population of monomeric gp140 when subjected to size-exclusion chromatography (Figure 3.3 bottom panel, solid blue trace). A second pass of supernatant containing gp140 over the Ni-NTA column resulted in a higher fraction of trimeric gp140 (dotted blue trace), indicating a difference in Ni-NTA affinity between oligomers, potentially resulting from differences in accessibility to the C-terminal His_6-tag. Coomassie blue staining of boiled, non-reduced, and boiled, reduced SOSVP 6R trimer fractions appeared identical to their SOSVP 4R counterparts (data not shown here). An anti-His_6 Western blot of the SOSVP 6R fractions showed ambiguous results (Figure 3.4, bottom panel). Fraction A6 or A7, which corresponded to trimeric protein for UC1 or 7312A SOSVP 6R respectively, did not appear to show cleavage due to the absence of the $gp41_{ECTO}$ band under reducing conditions (lanes 2 and 6). This band did appear for Fractions A11 and A12 (lanes 4 and 8), which corresponded to monomeric gp140. However, there is also some evidence of signal for the non-reduced samples of those fractions, which could have occurred as a result of contamination between lanes. At most, these results suggest that SOSVP 6R gp140 monomers may be cleaved, but that gp140 trimers were not cleaved.

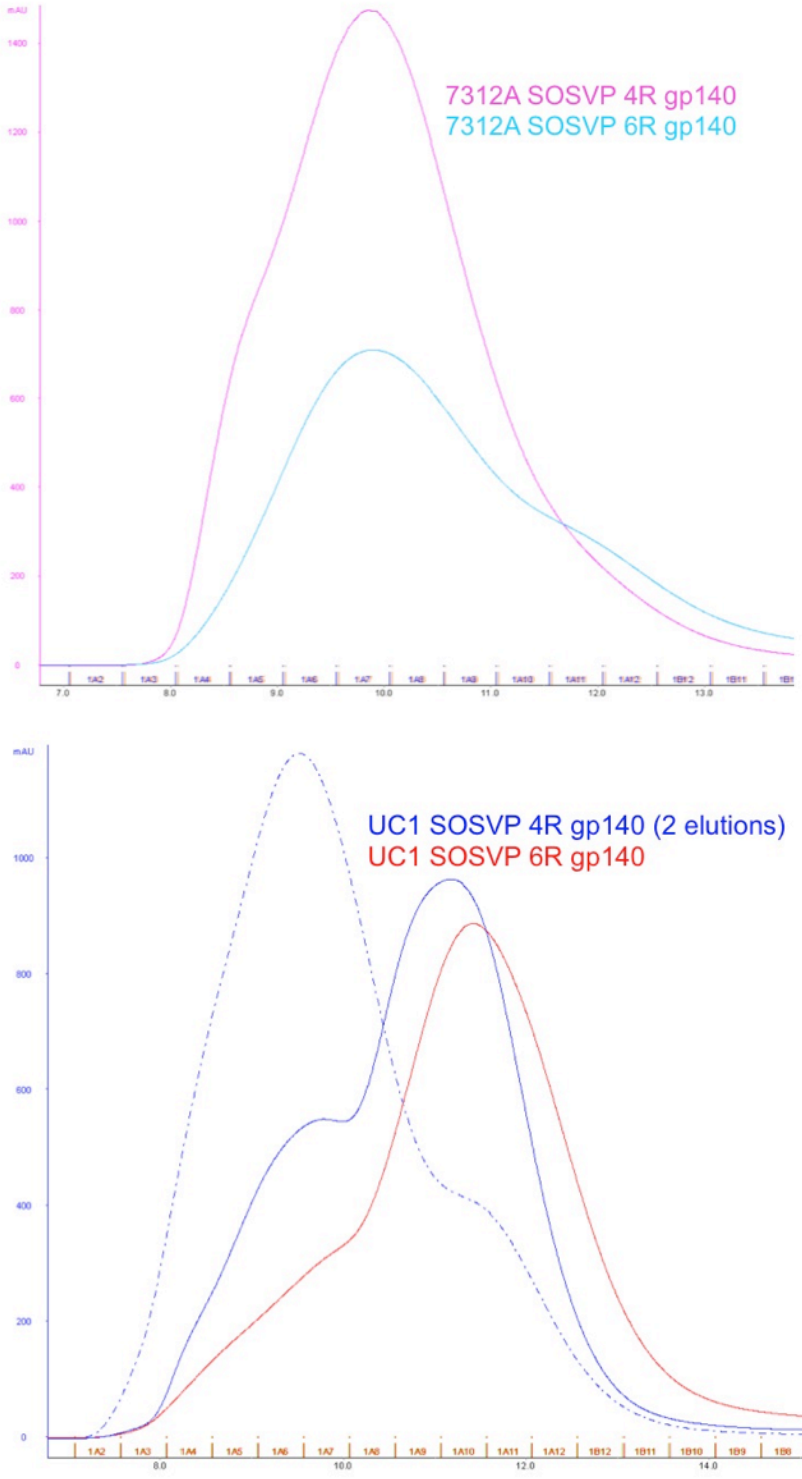

<u>Figure 3.3</u> Size-exclusion chromatography elution profile of 7312A and UC1 SOSVP 4R and 6R gp140 trimers. Trimers migrated around 9-10 ml, monomers ran around 12 ml, and the void volume of the S200 10/300 was around 8 ml.

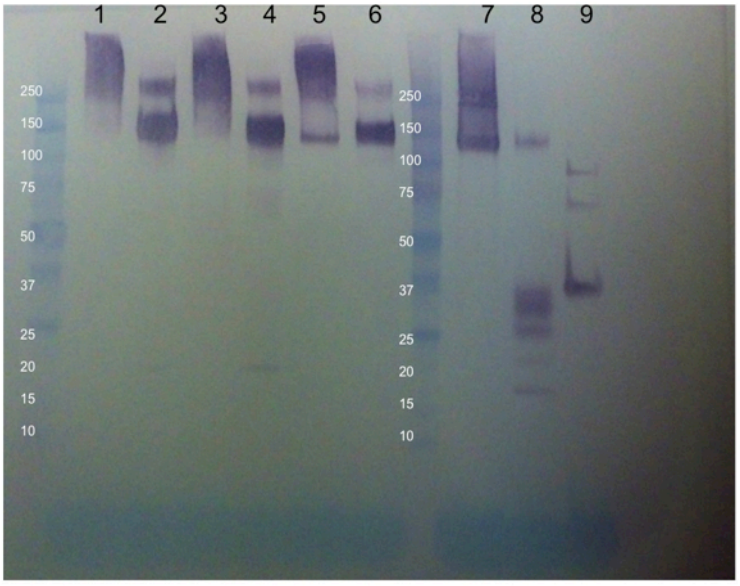

1. 7312A 4R A8 non-reducing
2. 7312A 4R A8 reducing
3. 7312A 4R A9 non-reducing
4. 7312A 4R A9 reducing
5. UC1 4R A6 non-reducing
6. UC1 4R A6 reducing
7. BG505-SOSIP non-reducing
8. BG505-SOSIP reducing
9. tdTomato (anti-His control)

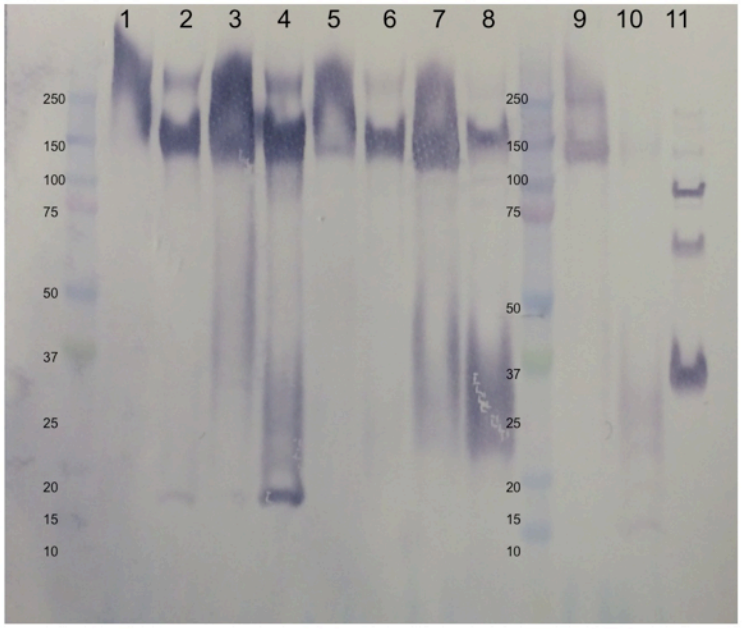

1. 7312A 6R A7 non-reducing
2. 7312A 6R A7 reducing
3. 7312A 6R A12 non-reducing
4. 7312A 6R A12 reducing
5. UC1 6R A6 non-reducing
6. UC1 6R A6 reducing
7. UC1 6R A11 non-reducing
8. UC1 6R A11 reducing
9. BG505-SOSIP non-reducing
10. BG505-SOSIP reducing
11. tdTomato (anti-His control)

Figure 3.4 Anti-His_6 western blot for 7312A SOSVP 4R (top), 6R (bottom) and UC1 SOSVP 4R (top), 6R (bottom). Indicated fractions from SEC elution of proteins were boiled in buffer with and without DTT for reducing and non-reducing conditions, respectively. The samples were run on AnyKD (BioRad) SDS-PAGE gels and transferred to nitrocellulose for western blotting with anti-His_6 tag antibody.

Analysis of purified HIV-2 SOSVP RRRR (4R) protein via SEC-MALS.

To determine the oligomeric states of various fractions in the SEC elution of HIV-2 SOSVP 4R trimer proteins, a size exclusion chromatography system (AKTA, GE) was coupled in-line with a UV detector, a multi-angle light scattering (MALS) detector, a quasi-elastic light scattering (QELS) detector, and a refractive index (RI) detector (Wyatt Technologies). We characterized the molar mass of the entire glycoprotein using the RI signal (both carbohydrate and protein contributions). The results (see Table 3.1) indicated that fractions A8 and A9 of the 7312A SOSVP 4R trace and that fraction A6 of the UC1 SOSVP 4R trace (see Figure 3.3) were likely HIV-2 trimers. This measurement does not distinguish between a cleaved or an uncleaved trimer, as both have the same molar mass.

*All 4R SOSVPs expressed in 293-6E cells		Calculated $MM_{protein}$ of monomer	**$MM_{glycoprotein}$ from SEC-UV/MALS/RI**	Hydrodynamic radius r_H from QELS/RI/DLS (nm)
7312A_SOSVP 4R peak A4+A5	Early "aggregate" shoulder	77,411.6	**1,100,000**	14.8
7312A_SOSVP 4R peak A8+A9	Main peak	77,411.6	**389,000**	8.4
UC1_SOSVP 4R peak A4	Early "aggregate" shoulder	77,443.2	**1,480,000**	15.6
UC1_SOSVP 4R peak A6	Middle peak, 50% of tall peak	77,443.2	**452,000**	8.7
UC1_SOSVP 4R peak A11+A12	Third, tallest peak – perhaps monomer?	77,443.2	**122,700**	4.1
Untreated BG505 SOSIP (GnTI-/-)[1]		74,332.6	**394,200 (357,000[2])**	12.3

Table 3.1 SEC-MALS analysis of HIV-2 SOSVP 4R trimers. Highlighted values correspond to the molar mass of trimeric gp140, in agreement with BG505 SOSIP trimers ([1] and [2] from (Depetris et al., 2012)).

Analysis of the HIV-2 SOSVP trimers via negative stain electron microscopy

Negative stain EM has been used as an assay to study the overall behavior and appearance of HIV-1 soluble trimers (Georgiev et al., 2015; Sanders et al., 2013; Scharf et al., 2014). Native-like, well-behaved, cleaved trimers generally appear as unaggregated, consistently compact single particles amenable to 3D reconstruction (Ringe et al., 2013). To perform this analysis on HIV-2 SOSVP trimers, we used a T12 electron microscope to image negatively stained (using 2% uranyl acetate) 4R and 6R proteins (at 0.01 mg/ml) adsorbed onto glow-discharged holey carbon grids.

7312A and UC1 SOSVP 4R trimers appeared aggregated and heterogeneous, often forming filament-like structures (Figure 3.5, left panels). This may have been caused by inherent instability of the uncleaved trimers or adverse reactions of the proteins to staining. 7312A and UC1 SOSVP 6R trimers (Figure 3.5, right panels) appeared more homogeneous in particle size, although we could not locate many particles with the distinctive trimeric shape by visual inspection (i.e., presence of a three-fold rotational axis). There was a great deal of protein "debris" evident on the SOSVP 6R grids, which could have been caused by the grids not having been made using fresh protein preps. Staining technique could also be a factor, as the standard procedure calls for waiting for the grid to dry completely during the protein adsorption step. Proteins with inherent instability may suffer from drying and destruction of morphology before the stain is applied, so from this point we began to apply stain when the grid was still slightly wet (Alasdair McDowell, personal communication).

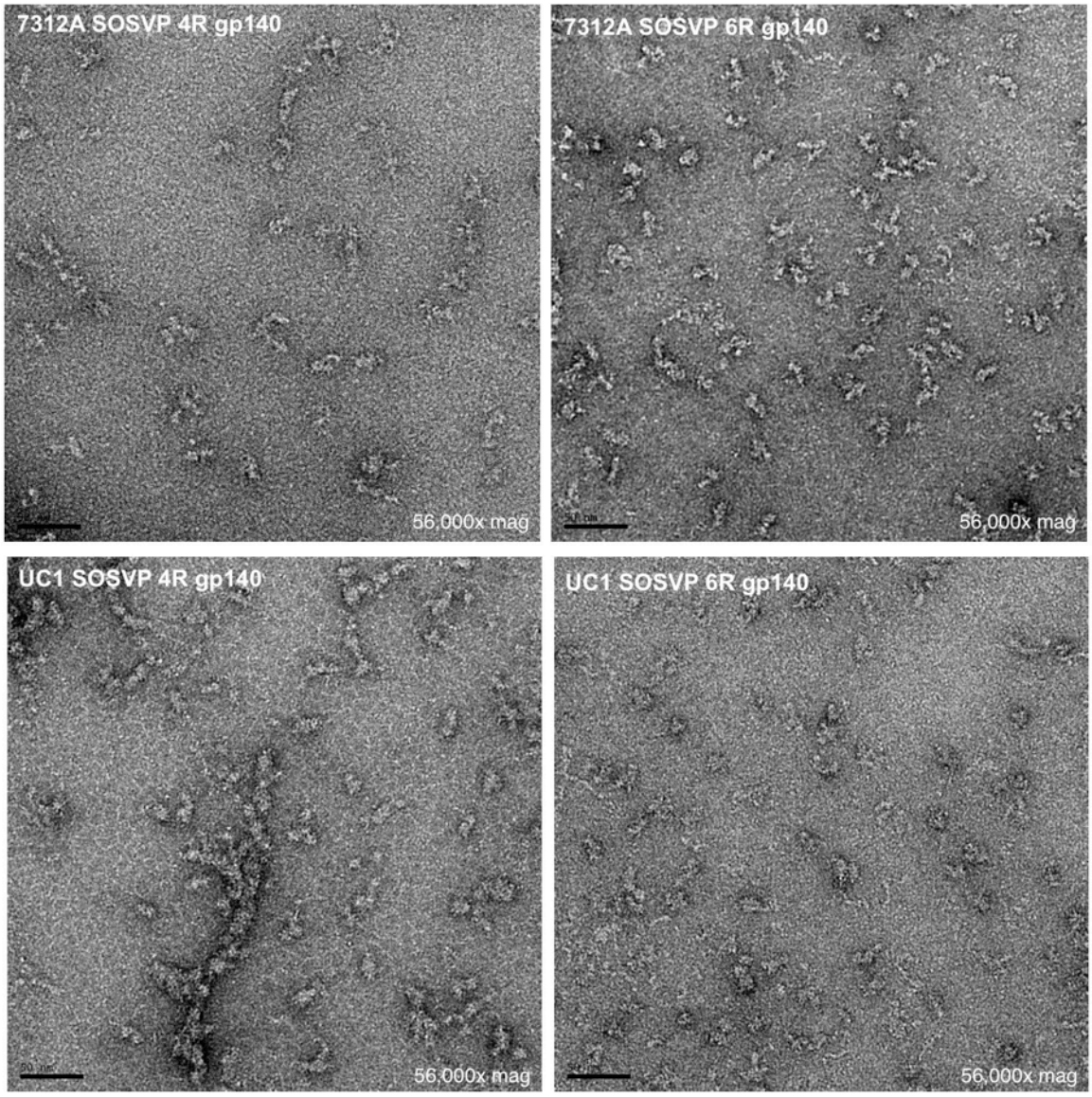

Figure 3.5 Negative stain electron micrographs of 7312A and UC1 4R (left) and 6R particles (right). Protein samples were purified via Ni-NTA affinity chromatography followed by size-exclusion chromatography. Fractions from the latter were taken and diluted to 0.01 mg/ml.

Design, mutagenesis, protein expression and purification of non-SOSVP HIV-2 gp140 trimers.

Since neither HIV-2 SOSVP 4R nor 6R trimers appeared ideal from Western blot and EM results, we pursued a new rationale for construct design. Given that little is known about HIV-2 Env in general, literature was consulted for both HIV-2 and for SIV, its most closely related virus. In addition, given the known differences between HIV-1 and -2, we hypothesized that the SOSIP mutations that were optimized for HIV-1 may not be appropriate for creating well-behaved HIV-2 trimers. Soluble, wild-type HIV-1 gp140 trimers have historically been difficult to obtain (Broder et al., 1994; Earl et al., 1994; Earl et al., 1992; Earl et al., 1991). SIV gp140 trimers, on the other hand, were readily expressed in the Lec3.2.8.1 system (Chen et al., 2000). Zhang, et al created a chimeric gp140 protein (Zhang et al., 2001) using HIV-1 strain ADA gp120 and SIV mac32H gp41 ectomain which was reproducibly stable with no additional alterations that were typically used for making soluble HIV gp140 trimers (e.g., engineered disulfide bond, GCN4 leucine zipper). These results support the possibility that HIV-2 trimers could potentially be expressed stably as wild-type, without SOSIP-like modifications.

The rationale for the SOS mutation is to covalently link the cleaved gp120 and $gp41_{ECTO}$, and the IP mutation is to destabilize the gp41-gp41 postfusion interface to promote the stability of the prefusion configuration of Env trimers. The postfusion state of SIVmac Env has been shown to be less stable than that of HIV-1 Env (Liu et al., 2002; Sanders et al., 2002), and the T_m of SIV gp41 (40°C) is lower than that of HIV-1 gp41 (66°C) (Malashkevich et al., 1998). From these results, we infer that HIV-2 Env may also

be inherently destabilized in its gp41 region compared to HIV-1 Env, and may not need the V to P mutation (I to P in HIV-1) for further destabilization (Center et al., 1997).

With these insights, we designed two new sets of HIV-2 gp140 trimer constructs (see Figure 3.2). The first set began with reversion of all SOSVP-related mutations to wild-type, with or without RRRRRR (6R) proteolytic enhancement. We then added back SOS or VP mutations alone, again with or without 6R. The rationale here was to capture the point at which any of these mutations, if at all, became relevant for optimization of soluble HIV-2 gp140 trimer production. The second set of constructs did not have the SOS mutation but used a flexible GGGGSGGGGS linker in place of the native Furin cleavage site, since the space resulting from cleavage allows the resultant gp120 and gp41 to fall into their native conformation within the trimer. A sufficiently long GS linker would serve the same purpose, and it has been shown to effectively make "native flexible linker" (NFL) trimers (Sharma, et al., 2015)(Georgiev et al., 2015) that are well behaved trimers in a native-like conformation. NFL trimers contain both the linker as well as the I to P (V to P in HIV-2) mutation. We also created a version without the V to P mutation, called GS WT. Several of these constructs were expressed and purified as previously stated, and their SEC elution profiles are shown in Figure 3.6. Most of the proteins featured a taller trimer peak (centered around fractions A6 or A7), with a shorter multimer or aggregate peak running slightly larger. There was little to no evidence of gp140 monomers, in contrast to results for the previous SOSVP 4R or 6R proteins. Coomassie blue stained gels of a few representative elutions are shown in Figure 3.7. These constructs looked similar to previous sets of constructs on non-reducing SDS-PAGE, but the samples under reducing conditions showed an additional band

corresponding to roughly 140 kDa. This band was previously not seen on gels of SOSVP 4R or 6R (Figure 3.4) but was evident in reduced BG505 SOSIP controls on the same gel.

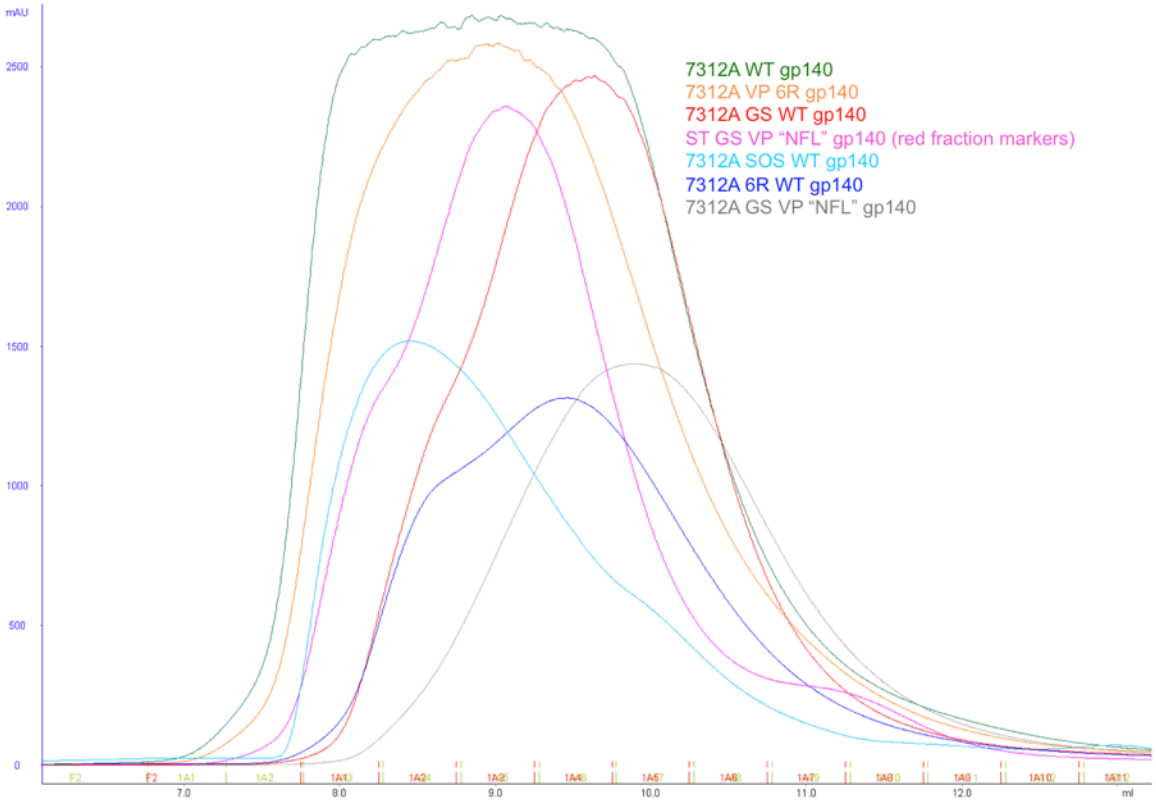

Figure 3.6 Size-exclusion chromatography elution profile for initial HIV-2 new trimers. Trimers generally ran around 9-10 ml, monomers ran around 12 ml, and aggregates ran around 8 ml. ST GS VP "NFL" gp140 (magenta curve) was run on a different AKTA, so the fraction markers (in red) are slightly offset relative to that of the other samples (in light green).

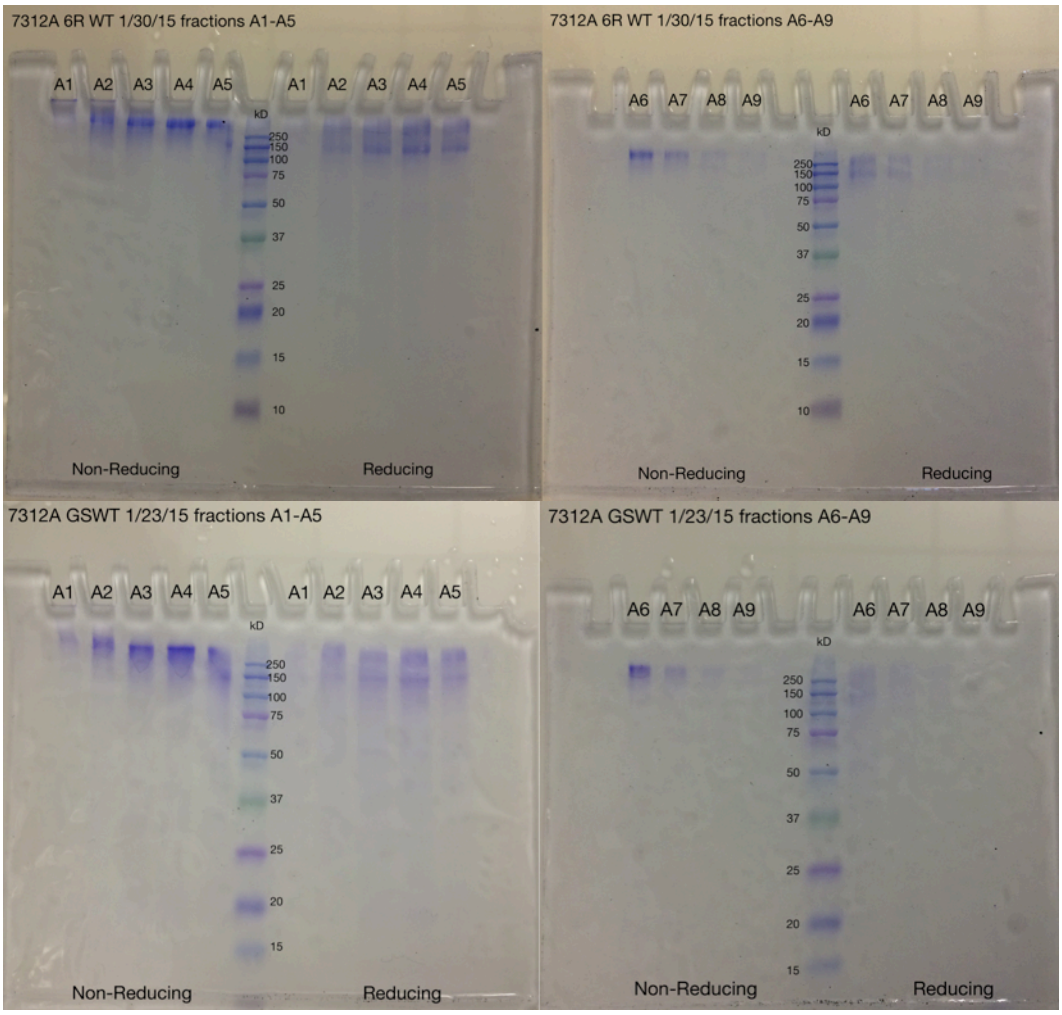

Figure 3.7 Example of SDS-PAGE analysis of initial HIV-2 new trimers. Samples under reducing conditions exhibit a new band at 140 kDa, corresponding to a gp140 monomer.

Analysis of non-SOSVP HIV-2 trimers via negative stain electron microscopy

Several non-SOSVP constructs were analyzed by negative stain EM as previously described (a few examples shown in Figure 3.8, top panels). Overall, the morphologies of these newer trimer constructs were consistently better than HIV-2 SOSVP trimers upon visual inspection. 7312A GS WT particles looked especially promising, as they were more compact and homogeneous than previous HIV-2 constructs, with distinguishing features instead of an amorphous mass. 1,600 particles were picked from around 100 images for reference-free 2D class averages (Figure 3.8, bottommost panel). The presence of several classes whose signals did not converge indicated that the sample was still not appropriate for 3D reconstruction. However, several classes exhibited a three-fold axis of symmetry indicating possible trimers (Figure 3.8, last row).

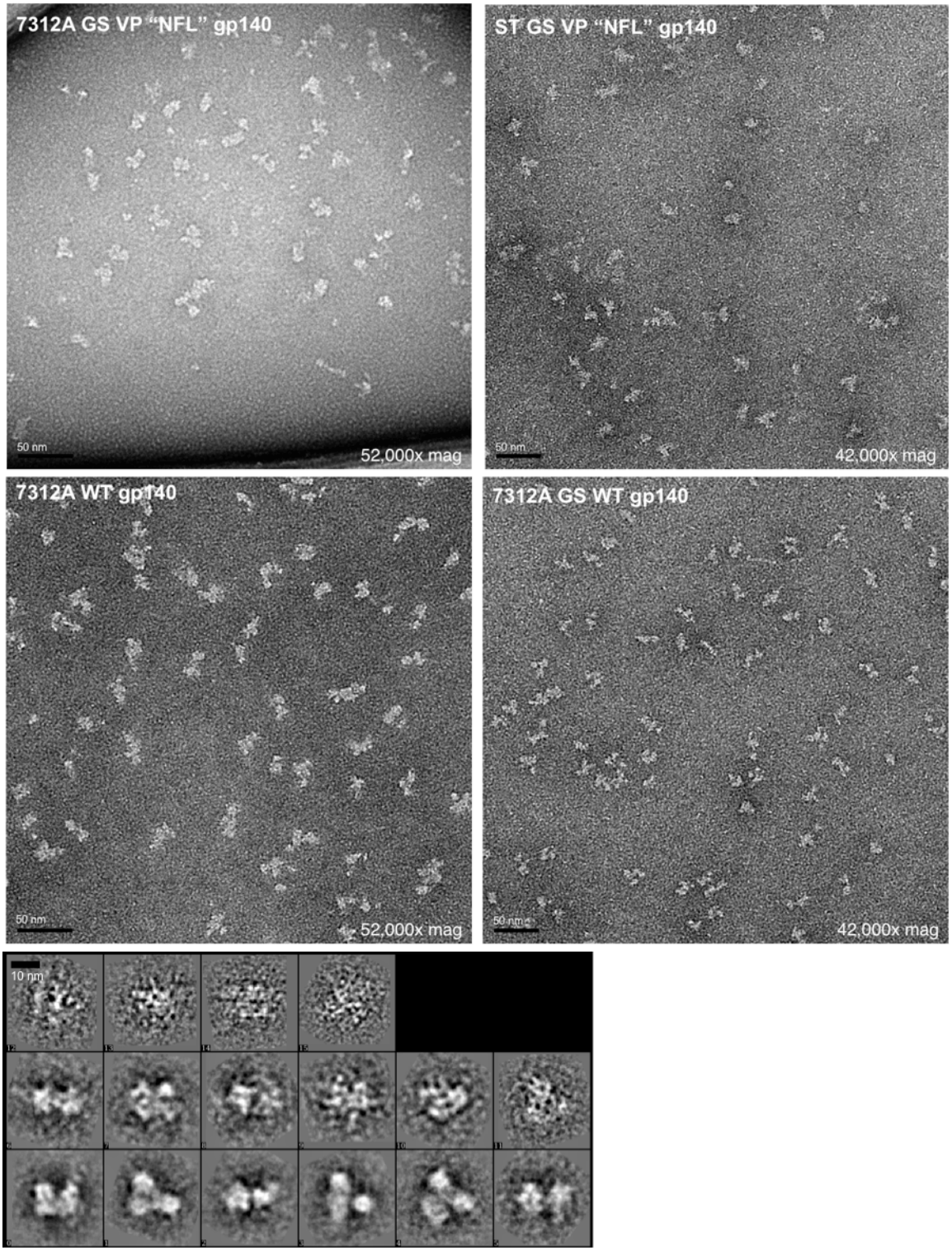

Figure 3.8 Example of negative stain electron micrographs of new trimers with initial 2D class averages from 1,600 particles of 7312A GS WT gp140.

Discussion and future directions

Over the last few decades, the majority of efforts to make a native-like, soluble, readily expressed, cleaved gp140 trimer has been applied to HIV-1. Recently, this work has culminated in the long-awaited X-ray and EM structures of an intact HIV-1 trimer (Julien et al., 2013; Lyumkis et al., 2013). The potential impact of the insight gained from these structures is enormous, and we were motivated by similar reasons to pursue the analogous target in HIV-2. A well-behaved, trimeric HIV-2 gp140 would lend itself to structural studies to answer compelling questions about its apparently lower pathogenicity and virulence. In our initial efforts, mimicking the mutations optimized for HIV-1 SOSIP.664 trimers proved to be a generally unproductive strategy. Though the two are closely related, HIV-2 Env trimer likely exhibits inherent, even if subtle differences in stability and conformation compared to HIV-1. We have yet to fully appreciate these distinguishing features in HIV-2, so designing new constructs starting from the wild-type version of HIV-2 gp140 may provide a promising route. Currently, our best lead is the 7312A GS WT construct, which has reproducibly appeared compact and homogeneous when analyzed via negative stain EM. Several strategies can now be employed to further improve this and other constructs to obtain a more useful reagent for studying native-like HIV-2 Env trimers.

The first step should be performing additional EM analyses of 7312A GS WT using fresh protein, wet-stained sample, and minimally handled grids to prevent bending. Experimenting with stain optimization and grid washing may also benefit the quality of particles. 7312A GS WT should also be purified in complex with CD4 and/or Fabs from anti-HIV-2 antibodies to enhance 2D class averaging of particles. The next step should be

a comparative study of all the proteins from the constructs listed in Figure 3.2. We have purified protein for all versions of the 7312A strain except for VP WT and SOS 6R. Systematic analysis of each SOSVP and non-SOSVP version of trimers using SEC, SDS-PAGE, anti-His_6 Western blotting, SEC-MALS with protein-conjugate analysis (to resolve glycosylation), and negative-stain EM could yield a wealth of information about the contribution of each modification to wild-type as well as synergistic effects of combined modifications. Any trimers that look compact and homogeneous under EM should be co-purified in complex with binding partners (CD4 and/or Fabs) to enhance 2D class averaging. Genes for seven anti-HIV-2 antibody Fabs have been cloned and are ready for expression. As negative-stain EM is an equipment-heavy and qualitative assay for trimer morphology, a better method may involve directly measuring relative protein stabilities of different trimer proteins by modulating temperature. Optimizing the co-transfection of cleavable constructs (all but the ones with GS linker) with different ratios of sFurin DNA may improve the fraction of fully cleaved, soluble trimers. As previously demonstrated (Guenaga et al., 2015), the use of negative selection to eliminate poorly-formed trimers may also help with 2D class averaging. Finally, the construct design of trimers can be further optimized. PNAS/JVI NFL makes a 20-mer GlySer linker and has found longer flexible linkers to be better for their constructs.

Materials and methods

HIV-2 gp140 trimer constructs

The genes for all HIV-2 SOSVP trimers were assembled using synthetic gblocks (Integrated DNA Technologies) via touchdown PCR and subcloned into the pTT5 vector. We included restriction sites for EcoRI and NotI for subcloning, the signal peptide with sequence MDAMKRGLCCVLLLCGAVFVSPAGA to facilitate secretion from HEK293 cells. HEK293-6E cells were transiently transfected using PEI with DNA corresponding to the trimer. All non-GlySer linker constructs were co-transfected with soluble Furin in a SOSVP:Furin ratio of 4:1. All proteins were purified via Ni-NTA affinity purification followed by size-exclusion chromatography on a Superdex 200 10/300 column. One liter of optimized HEK293-6E cell expression yielded approximately 0.5 to 2 mg of purified protein.

Negative stain electron microscopy

Negative stain grids were prepared by applying ~10ug/ml of the purified trimer to a freshly glow discharged ultrathin carbon film coated 400 Cu mesh grid (Ted Pella) and stained with 2% Uranyl acetate. Grids were viewed under FEI Tecnai T12 electron microscope operating at 120kV and imaged at a maginification of 42000X. Images were acquired on a Gatan 2kX2k CCD camera at ~1um defocus. Particles were picked manually picked up, and CTF estimation and phase flipping were performed using EMAN2. Reference-free 2D class averages were also calculated using EMAN2.

References

HIV Sequence Compendium 2013. Foley B, Leitner T, Apetrei C, Hahn B, Mizrachi I, Mullins J, Rambaut A, Wolinsky S, and Korber B, Eds. Published by Theoretical Biology and Biophysics Group, Los Alamos National Laboratory, NM, LA-UR 13-26007.

Shailendra Kumar Sharma, Natalia de Val, Shridhar Bale, Javier Guenaga, Karen Tran, Yu Feng, Viktoriya Dubrovskaya, Andrew B. Ward, Richard T. Wyatt, Cleavage-Independent HIV-1 Env Trimers Engineered as Soluble Native Spike Mimetics for Vaccine Design, Cell Reports, Available online 16 April 2015

Binley, J.M., Sanders, R.W., Clas, B., Schuelke, N., Master, A., Guo, Y., Kajumo, F., Anselma, D.J., Maddon, P.J., Olson, W.C.*, et al.* (2000). A recombinant human immunodeficiency virus type 1 envelope glycoprotein complex stabilized by an intermolecular disulfide bond between the gp120 and gp41 subunits is an antigenic mimic of the trimeric virion-associated structure. Journal of virology *74*, 627-643.

Binley, J.M., Sanders, R.W., Master, A., Cayanan, C.S., Wiley, C.L., Schiffner, L., Travis, B., Kuhmann, S., Burton, D.R., Hu, S.L.*, et al.* (2002). Enhancing the proteolytic maturation of human immunodeficiency virus type 1 envelope glycoproteins. Journal of virology *76*, 2606-2616.

Broder, C.C., Earl, P.L., Long, D., Abedon, S.T., Moss, B., and Doms, R.W. (1994). Antigenic implications of human immunodeficiency virus type 1 envelope quaternary structure: oligomer-specific and -sensitive monoclonal antibodies. Proceedings of the National Academy of Sciences of the United States of America *91*, 11699-11703.

Center, R.J., Kemp, B.E., and Poumbourios, P. (1997). Human immunodeficiency virus type 1 and 2 envelope glycoproteins oligomerize through conserved sequences. Journal of virology *71*, 5706-5711.

Chen, B., Zhou, G., Kim, M., Chishti, Y., Hussey, R.E., Ely, B., Skehel, J.J., Reinherz, E.L., Harrison, S.C., and Wiley, D.C. (2000). Expression, purification, and characterization of gp160e, the soluble, trimeric ectodomain of the simian immunodeficiency virus envelope glycoprotein, gp160. The Journal of biological chemistry *275*, 34946-34953.

Depetris, R.S., Julien, J.P., Khayat, R., Lee, J.H., Pejchal, R., Katpally, U., Cocco, N., Kachare, M., Massi, E., David, K.B.*, et al.* (2012). Partial enzymatic deglycosylation preserves the structure of cleaved recombinant HIV-1 envelope glycoprotein trimers. The Journal of biological chemistry *287*, 24239-24254.

Earl, P.L., Broder, C.C., Long, D., Lee, S.A., Peterson, J., Chakrabarti, S., Doms, R.W., and Moss, B. (1994). Native oligomeric human immunodeficiency virus type 1 envelope glycoprotein elicits diverse monoclonal antibody reactivities. Journal of virology *68*, 3015-3026.

Earl, P.L., Doms, R.W., and Moss, B. (1992). Multimeric CD4 binding exhibited by human and simian immunodeficiency virus envelope protein dimers. Journal of virology *66*, 5610-5614.

Earl, P.L., Koenig, S., and Moss, B. (1991). Biological and immunological properties of human immunodeficiency virus type 1 envelope glycoprotein: analysis of proteins with truncations and deletions expressed by recombinant vaccinia viruses. Journal of virology *65*, 31-41.

Georgiev, I.S., Joyce, M.G., Yang, Y., Sastry, M., Zhang, B., Baxa, U., Chen, R.E., Druz, A., Lees, C.R., Narpala, S.*, et al.* (2015). Single-chain soluble BG505.SOSIP gp140 trimers as structural and antigenic mimics of mature closed HIV-1 Env. Journal of virology.

Guenaga, J., de Val, N., Tran, K., Feng, Y., Satchwell, K., Ward, A.B., and Wyatt, R.T. (2015). Well-ordered trimeric HIV-1 subtype B and C soluble spike mimetics generated by negative selection display native-like properties. PLoS pathogens *11*, e1004570.

Julien, J.P., Cupo, A., Sok, D., Stanfield, R.L., Lyumkis, D., Deller, M.C., Klasse, P.J., Burton, D.R., Sanders, R.W., Moore, J.P.*, et al.* (2013). Crystal structure of a soluble cleaved HIV-1 envelope trimer. Science *342*, 1477-1483.

Liu, J., Wang, S., Hoxie, J.A., LaBranche, C.C., and Lu, M. (2002). Mutations that destabilize the gp41 core are determinants for stabilizing the simian immunodeficiency virus-CPmac envelope glycoprotein complex. The Journal of biological chemistry *277*, 12891-12900.

Lyumkis, D., Julien, J.P., de Val, N., Cupo, A., Potter, C.S., Klasse, P.J., Burton, D.R., Sanders, R.W., Moore, J.P., Carragher, B.*, et al.* (2013). Cryo-EM structure of a fully glycosylated soluble cleaved HIV-1 envelope trimer. Science *342*, 1484-1490.

Malashkevich, V.N., Chan, D.C., Chutkowski, C.T., and Kim, P.S. (1998). Crystal structure of the simian immunodeficiency virus (SIV) gp41 core: conserved helical interactions underlie the broad inhibitory activity of gp41 peptides. Proceedings of the National Academy of Sciences of the United States of America *95*, 9134-9139.

Poignard, P., Saphire, E.O., Parren, P.W., and Burton, D.R. (2001). gp120: Biologic aspects of structural features. Annual review of immunology *19*, 253-274.

Ringe, R.P., Sanders, R.W., Yasmeen, A., Kim, H.J., Lee, J.H., Cupo, A., Korzun, J., Derking, R., van Montfort, T., Julien, J.P., *et al.* (2013). Cleavage strongly influences whether soluble HIV-1 envelope glycoprotein trimers adopt a native-like conformation. Proceedings of the National Academy of Sciences of the United States of America *110*, 18256-18261.

Sanders, R.W., Derking, R., Cupo, A., Julien, J.P., Yasmeen, A., de Val, N., Kim, H.J., Blattner, C., de la Pena, A.T., Korzun, J., *et al.* (2013). A next-generation cleaved, soluble HIV-1 Env trimer, BG505 SOSIP.664 gp140, expresses multiple epitopes for broadly neutralizing but not non-neutralizing antibodies. PLoS pathogens *9*, e1003618.

Sanders, R.W., Vesanen, M., Schuelke, N., Master, A., Schiffner, L., Kalyanaraman, R., Paluch, M., Berkhout, B., Maddon, P.J., Olson, W.C., *et al.* (2002). Stabilization of the soluble, cleaved, trimeric form of the envelope glycoprotein complex of human immunodeficiency virus type 1. Journal of virology *76*, 8875-8889.

Scharf, L., Scheid, J.F., Lee, J.H., West, A.P., Jr., Chen, C., Gao, H., Gnanapragasam, P.N., Mares, R., Seaman, M.S., Ward, A.B., *et al.* (2014). Antibody 8ANC195 reveals a site of broad vulnerability on the HIV-1 envelope spike. Cell reports *7*, 785-795.

Zhang, C.W., Chishti, Y., Hussey, R.E., and Reinherz, E.L. (2001). Expression, purification, and characterization of recombinant HIV gp140. The gp41 ectodomain of HIV or simian immunodeficiency virus is sufficient to maintain the retroviral envelope glycoprotein as a trimer. The Journal of biological chemistry *276*, 39577-39585.